UNIVERSIDADE DE SÃO PAULO
INSTITUTO DE FÍSICA DE SÃO CARLOS

HIGOR VINÍCIUS DIAS ROSA

Septins and flaviviral proteases: a structural analysis

São Carlos
2022

HIGOR VINÍCIUS DIAS ROSA

Septins and flaviviral proteases: a structural analysis

Dissertation presented to the Graduate Program in Physics at the Instituto de Física de São Carlos, Universidade de São Paulo to obtain the degree of Master of Science.

Concentration area: Applied Physics
Option: Biomolecular Physics
Advisor:
Prof. Dr. Richard Charles Garratt
Co-Advisor:
Profª. Drª. Ana Paula Ulian Araújo

Original Version

São Carlos
2022

I AUTHORIZE THE REPRODUCTION AND DISSEMINATION OF TOTAL OR PARTIAL COPIES OF THIS DOCUMENT, BY CONVENTIONAL OR ELECTRONIC MEDIA FOR STUDY OR RESEARCH PURPOSE, SINCE IT IS REFERENCED.

Rosa, Higor Vinícius Dias
Septins and flaviviral proteases: a structural analysis / Higor Vinícius Dias Rosa; advisor Richard Charles Garratt; co-advisor Ana Paula Ulian de Araujo -- São Carlos 2022.
117 p.

Dissertation (Master's degree - Graduate Program in Biomolecular Physics) -- Instituto de Física de São Carlos, Universidade de São Paulo - Brasil , 2022.

1. Septins. 2. Flaviviral proteases. 3. Microcephaly. I. Garratt, Richard Charles , advisor. II. Araujo, Ana Paula Ulian de, co-advisor. III. Title.

FOLHA DE APROVAÇÃO

Higor Vinícius Dias Rosa

Dissertação apresentada ao Instituto de Física de São Carlos da Universidade de São Paulo para obtenção do título de Mestre em Ciências. Área de Concentração: Física Aplicada - Opção: Física Biomolecular.

Aprovado(a) em: 25/03/2022

Comissão Julgadora

Dr(a). Richard Charles Garratt

Instituição: (IFSC/USP)

Dr(a). Jorg Köbarg

Instituição: (UNICAMP/Campinas)

Dr(a). Shaker Chuck Farah

Instituição: (IQ/USP)

With all my love, to everyone
who shared a part of their lives and knowledge with me,
in special JR and MH for supporting and inspiring me ever since.

ACKNOWLEDGEMENTS

"Be or not to be?"

Well, of course, without the support from many people, I am sure that (apart from continuing to know nothing) I would not have become even a part of what I am today, accomplishing a lot lesser, foolishly spending even more time and effort individually on the same unfortunate tasks, and ultimately being a lot less happy and fulfilled. Therefore, if there is an essential section in this document, this is it! They are the people who made this work progress. They are the ones who shall be awarded and acknowledged for everything that derives from these 100 pages. I sincerely hope these words can touch their hearts as a genuine recognition for all the days and nights, smiles and tears they spent to see the accomplishment of this document.

I am doing my best to remember here all the ones who truly contribute to this study. Still, it is really difficult to select some people and write the right words about their real support and do not state even a state for others, who also were crucial for my development and for the success of this study. For these friends, I would like to heartedly thank them for sharing part of their lights in my support, even without demanding to star. As a "supporting player" in some music bands, I know how important you were (and are) for the harmony, rhythm and balance required for the lead singer to shine. Sincerely, thank you for helping me!

In this way, after this long digression, I would like to start my acknowledgements first towards my supervisor Professor Richard, for being, mainly, a representation of genuine passion for our beloved septins, for structural biology and science in general. Seeing the sparkle in your eyes speaking about the torsion angles of the i+1, i+2 residues in a β-turn (and how one could "magically" retrieve the 3D structure just from the knowing the aa sequence for this loop), made me realise, after a long reflection time, it was not just simple information being transmitted (as one would retrieve from a book), but an emotionally embarked knowledge passed from the inner heart, naturally addressed to the recipients' heart, which, in this way, will never be forgotten. Your way of connecting people and encouraging collaborations between everyone is really inspiring. Thank you also for all the patience, support and for, of course, the infinite recommendation letters and e-mails answered later in the night, or weekends and even more our holiday meetings you attend just to hear sometimes a draft of a theory on how a specific residue of a septin would be crucial for the stabilisation of a whole interface, during septin heterocomplex assembly. Your way of stimulating

criticism and investigation over the sequences, structures and scientific knowledge, in general, was fundamental for my development. With these practices, you foster the importance of planning, proposing and addressing questions precisely and not only doing experiments to get more and more data without a previous question in mind. This has really changed my way of working, and I am sure, by doing that, you have completely transformed my evolution as a scientist, and I will be eternally grateful.

Professor Ana Paula, first of all, how can I write something to acknowledge somebody who became a mother for me in São Carlos, at least in my respect and consideration, due to your endless efforts in helping me grow not only as a scientist but as a person. I am immensely grateful for you taking this teenage freshman boy from your molecular biology classes and introducing him to the world of real scientific research. Your confidence in letting me play alone with the ÄKTAs (and other expensive equipment) late in the night (when no one would want to stay to wait for another run on these "big" SEC columns) was fundamental for my early independence in the lab. By giving me the freedom to learn and explore the pros and cons of each different biophysical and biochemical technique and later discuss and propose experiments, with this in mind, you were crucial for my growth in the field. Apart from this, your daily advice was crucial not only for the progress of my projects but also helped me in some decisions in other spheres of my life and career. Thank you for always asking and caring about me not only as a student but as a person, since very early. By the way, I really appreciate you never directly complained about my excessive requests for recommendation letters and absences from the lab due to these extracurricular courses, workshops, and preparations for the application processes. I am leaving your student room and lab with a reluctant heavy heart, and I will always be in debt with you for all these past years.

A special acknowledgement for Professor Ricardo (*in memoriam*), who also introduced me to the scientific thinking during his classes and further nurtured this during our septin group meetings. I must confess I truly enjoyed when we entered into debates over some results and experiments and the particular way you provoked us to think over the implications of the data analytically. I really missed your contributions as our "reviewer #1" in these intellectual challenges. I will never forget my first presentation at this septin meeting as an undergraduate, in which you entered the room and objected to the title, saying it was too audacious, but at the end compliment me saying the study had fulfilled all the expectations raised from the title. You have made real contributions with your after-meeting advice on my

career, and you would have been essential in discussing and revising part of this manuscript, but for all this help, I really hope your soul rest in peace.

How could I not say a state to express my gratitude to all the staff at the Biophysics lab (Belzinha, Drê, Fernando, Raphael), with whom I passed most of my time, and who were elemental for the achievement of this and many other fruitful studies. I could not have been more fortunate to have such friendly and helpful people around. You not only made my work easier but turned the lab environment into a family and a home in São Carlos. I will really miss talking with you all at the Cafe before, during and after the experiments, particularly motivating me when things went wrong. I apologize once more for all the times I almost "collided" with you all while running up and downstairs. Luckily, I retired from the athletics team, and now this would not be a problem anymore.

More specifically, I would like to thank you, Bel, for teaching me the very best of the purification methods (even though some "columns jackets" did not survive in the process), after many others gave up giving attention to this hyperactive person, and for always supplying us with all we needed (from reagents to the best "pães de queijo").

Andressa, the training on the many techniques available in the lab and the mentoring you gave me, apart from the helpfully and pleasant brainstorms and discussions we always had, were the basis for ideas and projects that many in the lab developed. You are at the heart of this septin group, and I cannot remember a single project in this group that has not involved you or your help to some extent. I feel peaceful to know that many new privileged students will be very successful in their projects to have you as a guide to thrive in this turbulent research environment. Keep pushing our "septinologists" in your unique way!

To the master of microscopes and septins Deborah, a real big sister in all these years in São Carlos, who helped in the most remarkable projects and in my most difficult times in life! You know how you were vital to this project. Our countless conversations about the most diverse topics during the preparation and collection of dozens (if not hundreds) of grids shaped this project itself and how I perceive science and life in general. We have already talked about that many times: you really know what needs to be done next, and you have my full support and trust for everything! I am very happy to share these years with you. I hope our paths cross again in the future (and they will)!

To all current members of the septin group (Adriano, Dani, Diego, Eloy, Ítalo, Gabriel, Giovanna, Nilton, Rafael and Humberto) and past members whom I had the contact ("Jesus", Paty, Ana Elisa, Samuel, Sinara, Carla, Helô, Marina, Paola, Mari, and Ton), I would like to thank you so much for all the moments, discussions and guidance you all gave

me. It was a lot easier to get into this amazing, although sometimes confusing, world of septins with your help. For the current and future members, if I had to say something to encourage you, is to do not give up on the difficulties these tricky “serpentinas” may pose to you, take them as a way to learn and then one day you will probably look back and be glad on this. You are really advancing our knowledge forward, even (and probably more fascinatingly) when things may do not work as we hypothesize! These little untamed beasts “were born to be wild” and different from everything else, do not be surprised if you found something amazingly singular about them. There is still so much to be learned and many challenges and adventures to embark on.

Additionally, I would like to hugely thank my friends from Professor Glaucius Oliva Lab (André, Gabi, Rapha, Victor, Nathy and Marjorie) for helping me to enter the field of viral proteases and doing a lot of research in this, not Only with ZIKV and YFV but also with Covid-19 more recently. I would like to particularly thank Gabi for being a huge friend and helper since the very begging of my bachelor degree and particularly during my masters, spending a lot of time discussing and preparing the plasmids and proteases for this study. I would not have come even half this far without your help! Thank you so much, I will really miss you. I would also like to thank Nathy for giving me the ZIKV proteases and motivating me since the very begging of this study when I told you I would probably start something into this. Thank you so much, guys, for all the help.

Maybe this is not the right place to say this, but I would like to thank all the friends (from the Pulero, Vila, Bands, and others from the labs I have been in these years) who helped me grow and, most importantly, kept my mental health and sanity during this whole pandemic and even before. You were fundamental for all of this.

Last but not least, I would like to thank my parents and my sister for giving me full support and unparalleled love during my whole life, always encouraging me to pursue my dreams. You gave a lot more than I deserved, and I hope I can give you some joy and satisfaction to some extent, despite not being so near with you there anymore (physically, but not on the thoughts). I love you.

This study was financed in part by the Coordenação de Aperfeiçoamento de Pessoal de Nível Superior - Brasil (CAPES) - 88887.369815/2019-00 and in part by São Paulo Research Foundation (FAPESP) – grant 2019/22000-9.

"Gela-me a ideia de que a morte seja
O encontrar o mistério face a face
E conhecê-lo.
Por mais mal que seja
A vida e o mistério de a viver
E a ignorância em que a alma vive a vida,
Pior me [relampeja] pela alma
A ideia de que enfim tudo será
Sabido e claro..."

Fausto - **Fernando Pessoa** (1951)

ABSTRACT

ROSA, H. V. D. **Septins and flaviviral proteases:** a structural analysis**.** 2022. 117 p. Dissertation (Master in Science) - Instituto de Física de São Carlos, Universidade de São Paulo, São Carlos, 2022.

In 2016, a 26-fold increase in microcephaly cases during a Zika virus outbreak alarmed the country. In these cases, during infection, the virus has as its main target the neuronal progenitor cells (NPCs), decreasing their proliferation leading to cell death, which contributes to microcephaly. By identifying the isolated effect of viral proteins on these cells, Li *et al.* (2019) observed that the NS2B-NS3 protease is able to mediate virus neurotoxicity, through the cleavage of host proteins essential to neurogenesis (especially septins). There was a reduction in the levels of these proteins after overexpression of the protease, confirming them as a target. In the same study, the cytotoxic effects were related to the cleavage of the C-terminal domain of septin 2, rescuing cytokinesis after the expression of septin 2 "resistant" to the cleavage. Although the cellular effects (after cleavage) were determined, the immediate effect and the importance of the cleaved region in the formation of septin structures was still unclear. It was also unknown whether the septin cleavage was specific for Zika or whether other flavivirus proteases could cleave them. In this work, truncated septin constructions were used to assemble heterocomplexes in order to characterize them and evaluate their potential to polymerize. Proteolytic activity assays and interaction analyses involving septins, and different flavivirus proteases were also performed. Based on these studies, it was found that hexameric complexes are still able to be formed even in the absence of the C-terminal domains, despite influencing stability. However, when analysing the capacity to form filaments, it can be seen that the absence of these domains influences not only the morphology of the filaments formed but also the concentration required for the appearance of these high-order structures. More specifically, the C-terminal domain of SEPT2 cleaved by ZIKV protease proved to be critical for observing filaments at physiological concentrations, thus justifying the subsequent effects caused by its cleavage. At the same time, a specificity for the ZIKV protease in septin cleavage was observed when compared to YFV. The explanations given for the greater efficiency of this off-target cleavage are the closer correspondence between the sequence of the cleavage region in SEPT2 and the preferred sequence for ZIKV cleavage when compared to YFV, and the greater intrinsic catalytic efficiency of the protease from ZIKV. On the latter point, we observe that the two proteases

show differences in their oligomerization profiles in solution, which (allied to other factors) could have some influence on catalytic activity. Finally, from the analysis of the interaction of septins with inactive proteases, it can be verified that the cleavage occurs transiently, and a stable complex between these proteins cannot be obtained. A peptide representing the sequence of the SEPT2 cleavage region was synthesized, and preliminary co-crystallization assays were performed. A possible structure of this complex would be very interesting for understanding the cleavage process and for drug development against microcephaly. We hope that all these results will help understand the implications of septin-2 cleavage and its relationship to the microcephaly caused by Zika virus infection.

Keywords: Septins. Flaviviral proteases. Microcephaly.

RESUMO

ROSA, H. V. D. **Septinas e proteases flavivirais:** uma análise estrutural**.** 2022. 117 p. Dissertação (Mestrado em Ciências) - Instituto de Física de São Carlos, Universidade de São Paulo, São Carlos, 2022.

Em 2016, um aumento de 26 vezes nos casos de microcefalia durante uma epidemia do vírus Zika alarmou o país. Nesses casos, durante a infecção, o vírus tem como alvo principal as células progenitoras neuronais (NPCs), diminuindo a sua proliferação levando à morte celular, que contribui para microcefalia. Ao identificar o efeito isolado de proteínas virais sobre essas células, Li *et al.* (2019) observaram que a protease NS2B-NS3 é capaz de mediar a neurotoxicidade do vírus, por meio da clivagem de proteínas do hospedeiro essenciais à neurogênese (em especial as septinas). Verificou-se uma redução nos níveis dessas proteínas após a superexpressão da protease, confirmando-as como alvo. No mesmo estudo, os efeitos citotóxicos foram relacionados à clivagem do C-terminal da septina 2, resgatando a citocinese após expressão de septinas 2 "resistentes" à clivagem. Apesar dos efeitos celulares (após a clivagem) terem sido determinados, o efeito imediato e a importância da região clivada na formação das estruturas de septinas ainda estava obscuro. Também não era entendido, se a clivagem de septinas era específica de Zika ou se outras proteases de flavivírus poderiam clivá-las. Assim, foram utilizadas construções truncadas de septinas para a montagem de heterocomplexos a fim de caracterizá-los e avaliar potenciais de polimerização. Foram realizados, também, ensaios da atividade proteolítica e análises da interação envolvendo septinas e diferentes proteases de flavivírus. A partir desses estudos, verificou-se que os complexos hexaméricos ainda conseguem ser formados na ausência desses C-terminais, apesar destes influenciarem na estabilidade. Contudo, quando analisada a capacidade de formação de filamentos, pode-se verificar que a ausência desses domínios influencia não só na morfologia dos filamentos formados, como também na concentração necessária para o aparecimento dessas estruturas de alta ordem. Mais especificamente o C-terminal da SEPT2 clivado pela protease de ZIKV, se mostrou crítico para a observação de filamentos em concentrações fisiológicas, justificando assim os efeitos posteriores causados em decorrência de sua clivagem. Paralelamente, observou-se uma especificidade da protease do ZIKV na clivagem de septinas, quando comparado ao YFV. As explicações dadas para uma maior eficiência dessa clivagem *off*-target são: maior correspondência entre a sequência da região de clivagem na SEPT2 e a sequência preferidas para clivagem ZIKV, quando comparada ao YFV, e maior eficiência catalítica intrínseca da protease de ZIKV vs. YFV. Para esse último

ponto, pode-se verificar que as duas proteases apresentam diferenças nos perfis de oligomerização em solução, o que (aliado a outros fatores) poderia ter algum efeito no aumento dessa atividade catalítica. Finalmente, a partir da análise da interação de septinas com proteases inativas, pode-se verificar que a clivagem ocorre de modo transiente e um complexo estável entre essas proteínas não pode ser obtido. Um peptídeo representando a sequência da região de clivagem da SEPT2 foi sintetizado e ensaios preliminares de co-cristalização foram feitos. Uma possível estrutura desse complexo seria muito interessante para o entendimento do processo de clivagem e desenvolvimento de fármacos contra a microcefalia. Esperamos que todos esses resultados ajudem a entender as implicações da clivagem da septina 2 e a relação com a microcefalia.

Palavras-chave: Septinas. Proteases flavivirais. Microcefalia.

LIST OF FIGURES

Figure 1.1 – **Flavivirus genome structure and protein expression.** 24

Figure 1.2 – **Structure of the *Zika* virus NS2B-NS3 complex (PDB 5GPI)** 25

Figure 1.3 – **Septins in the cellular context: from complexes to functions.** 26

Figure 1.4 – **Septins, the fourth component of the cytoskeleton.** 27

Figure 1.5 – **Structure and organization of human septins: primary structure to complexes.** 28

Figure 1.6 – **Septin hexamer structure.** 29

Figure 1.7 – **SEPT2 gene structure and the ZIKV protease cleavage site.** 30

Figure 4.1 – **Sequence identity, of each domain, between members of the same septin group.** 50

Figure 4.2 – **Alignment of the C-terminal domain sequences from the canonical isoforms of the septins from the SEPT2 group.** 51

Figure 4.3 – **PCR products from the amplification of the NG domains of septins 6 and 7.** 52

Figure 4.4 – **Restriction analyses of NG constructs (SEPT2, SEPT6, SEPT7) in the expression plasmids** 53

Figure 4.5 – **Affinity chromatography purification of the 2NGC-6NGC-7NGC septin complex.** 55

Figure 4.6 – **Size exclusion chromatography purification of the 2NGC-6NGC-7NGC septin complex.** 56

Figure 4.7 – **Affinity chromatography purification of the 2NG-6NGC-7NGC septin complex.** 57

Figure 4.8 – **Size exclusion chromatography purification of the 2NG-6NGC-7NGC septin complex.** 58

Figure 4.9 – **Affinity chromatography purification of the 2NGC-6NG-7NG septin complex.** 60

Figure 4.10 – **Size exclusion chromatography purification of the 2NGC-6NG-7NG septin complex.** 61

Figure 4.11 – **Affinity chromatography purification of the 2NG-6NG-7NG septin complex.** 62

Figure 4.12 – **Size exclusion chromatography purification of the 2NG-6NG-7NG septin complex.** 63

Figure 4.13 – **SEC-MALS profiles of full-length and truncated septin complexes.** 65

Figure 4.14 – **Micrographs of the SEPT2NGC/6NGC/7NGC hexameric complex at high ionic strength.** 67

Figure 4.15 – **Micrographs of the SEPT2NG/6NGC/7NGC (2ΔC) hexameric complex at high ionic strength.** 68

Figure 4.16 – **Micrographs of the SEPT2NGC/6NG/7NG (67ΔC) hexameric complex at high ionic strength.** 69

Figure 4.17 – **Micrographs of the SEPT2NG/6NG/7NG (ΔC) hexameric complex at high ionic strength.** 70

Figure 4.18 – **PIP-Strip analysis of different complexes.** 73

Figure 4.19 – **Micrographs of the SEPT2NGC/6NGC/7NGC hexameric complex under polymerizing conditions.** group members. 76

Figure 4.20 – **Micrographs of the SEPT2NG/6NGC/7NGC hexameric complex under polymerizing conditions.** 79

Figure 4.21 – **Micrographs of the SEPT2NGC/6NG/7NG hexameric complex under polymerizing conditions.** 81

Figure 4.22 – **Micrographs of the SEPT2NG/6NG/7NG hexameric complex under polymerizing conditions.** 82

Figure 4.23 – **Systematic analysis of the polymerization capacities of wild and truncated hexameric complexes as a function of their concentrations (100, 200, 400 and 800 nM).** 84

Figure 5.1 – ***In vitro* proteolytic assays**. 88

Figure 5.2 – **Cloning of the ZIKV NS2B3S135A.** 90

Figure 5.3 – **Purification of ZIKV NS2B3^{S135A} protease.** 91

Figure 5.4 – **Purification of YFV NS2B3^{S138A} protease.** 92

Figure 5.5 – **SEC-MALS profiles of ZIKV and YFV NS2B3 proteases (natives WT and inactive mutants).** 93

Figure 5.6 – **Co-purification of septins and ZIKV inactive protease.** 95

Figure 5.7 – **SEC-MALS profile of 2NGC-6G dimer incubated with ZIKV NS2B3^{S135A} protease.** 96

Figure 5.8 – **Microcrystals observed in the crystallization assays of the ZIKV NS2B3^{S135A} protease incubated with a peptide covering the cleavage region on the SEPT2.** 97

CONTENTS

1 INTRODUCTION 23

1.1 Viruses causing congenital effects: the Zika epidemic and microcephaly 23

1.2 Septins 26

1.3 Cleavage of septins by the Zika NS2B-NS3 protease 29

1.4 Justification 30

2 OBJECTIVES 33

2.1 Central Objective 33

2.2 Specific objectives 33

2.2.1 Part A: Structural relevance of the C-terminal domain for septins 33

2.2.2 Part B: Interactions between septins and flaviviral proteases 34

3 MATERIALS AND METHODS 35

3.1 Bioinformatics: 35

3.1.1 Sequence analysis: Alignments and Pairwise distance calculation for each domain 35

3.2 Heterologous protein production: Cloning 35

3.2.1 Cloning of the truncated septin constructs 35

3.2.2 Construction of the catalytically inactive flaviviral proteases 37

3.3 Heterologous Expression 38

3.3.1 Expression of truncated and full-length septin complexes 38

3.3.2 Expression of the mutant flaviviral proteases 39

3.4 Septin purification 40

3.4.1 Cell lysis and clarification of the septin complexes 40

3.4.2 Affinity purification of the septin complexes 40

3.4.3 Size exclusion chromatography (SEC) purification of the septin complexes 41

3.5 Flaviviral proteases purification 41

3.5.1 Cell lysis and clarification of the flaviviral proteases 41

3.5.2 First affinity purification of the flaviviral proteases 42

3.5.3 Dialysis and TEV cleavage of the flaviviral proteases 42

3.5.4 Second affinity purification of the flaviviral proteases 42

3.5.5 Size exclusion chromatography (SEC) purification of the septin complexes 42

3.6 Analysis of the septin C-terminal domain influence on the oligomeric state, heterocomplex assembly and filament polymerization of septins 43

3.6.1 Size Exclusion Chromatography Coupled to Multiple Angle Light Scattering (SEC-MALS) to characterize the septin complexes 43

3.6.2 Preparation of Grids for Transmission Electron Microscopy (TEM) 43

3.6.3 Evaluating the C-terminal truncations effects on heterocomplex assembly 44

3.6.4 Polymerisation assays: the effect of protein concentration on filament formation 44

3.6.5 Evaluating septin interaction with lipids via PIP Strips 45

3.7 Biophysical analysis of the flaviviral proteases 45

3.7.1 *In vitro* protease assay 45

3.7.2 Quantification of proteolytic activity by fluorescent assays 46

3.7.3 Oligomeric state analysis of the flaviviral proteases (SEC-MALS) 46

3.7.4 Co-purification of septins and inactive proteases 46

3.7.5 Size Exclusion Chromatography Coupled to Multiple Angle Light Scattering (SEC-MALS) of septin and proteases complexes 47

3.7.6 Crystallisation Assays with peptides 47

4 RESULTS: STRUCTURAL AND FUNCTIONAL RELEVANCE OF THE C-TERMINAL DOMAIN IN SEPTINS 49

4.1 Alignments and analyses of the sequential identities of the N, G and C domains 49

4.1.1 Alignment of each individual domain 49

4.1.2 Identity between subgroup members in each domain: 49

4.2 Septin complexes production: from cloning to purification 52

4.2.1 Production of truncated constructs lacking the C-terminal domain (NG) 52

4.2.2 The rationale behind the choice of truncated complexes to be purified and studied 54

4.2.3 Purification and analysis of the 2NGC-6NGC-7NGC complex 54

4.2.4 Purification and analysis of the 2NG-6NGC-7NGC complex 57

4.2.5 Purification and analysis of the 2NGC-6NG-7NG complex 59

4.2.6 Purification and analysis of the 2NG-6NG-7NG complex 62

4.3 Analysing the influence of the C-terminal domains on the oligomeric state and the complex self-assembly (in high ionic strength conditions) 64

4.3.1 Analysis of molecular masses of complexes by SEC-MALS 65

4.3.2 Analysis of the assembly of hexameric complexes by electron microscopy (negative stain) under conditions of high ionic strength 66

(1) WT complex in a high-ionic strength buffer 67

SEPT 2ΔC complex in a high-ionic strength buffer 68

(2) SEPT 67ΔC complex in a high-ionic strength buffer 69

(3) SEPT ΔC complex in a high-ionic strength buffer 70

4.4 Analysis of the influence of C-terminal domains on the capacity of interaction with membranes (PIP-Strips) 72

4.5 Analysis of the influence of C-terminal domains on the polymerization process 74

4.5.1 WT complex under polymerising conditions: the loose and tight filament spacings 76

4.5.2 SEPT 2ΔC complex in a low ionic strength buffer: the ZIKV protease cleavage effect on polymerization 78

4.5.3 SEPT 67ΔC complex in a low ionic strength buffer: formation of paired filaments and only tight filament spacing 80

4.5.4 SEPTΔC complex in a low ionic strength buffer 82

4.6 Conclusion 85

5 RESULTS: FLAVIVIRAL PROTEASES AND THE INTERACTION WITH SEPTINS 87

5.1 *In vitro* Proteolytic Assays 87

5.2 Production of catalytically inactive mutant flaviviral NS2B3 proteases 90

5.3 Purification of inactive flaviviral proteases and proteolytic activity assays 90

5.3.1 An oligomeric state analysis of the flaviviral proteases (SEC-MALS) 93

5.3.2 Confirming the loss of catalytic activity in the mutant flaviviral proteases through *in vitro* proteolytic assays 94

5.4 Interaction and complex formation between septins and ZIKV inactive protease 95

5.4.1 Pull-down assay with septins and ZIKV inactive protease 95

5.4.2 SEC-MALS analysis of the incubation between septins and ZIKV inactive protease 96

5.4.3 Co-crystallization assays with SEPT2 peptides containing the cleavage residues 97

5.5 Conclusion 98

6 FINAL REMARKS AND FUTURE PERSPECTIVES 99

REFERENCES 101

1 INTRODUCTION

1.1 Viruses causing congenital effects: the Zika epidemic and microcephaly

Viral infections during pregnancy have been identified as the cause of congenital effects for a long time.[1] The so-called "vertical transmissions," which occur when the infectious agent promotes infection in the fetus or new-born after maternal exposure, have well-known and studied effects. As an example, vertical transmission infections involving rubella virus and cytomegalovirus have already been described and associated with neurological and cardiac anomalies, as well as other types of congenital physical and psychological disorders.[2-3]

Recently, an epidemic of the Zika virus has highlighted, once again, the relationship between viral infections during pregnancy and consequent congenital effects. The rapid transmission of this arbovirus meant that, during the peak of the epidemic in Brazil in 2016, a 26-fold increase in the incidence of microcephaly[4] cases in the country was reported. Until July 2019 (the last epidemiologic report[5] of Zika by WHO), 246,282 cases had been confirmed in the Americas alone[6] and the virus was present in 87 countries worldwide, representing a significant challenge for international public health.[7]

Microcephaly, resulting from fetal viral infection and characterized by a drastic reduction in brain size, is considered the primary indication of the so-called Congenital Zika Syndrome. Other characteristics resulting from the infection are also associated with this condition, such as: delayed intrauterine growth, severe impact on the central nervous system, cerebral calcifications, among other abnormalities related to the nervous system.[8-10]

Several changes in biomolecules and biological processes that lead to microcephaly (due to Zika virus infection) have been recently identified.[11] Although the detailed mechanism (behind these alterations) has not yet been completely elucidated, most of the changes are related and have as the main target the human neuronal progenitor cells (hNPCs).[12] Drastic changes in the transcriptional profile of these cells are observed, with activation of caspases, inhibition of interferon signalling pathways (in charge of the antiviral responses), in addition to blocks at crucial stages for neurogenesis.[13-16] Essentially, different failures and deficiencies are seen during the cell cycle. These are more evident during cell division, causing delays, the presence of multinucleated cells, and the induction of apoptosis.[11,13-14]

The Zika virus, which causes these different effects, belongs to the Flaviviridae family and to the Flavivirus genus, which also includes the Yellow Fever, the Dengue and the Japanese Encephalitis viruses. Viruses belonging to this genus contain genetic material composed of a single positive strand of 11kb RNA that encodes a single open reading frame (ORF). This ORF contains the coding sequence for a single polyprotein (Figure 1.1), translated by the host, in addition to non-coding regions that flank it (associated with the control of translation and viral replication).[15]

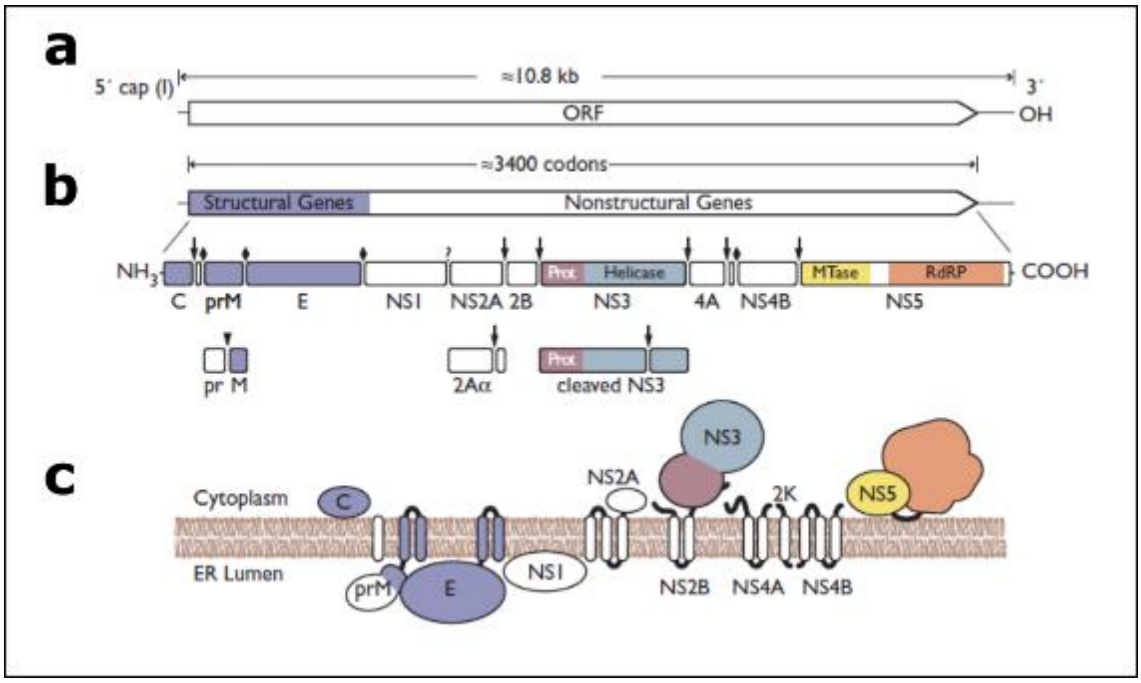

Figure 1.1 – **Flavivirus genome structure and protein expression.** In a., the structure of the ORF and the genome. The flanking regions of the ORF possess noncoding sequences, functionally significant. In b., the polyprotein structure is shown. Structural and Non-structural genes are highlighted. The boxes below depict both the precursors of the proteins (before the cleavage by the protease) and the mature processed proteins. Larger arrows (in black) indicate the NS2B-NS3 serine protease cleavage sites in the polyprotein. In c., the polyprotein membrane topology.

Source: Adapted from LINDENBACH.[15]

The cleavage of this polyprotein is essential for virus replication and is performed in part by host proteases but, mainly, by the complex between the serine protease domain of the non-structural protein 3 (NS3) interacting with the C-terminal portion of the non-structural protein 2 (NS2B). With the formation of the functional NS2B-NS3 heterodimer, the processing and separation of different viral proteins, previously synthesized as a single polyprotein, are possible, making them active and mature.[16]

Recent studies have tried to identify how each Zika virus protein promotes the changes observed in hosts, isolating the biological effect of each and comparing it with phenotypes observed after viral infection as a whole.[14, 17]

It can be seen, for example, that the NS2B-NS3 heterodimer (Figure 1.2) can also cleave host proteins containing the cleavage sites recognised by the protease.[18] When a truncated NS2B protein construct fused to the serine protease domain of NS3 is overexpressed in hNPCs, it can be seen that this construct (NS2B3) is able to mediate the same cytotoxic effects of Zika virus infection: cells with multiple centrosomes, failures and delays in cell division, increased apoptosis and the formation of multipolar spindles.[19]

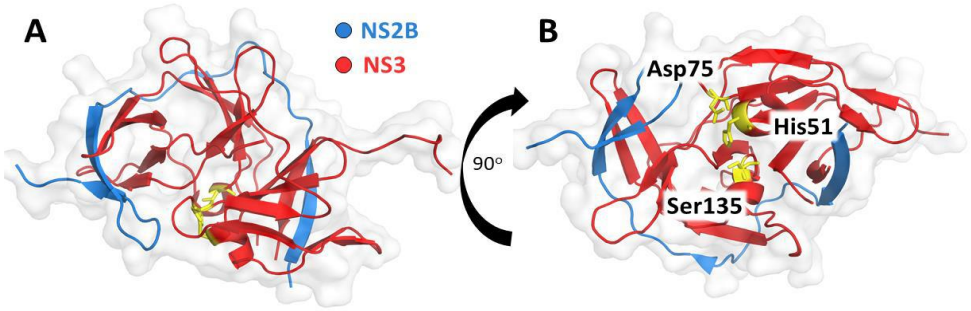

Figure 1.2 – **Structure of the *Zika* virus NS2B-NS3 complex (PDB 5GPI)**. In a., the structure of the NS2B (blue) complex with the NS3 (red) is displayed. In b., the catalytic triad typical for a serine protease (with residues His51, Asp75 and Ser135) is displayed in yellow.

Source: Kindly provided by G. Noske.

In order to identify the molecular targets of the NS2B-NS3 protease, Li *et al.*[19] performed quantitative proteomics analyses (co-purification with the inactive protease NS2B-NS3^{S135A} followed by mass spectrometry analyses of the co-purified proteins). In this analysis, it is assumed that proteins identified as interaction partners of the protease could possibly be cleaved by it. The different proteins identified could then be grouped into different specific interaction modules, according to the cellular function they are involved in: cytoskeleton, protein folding, proteasome, RNA binding and processing, chromosome maintenance, metabolism and ribosome.

The specific interaction module related to the cytoskeleton, which could be directly related to the different cellular phenotypes most observed during infection with the virus (problems in cytokinesis, presence of multinucleated cells), showed hits for cytoskeletal proteins called septins, in particular the septins 2 (SEPT2), 7 (SEPT7) and 9 (SEPT9). Interactions with the NS3 protease were confirmed for septins 2 and 7 and increased in the presence of the NS2B protein. It was also possible to observe a reduction in the

endogenous levels of septins after transfection with the gene for the overexpression of active NS2B-NS3 but not with the inactive mutant protease in which the catalytic serine had been substituted by an alanine. In summary, this indicates that septins are, in fact, a molecular target for the protease (albeit presumably accidental).

1.2 Septins

Septins are a family of proteins highly conserved in eukaryotes, which bind to the nucleotide guanosine triphosphate (GTP) and interact to form heterocomplexes. Septins were first observed in studies with mutants that failed to perform cytokinesis in yeast (Saccharomyces *cerevisiae)* in the 1970s. [20-22] Subsequently, these genes were associated with the formation of the dividing septum, [23-26] allowing the separation of cells formed during cell division, conferring on them the name of septins. Since then, they have been seen in several organisms such as fungi,[27-28] animals,[29-30] protozoa[31] and algae.[32-33]

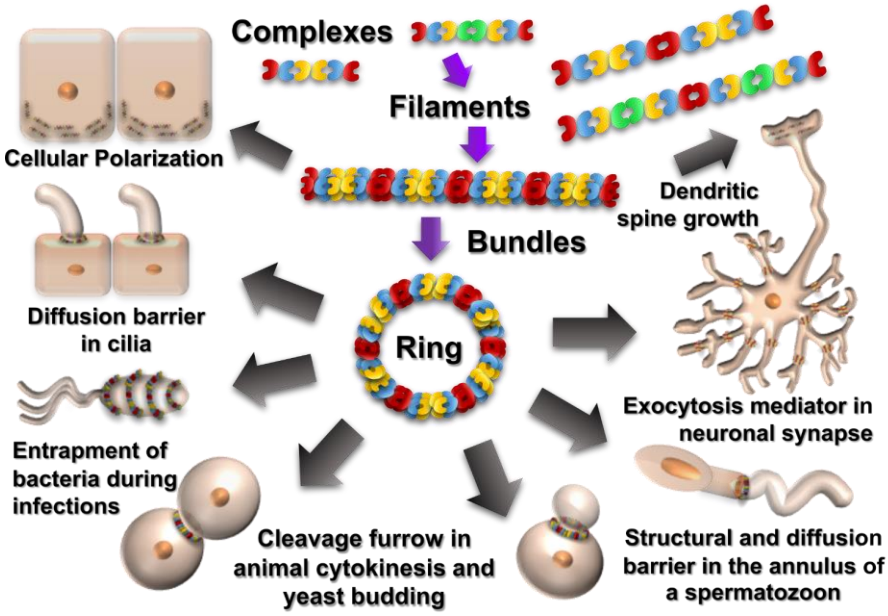

Figure 1.3 – **Septins in the cellular context: from complexes to functions.**

Source: By the author.

After identifying their active presence in the cytokinesis process, septins have been associated with other cellular functions, such as: membrane compartmentalization, epithelial cell polarization, organization and dynamics of microtubules and actin filaments, and others (Figure 1.3).[34-42] Due to the diversity and importance of the functions performed, septins are classified as the fourth component of the cytoskeleton, together with actins, intermediate

filaments and microtubules.[37] Amongst all these cytoskeletal components, the septins filaments are the narrowest (Figure 1.4). Like intermediate filaments, septins polymerize into non-polar filaments.[43-45]

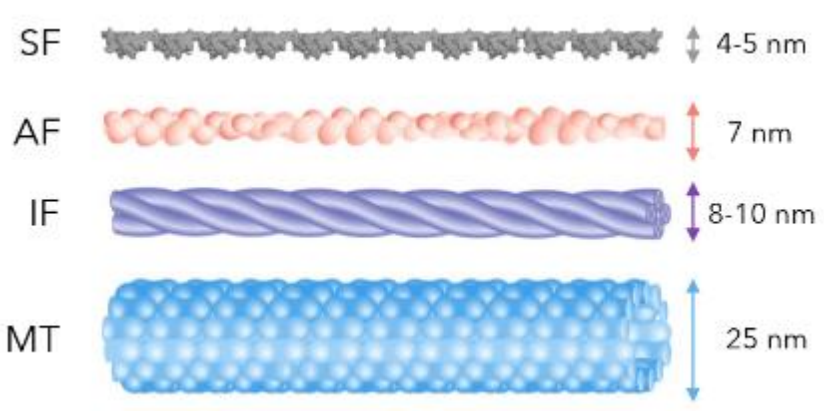

Figure 1.4 – **Septins, the fourth component of the cytoskeleton.** The four components are displayed in this figure: the septin filaments (SF), actin filaments (SF), intermediate filaments (SF), and microtubules (MT). At the right side of each filament is shown the approximate diameter of each filament once polymerized.

Source By the author.

Septins have three structural domains:[46-47] a central guanine binding (GTP/GDP) domain (G-domain), flanked by the N-terminal and C-terminal domains (Figure 1.5). The N-terminal domain is poorly conserved and includes, in most septins, a polybasic region (PB1) related to interaction with membrane lipids (where it is possible to observe an α helix called α0),[48-49] as well as an unstructured upstream sequences, sometimes enriched in prolines related to the interaction with other proteins and components of the cytoskeleton, prior to the polybasic region.[50-51] The highly conserved central domain is called the G-domain and it interacts with the guanine nucleotide.[52] The C-terminal domain is quite variable and is found right after a highly conserved region of the G-domain, characteristic of septins, called the septin unique element (SUE).[43,53.] This C-terminal domain can contain within its sequence coiled coil regions. These structural motifs are presumed to be important for the interaction of septins with other septins, partner proteins and lipid membranes.[45-47, 54-56]

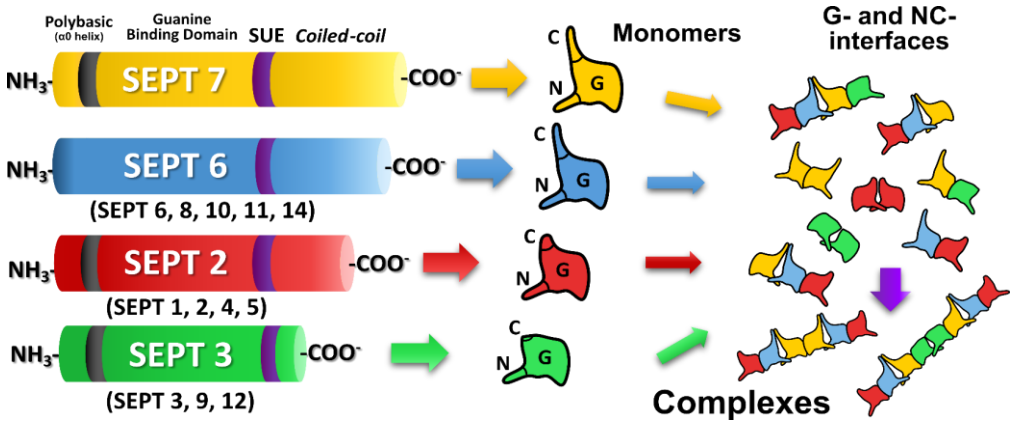

Figure 1.5 – **Structure and organization of human septins: primary structure to complexes.**

Source: By the author.

In humans, there are 13 genes that code for septins (which can generate dozens of isoforms by alternative splicing).[57-59] Based on the sequential similarity between these genes, it is possible to group them into four groups that are represented by septins 2 (SEPT2), 3 (SEPT3), 6 (SEPT6) and 7 (SEPT7). The members of each group are shown in Figure 1.5. These groups show differences in the length of the C-terminal region and in their catalytic activity, with each group occupying a specific position in the formation of complexes. It has been proposed that members of the same group can be interchanged in the formation of these structures.[37,52,58] In the case of human septins, these hetero-oligomeric complexes may be either hexamers (composed of two copies each of members of the SEPT2, SEPT6 and SEPT7 groups) or octamers in which all four groups are present.

Septins subunits in the complexes interact using two opposite interfaces. [43] The so-called G-interface directly involves the region close to the binding site of the guanine nucleotides of the interacting subunits. The NC interface, as opposed to the G interface, involves the N- and C-terminal ends of the G domain, as well as portions of the N- and C-terminal domains, such as the α0 helices. Figure 1.6 shows the arrangement of a hexamer composed of two copies each of SEPT2, SEPT6 and SEPT7.

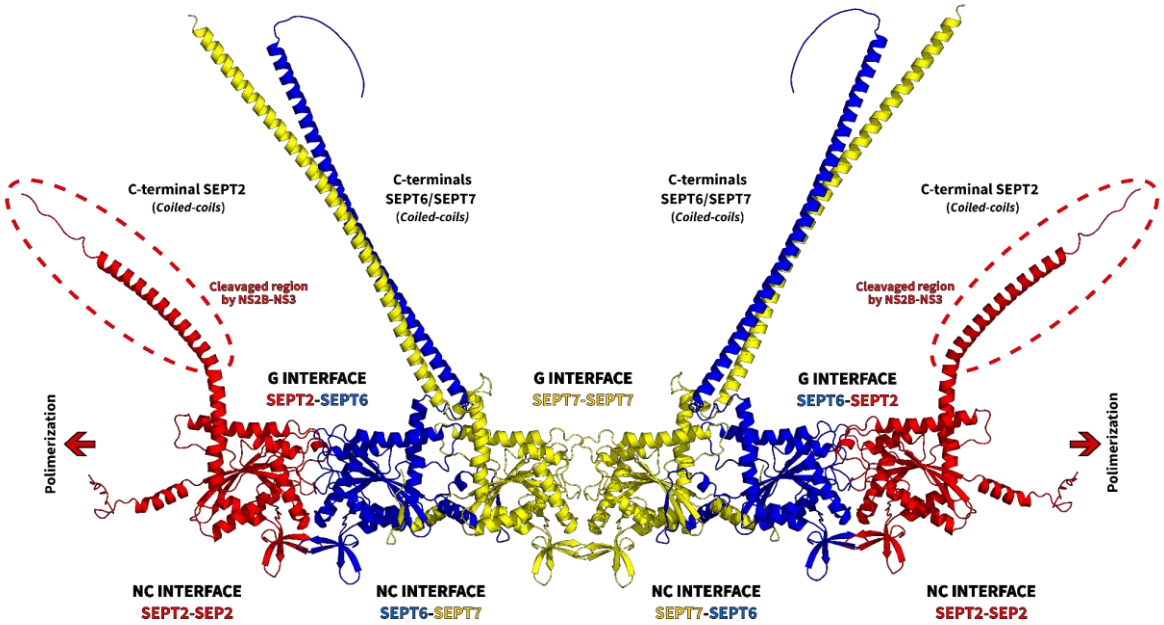

Figure 1.6 – **Septin hexamer structure.** The G and NC interfaces found in the heterocomplex formed from the interaction between septin 2 (red) and septin 6 (blue) and between two subunits of septin 7 (yellow) are shown. The C-terminal domains, which are not visualized in the structures of septin heterocomplexes [43, 60] deposited on PDB (due to the absence of density), are seen here as modelled by AlphaFold. [61] Horizontal arrows indicate the direction of polymerization via the septin 2 homodimeric NC interface. The dashed circle indicates the C-terminal region of septin 2 cleaved by the Zika NS2B-NS3 protease.

Source: By the author.

The subunit interactions observed in the published human heterocomplex structures are formed by the proteins SEPT2-SEPT6-SEPT7 in a palindromic distribution,[43,60] through the G interface between SEPT2/SEPT6 and SEPT7/SEPT7, as well as through the NC interfaces between SEPT6/ SEPT7 and SEPT2-SEPT2.[52] According to the corrected model for the order of septins in the complex, recently proposed by Mendonça *et al.*[62] and Soroor *et al.*[63] and further corroborated by others in the literature,[64] the presence of septin 2 (SEPT2) is seen in at the polymerising extremity, whether it is a hexameric or an octameric complex.

1.3 Cleavage of septins by the Zika NS2B-NS3 protease

Once the host proteins that are the targets of protease cleavage (responsible for the phenotypes observed in NPCs after Zika virus infection) were identified and confirmed, the affected regions in these targets (septins) due to this degradation were identified. It was observed that only septin 2 is cleaved by the protease (SEPT7 and SEPT9 possibly formed part of the same complex). The cleavage of SEPT2 occurs in a region near the end of the G domain, which causes the complete loss of the C-terminal domain after the cleavage.[19]

In the same study, the authors identified the sequence of amino acids that make up the specific cleavage site of the protease ($_{305}$KRG$_{307}$), which enables the cleavage of SEPT2 (Figure 1.7). When eliminating this site, through a point mutation of a residue (SEPT2^{R306A}), it was observed that the protease became incapable of degrading the mutant septin. [19] Furthermore, by promoting the expression of this SEPT2^{R306A} mutant septin, it was possible to rescue the normal functions and phenotypes partially, even during the overexpression of the NS2B-NS3 protease in hNPCs.[19]

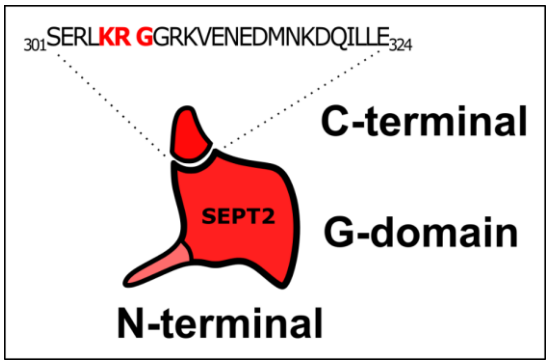

Figure 1.7 – SEPT2 gene structure and the ZIKV protease cleavage site. Schematic showing the domains of septin 2, highlighting the C-terminal domain (residues 301-324), containing the protease cleavage site (residues in red). The cleavage occurs between an arginine and a glycine (in red).

Source: By the author.

1.4 Justification

Although the study by Li *et al.*[19] was a pioneer in identifying septins as molecular targets of the NS2B-NS3 protease (mediator of cytotoxic effects related to congenital Zika syndrome), the structural and molecular consequences of septin cleavage remain open to investigation, as do issues related to the specificity of effects caused in hNPCs arising from Zika virus infection, as opposed to other flaviviruses.

It is not well understood whether septin cleavage is a phenomenon specific to Zika protease or whether other flaviviral proteases are also able to cleave them. Although the Zika NS2B-NS3 protease has already been shown to be more efficient than the proteases from other flaviviruses,[65] the cleavage and cytotoxic effects leading to microcephaly may be more observed (after Zika infection) due to enhanced viral accessibility to target regions and molecules, crossing membranes and other barriers.[66-67] More extensive studies should be carried out to comparatively evaluate the effect and interaction of proteases from other flaviviruses on septins.

Furthermore, although the cellular consequences have been determined, the immediate effect of the cleavage of the C-terminal domain of septin 2 on the formation of the septin heterocomplex, or even on the properties of the filaments and high-order structures of septins, is not yet known. Based on the new order model proposed by Mendonça *et al.*[62] and Soroor *et al.*[63] and which states that septin 2 occupies the end of the filaments, the cleavage of the C-terminal region of this septin would not be expected to be related to the formation of hexameric (or octameric) complexes, but more likely involved both in the polymerization of these complexes into filaments and in the formation of lateral interactions between filaments. Overall, little is understood about the specific interactions and functions of the N- and C-terminal domains of septins. Thus, the effort to clarify which regions are necessary and sufficient for the formation of complexes and filaments, as well as for the formation of lateral interactions between filaments, which may be related and necessary to the formation of high-order bundles and structures, should be encouraged.

2 OBJECTIVES

2.1 Central Objective

The main goal of this project was to investigate the effect of cleavage of SEPT2 (due to the action of flaviviral proteases) on the structural organization of the septin complex in which it participates as well as its impact on complex polymerization into filaments. For this, we produced and compared complexes containing full-length septins and septins with their C-terminal domains truncated. More specifically, the truncated forms investigated were those of SEPT6, SEPT7, and SEPT2, the latter mimicking the effect of ZIKV protease cleavage. In addition, we aimed to analyse the possible interactions of these constructs with flaviviral proteases.

2.2 Specific objectives

In order to accomplish the general objective, we divided the project into two parts and for each, we proposed some specific goals as follows:

2.2.1 Part A: Structural relevance of the C-terminal domain for septins

a) Construct truncated versions containing only the N-terminal (N) and GTP binding (G) domains of human septin 2 (SEPT2NG).

b) Co-express and co-purify complexes containing (SEPT2NGC (full-length) and/or, SEPT2NG (truncated).

c) Evaluate the formation of complexes and possible alterations in the oligomeric state resulting from the absence of the C-terminal domain (C) of septin 2 by SEC-MALS.

d) Characterize and analyse the importance of this C-terminal domain in the ultra-structural organization of complexes using Transmission Electron Microscopy (TEM), aiming to evaluate the effect of this domain on the process of hexameric complex assembly, on polymerization, and additionally on septin interaction with lipids.

e) Comparatively evaluate the importance of the C-terminal domain of septins 6 (SEPT6) and 7 (SEPT7) for complex formation and polymerization.

2.2.2 Part B: Interactions between septins and flaviviral proteases

a) Test the *in vitro* activity of the Yellow Fever virus (YFV) NS2B-NS3 protease on full-length SEPT2 (SEPT2NGC) in order to evaluate the capacity and efficiency of septin cleavage between different flaviviral proteases (compared with ZIKV).

b) Produce the inactive Zika virus NS2B-NS3 protease (mutant S135A).

c) Verify the stability of the complex between NS2B-NS3S135A and full-length SEPT2.

d) Perform *in vitro* activity tests (on septins) with different proteases.

3 MATERIALS AND METHODS

3.1 Bioinformatics:

3.1.1 Sequence analysis: Alignments and Pairwise distance calculation for each domain

Sequences of the isoforms of all 13 human septins (44 isoforms) were obtained at UniProt and were downloaded as a multi fasta file. Then, the full-length sequences were split into three files, each one containing the sequences of a domain (N, G or C), including all the 44 isoforms. The ranges of each domain (and their respective coordinates) were obtained from sequence alignments for the canonical septins, previously curated using structural data.[68-69] These sequences were then aligned with the software MEGAX,[70] applying the MUSCLE algorithm,[71] with default parameters for gap penalties. Some intricate regions and peculiarities were curated manually, based on structural information.

Once the alignments were obtained for each septin domain, these results were applied to pairwise distance calculations also using the MEGAX software. For these calculations, the bootstrap method provided the variance estimation (the number of bootstrap replications was 1000). The substitution model used was Amino-Acid, displaying the information using the p-distance method, in which 0.0 means 100% of similarity between residues in the sequences and 1.0 means 0% of similarity. The averages amongst all human septin sequences and within members of each septin group were calculated from the data displayed in the matrix.

3.2 Heterologous protein production: Cloning

3.2.1 Cloning of the truncated septin constructs

To assemble the truncated construct mimicking protease cleavage, the coding sequence of septin 2 (SEPT2) (GenBank: NM_004404) was used as a template. Homologous sites in septin 6 (SEPT6) (GenBank: NM_145799) and septin 7 (SEPT7) (GenBank: NM_001788) were similarly used for the production of the equivalent truncated versions, even though these are not naturally generated by viral protease cleavage. The plasmids containing these full-length sequences were already available in our research group. Again,

the definitions of the flanking regions of each septin domain were evaluated based on structural alignments).[68]

The amplification of the nucleotide sequence referring to the desired regions of each protein was performed using the polymerase chain reaction (PCR), using oligonucleotide primers, based on the sequences deposited in GenBank, which are shown in Table 3.1.

Table 3.1 – Oligonucleotides used for to amplify the region of interest for the production of NG constructs. Restriction sites are highlighted in blue, and terminator codons in red.

Oligonucleotides	Restriction enzyme	Sequence (5' to 3')	T_{m*}
SEPT6NG *Forward*	*Nco*I	A**ccatgg**cagcgaccgatatag	59
SEPT6NG *Reverse*	*Hind*III	c**aagctttta**ctcctccagcttacagcg	61
SEPT7NG *Forward*	*Bam*HI	g**ggatcc**gatggtagctcaacagaagaac	62
SEPT7NG *Reverse*	*Pst*I	gc**ctgcagtta**agtcacagctgcaagttttc	63

* The T_m calculation was performed via *OlygoAnalyzer* server IDT (https://www.idtdna.com/pages/tools/oligoanalyzer)

Source: By the author.

The PCR cycles were performed in a Veritii 96-well Thermal Cycler (Applied Biosystems) using the high-fidelity polymerase *Phusion* (Cellco) under conditions described by the manufacturer. These cycles consisted of denaturation, annealing and extension steps, as shown in

Table 3.2. The PCR products were analysed in 0.8% agarose gels containing ethidium bromide (Bio-Rad) and TAE 1X buffer (8 mM Tris-Acetate pH 8,0 and 0.2 mM EDTA).

Table 3.2 – Representation of the cycles employed to amplify the regions of interest for the production of NG constructs.

	Step	Temperature (ºC)	Duration (s)
1X	Initial Denaturation	98	30
	Denaturation	98	10
35X	Hybridization	$T_{m'}$+ 3*	30
	Extension	72	30
1X	Final Extension	72	600

*$T_{m'} = (T_{m(Fw)} + T_{m(Rv)})/2$, represents the average Tm between primers. Addition of 3 ºC in Tm is recommended for *Phusion*™.

Source: By the author.

The amplified products were purified from these gels using the Wizard ® SV Gel and PCR Clean-Up System (Promega), following the manufacturer´s instructions, and their concentrations were quantified using a Nanodrop™ 2000 spectrophotometer (Thermo Scientific).

To allow insertion into pGEM-T cloning plasmids, a protocol for adding 3' overhanging adenines was performed using *Taq* polymerase (NEB). After this tailing procedure, the ligation with the plasmid was accomplished using the T4 DNA ligase (Thermo), using conventional ligation procedures (50 ng of vector, molar ratio vector/insert 3:1, 5 U T4 DNA ligase and [1X] enzyme buffer). After incubation for 16 hours at 4 ºC, the products were used to transform competent *E. coli* DH5-α in order to propagate these plasmids. The positive transformant colonies were selected using an LB medium containing both ampicillin (50 μg/mL) and the Blue-White selection markers: 80 μg/mL of 5-Bromo-4-Chloro-3-Indolyl β-D-Galactopyranoside (XGal) and 0.5 mM of Isopropyl β- d-1-thiogalactopyranoside (IPTG) for inducing expression.

After confirming the recombinant plasmids, these were isolated and purified, and then the regions of interest were characterized by colony *PCR*s and double digestion analysis using specific endonucleases, followed by electrophoresis in a 0.8 % agarose gel. Finally, the positive clones were sequenced using a 3130 Genetic Analyzer (Applied Biosciences) by the dideoxy chain-terminating method [72], to confirm the integrity and fidelity of these constructs.

The SEPT2NG construct was already available and had been made using the Gibson assembly approach in collaboration with Dr Éverton Silva. Therefore, only sequencing and cloning into expression vectors were required in this case.

3.2.2 Construction of the catalytically inactive flaviviral proteases

The inactive mutants of the Zika (ZIKV) and Yellow Fever (YFV) NS2B3 proteases were obtained by site-directed mutagenesis in plasmids containing the wild-type sequences available from CIBFar kindly provided by Dr Nathalya Mesquita and Gabriela Noske. The mutation of the catalytic serine (S135) to alanine is assumed to abolish the proteolytic activity of the enzyme.[19] Thus, PCR amplification of the full-length plasmids was performed (employing primers containing the mutated bases, shown in (

Table 3.3), followed by the digestion of methylated templates using Dpn I. Then, artificial phosphorylation reactions of the 3' portion (using PNK) and recircularization of

these plasmids (via T4 ligase) were performed, aiming for greater efficiency in bacterial transformation. Plasmids were then propagated and purified, allowing the constructs and mutations to be verified by colony PCRs, restriction analysis and sequencing, as described earlier.

Table 3.3 – Oligonucleotides used for making inactive proteases. Mutations are highlighted in blue.

Oligonucleotides	Sequence (5' to 3')	T_{m*}
ZIKV NS2B3 S135A Forward	ggcagggact **g** ccggtag	68
ZIKV NS2B3 S135A Reverse	ggatagtcgagggcaacagcg	70
YFV NS2B3 S138A Forward	ccaagtggcact **g** ctggttctc	70
YFV NS2B3 S138A Reverse	gtagtcaagggcaacccgccc	70

Source: By the author.

3.3 Heterologous Expression

3.3.1 Expression of truncated and full-length septin complexes

After confirming the sequences, they were subcloned into expression vectors. In order to allow for protein co-expression, the fragments were subcloned into bicistronic expression vectors (pETDuet, pRSFDuet). Aiming to maximize yields and provide easier exchangeability in assembling the different truncated and wild-type (WT) complexes, the sequences related to SEPT7 were cloned into the Multiple Cloning Site (MCS) 1 of pETDuet, exploiting the presence of a poly-histidine (His-tag) sequence upstream of the gene. The other two septins required for the hexamer assembly were inserted into the pRSFDuet: SEPT6 at the MCS-1 (without a His-tag), and SEPT2 at the MCS-2. The final constructs utilized in the present study are displayed in Table 3.4.

Table 3.4 – Constructs and plasmids of truncated and full-length septin complexes.

Name	Plasmid	MCS	Mass (kDa)	Coordinates*
His-SEPT7NGC	pETDuet	1	50.4	20-437
His-SEPT7NG	pETDuet	1	35.9	20-318
SEPT2NGC/SEPT6NGC	pRSFDuet	2/1	41.5/48.9	1-361/1-427
SEPT2NG/SEPT6NGC	pRSFDuet	2/1	36.2/48.9	1-308/1-427
SEPT2NGC/SEPT6NG	pRSFDuet	2/1	41.5/34.5	1-361/1-305
SEPT2NG/SEPT6NG	pRSFDuet	2/1	36.2/34.5	1-308/1-306

*Please be aware of the isoforms utilized in this study. The numbering may be different for others.

Source: By the author.

The expression and purification of septin complexes were conducted based on protocols already established in the literature and in the laboratory.[62,73]

Expression of the protein complexes was performed in *E. coli* Rosetta™ 2 (DE3) (Novagen) as host cells. To achieve the optimal stoichiometry of a 1:1:1 hetero-hexamer, SEPT2 and SEPT6 were expressed separately, using a larger culture volume to compensate for the lower level of expression of the pRSFDuet plasmid compared that of the SEPT7 in pETDuet. The ratio of expressed cultures was three parts of SEPT2/SEPT6 to one of SEPT7.

The transformants were selected on agar plates containing appropriate antibiotics for marker selection of the plasmids: ampicillin (50 μg/mL) for the pETDuet vector, kanamycin (30 μg/mL) for pRSFDuet, and chloramphenicol (34 μg/mL) for the selection of pRARE 2 (Rosetta). A pool of colonies was picked from the plate and grown in a 10 mL LB "pre-inoculum" overnight at 37 ºC, while shaking at 250 rpm. Samples of such overnight cultures were used to inoculate a 1 L culture of LB broth supplemented with 2 mM $MgCl_2$. Cells were grown under the same conditions as before. When the optical density at 600 nm (OD_{600}) reached 1–1.2, the temperature was decreased to 18 ºC and the expression was induced with 0.5 mM IPTG, and left at 150 rpm, for 20 h.

Finally, to achieve the correct proportion of the septins within the hexamer and allow for complex assembly, 3 L of SEPT2/SEPT6 were pooled with 1 L of SEPT7. After this, the cells were centrifugated at 10,000 g for 10 min at 4 ºC. The resulting pellet was either stored at -80 °C for purification at a later time or used immediately.

3.3.2 Expression of the mutant flaviviral proteases

For the purpose of expressing the mutant flaviviral proteases, protocols for the wild-type proteases already established in the literature and at the CIBFar were used. [65, 74] Protein expression was performed in the enriched Terrific Broth medium (TB) using *E. coli* Rosetta™ 2 cells transfected with the recombinant plasmids, previously cultured in an overnight 10 mL pre-inoculum flask containing antibiotics for selection of the positive transformants, under shaking (250 rpm) and at 37 ºC. Subsequently, 1 L of TB medium, also containing selection markers, was inoculated with the pre-inoculum and incubated, under the same temperature and rotation conditions, until the solution reached an OD_{600} of 1-1.2, allowing for the

induction of expression, using 0.5 mM IPTG, which was maintained for 20 h at 18 ºC and 150 rpm.

Finally, cells were harvested by centrifugation at 10,000 g for 10 min at 4 ºC. The resulting pellet was stored either at -80 °C for purification at a later time or used immediately.

3.4 Septin purification

3.4.1 Cell lysis and clarification of the septin complexes

The bacterial pellets were resuspended in 30 mL buffer A (25 mM Tris-HCl pH 7.8, containing 500 mM NaCl, 5 mM Mg Cl_2 and 5% [v/v] glycerol) for each 1 L of culture immediately before the start of the purification procedures. The solution was also incubated with lysozyme (100 ug) and benzonase nuclease (100 U) for 30 minutes, on an ice bath, prior to sonication. Phenylmethylsulfonyl (PMSF) protease inhibitor (1 mM) was also utilized to prepare septin samples for those experiments not involving the flaviviral proteases.

After this incubation, the cell suspension was subjected to sonication cycles of 30 sec "ON" followed by 30 sec "OFF" (20% amplitude), achieving a total of 5 "ON" min, using a 505 Sonic Dismembrator (Fisher Scientific) with a 1/2" tip.

Soluble fractions, containing target proteins, were separated from insoluble fractions by centrifugation (20,000 g for 45 min at 4 °C), Then this solution was further filtered before proceeding to the Ni-NTA affinity purification step, using 0.45 μm syringe filters (Millipore).

3.4.2 Affinity purification of the septin complexes

The filtered soluble fraction was loaded onto a HisTrap HP 5 mL column (GE Healthcare), pre-equilibrated, under a flux of 5 mL/min, with buffer A supplemented with 2%[v/v] of buffer B (25 mM Tris-HCl pH 7.8, 500 mM NaCl, 5 mM $MgCl_2$, 5% [v/v] glycerol and 500 mM Imidazole), to hamper promiscuous interactions within the Immobilized metal affinity chromatography (IMAC) column.

Firstly, the column was washed with the same equilibration mixture, until the UV baseline stabilization. Thereafter, a 10 mL solution of 0.1% Triton-X 100 was injected onto the column to better clean lipids and other components. Finally, the percentage of buffer B in this mixture was increased to 7 %[v/v] (35 mM Imidazole) to wash away other contaminants.

The septin hexameric complex was eluted during a linear gradient of 25 mL of buffer B ramping from 35 to 500 mM Imidazole (7 to 100 % of buffer B in the mixture).

The purity and integrity of all the septin complexes were analyzed on 12% SDS-PAGE, before proceeding to the following purification step, in order to select the best fractions with fewer contaminants and higher septin concentrations.

3.4.3 Size exclusion chromatography (SEC) purification of the septin complexes

Prior to the size exclusion chromatography, the selected fractions were concentrated in cycles of 5 min and 1000 g, using refrigerated microcentrifuges (4 ºC) using Amicon® centrifugal filters with a 50 kDa pore cut-off previously passivated by incubating them with 5 %[v/v] Triton-X 100 for 2 h.

Subsequently, to better separate hexamers from larger and smaller oligomeric states (aggregates, monomers, dimers, tetramers), the purified concentrated complexes were loaded onto a preparative HiLoad Superdex 200 16/600 column (GE Healthcare) pre-equilibrated with buffer C (25 mM Tris-HCl pH 7.8, 300 mM NaCl, 5 mM $MgCl_2$, 5% [v/v] glycerol). Samples were obtained through an isocratic elution, at a 1.0 at flux of mL/min, and protein and nucleotide absorbance were monitored at 280 and 254 nm, respectively. Fractions containing the complex were quantified and, when required, concentrated to 1 mg/mL. When not immediately used for the experiments, aliquots of 20 µL were frozen in liquid N_2 and stored at −80 ºC for further utilization. SEC purification, at a flux of 0.75 mL/min, was also performed using an analytical Superdex 200 10/300 Increase GL, under similar buffer conditions, when the injection volume was smaller and for those experiments in which protein purity was less critical.

3.5 Flaviviral proteases purification

3.5.1 Cell lysis and clarification of the flaviviral proteases

Cell lysis and clarification of the flaviviral proteases were done similarly to septins. Pellets were resuspended in 50 mL protease buffer A (50 mM Tris-HCl pH 8.0, 300 mM NaCl, 10% [v/v] glycerol) supplemented with 30 mM Imidazole. Again, the solution was incubated for 30 min with lysozyme and benzonase, in an ice bath. Here, PMSF protease inhibitor was not added, as protease activity assays would be subsequently performed. Dithiothreitol (DTT) (1 mM) was used as a reducing agent.

Sonication could be adjusted and intensified as these proteases are more thermally stable than the septins. Cycles consisted of 12 min of 30 sec "ON" followed by 45 sec "OFF"

(40% amplitude). Thereafter, clarification was done, and the soluble fraction was filtered before loading onto the IMAC column, as previously described for septins.

3.5.2 First affinity purification of the flaviviral proteases

For the first IMAC purification of the flaviviral proteases, a HisTrap HP 5 mL column (GE Healthcare) was pre-equilibrated with buffer A supplemented with 10%[v/v] of buffer B (50 mM Tris-HCl pH 7.8, 300 mM NaCl, 5 mM $MgCl_2$, 10% [v/v] glycerol and 300 mM Imidazole), under a flux of 5 mL/min.

After the first wash with 10 column volumes (CV) of the equilibration buffer, the elution started with an increase in the percentage of the protease buffer B in a linear gradient until it reached 100 %.

3.5.3 Dialysis and TEV cleavage of the flaviviral proteases

To enable the cleavage of the His-tag and the Small Ubiquitin-like Modifier (SUMO) fusion protein attached to the proteases, the peak fractions were subjected to overnight dialysis, at 4 ºC, on a 1 L dialysis buffer (50 mM Tris-HCl pH 7.8, 300 mM NaCl), inside dialysis membranes of 15 kDa pore cut-off, loaded with DTT (4 mM) and home-made Tobacco Etch Virus (TEV) protease (10 mg) each. After the first two hours, the dialysis reservoir buffer was replaced to allow for better dialysis, and then this was left overnight under mild rotation.

3.5.4 Second affinity purification of the flaviviral proteases

In order to separate the cleaved proteases from those that were not, an additional IMAC purification was performed. The IMAC column was pre-equilibrated with a freshly prepared dialysis buffer. The flow-through, containing the proteases without the fusion was collected, quantified and concentrated before proceeding with the subsequent purification step.

3.5.5 Size exclusion chromatography (SEC) purification of the septin complexes

Prior to the size exclusion chromatography, the selected fractions were concentrated in 10 min cycles and 3500 g, using a refrigerated microcentrifuge (8 ºC), using Amicon® centrifugal filters with a 10 kDa pore cut-off.

The purified concentrated proteases were loaded onto a preparative HiLoad Superdex 75 16/600 column (GE Healthcare) pre-equilibrated with protease buffer C (20 mM HEPES

pH 7.5, 500 mM NaCl, 5% [v/v] glycerol). Samples were obtained by isocratic elution at a flux of 1.0 mL/min, and protein and nucleotide absorbance were also monitored at 280 and 254 nm, respectively. Finally, samples were quantified, analysed by SDS-PAGE, and concentrated when required, under similar conditions as described earlier for these proteins.

3.6 Analysis of the septin C-terminal domain influence on the oligomeric state, heterocomplex assembly and filament polymerization of septins

3.6.1 Size Exclusion Chromatography Coupled to Multiple Angle Light Scattering (SEC-MALS) to characterize the septin complexes

Aliquots of the proteins were applied to a size exclusion column and analyzed by HPLC on a Waters 600 Controller chromatograph. Coupled with chromatography, the miniDAWN TREOS system (Wyatt Technology) determines the mass distribution, size and composition, and the OptiLab T-rEX system (Wyatt Technology) determines the differential refractive index. The oligomeric state and polydispersity of the sample were then determined by processing the data using the ASTRA7 *software* (Wyatt Technology).

3.6.2 Preparation of Grids for Transmission Electron Microscopy (TEM)

The capacity of complex formation and polymerization of the different septin constructs was evaluated by the technique of transmission electron microscopy. Purified septin complexes were prepared using the negative staining technique (Negative Stain). In this method, the samples were prepared on copper grids with a lacey-type carbon support film covering one side and an ultra-thin carbon film coating on the other side (Ted Pella, USA). For sample adhesion, the grids were negatively charged, using the Glow Discharge procedure, performed with an easiGlow equipment (Pelco, USA).

Samples were stained by applying 3 μL of 0.75 % aqueous solution of uranyl formate to the grid containing the sample. After 30 s, the uranyl formate solution was removed with conventional filter paper. The process was repeated one more time for more intense marking. Preparation of the grids was carried out in collaboration with the PhD student Deborah Cezar Mendonça.

The dried samples were analysed by transmission electron microscopy. Data acquisition was performed both at the facilities of the National Nanotechnology Laboratory (LNNano) of the National Center for Research in Energy and Materials, using the Talos F200C - FEI microscope, or at the São Carlos Institute of Chemistry (IQSC), at the University of São Paulo, using a JEOL-2100 (JEOL), operating at 200 kV, in conditions close to the

focus (~1µm defocus) with magnification from 40,000 to 60,000 times. The images obtained were analysed using the software ImageJ (NIH, USA).

3.6.3 Evaluating the C-terminal truncations effects on heterocomplex assembly

The ability of the different truncated complexes to assemble into hexamers was evaluated using TEM. For this purpose, the sample protein concentrations were diluted to physiological concentrations (100~200 nM), using high salt concentration buffer (300 mM NaCl), preserving, therefore, the high ionic strength of the solution, thereby debilitating filament formation,[45] but not heterocomplex assembly.

3.6.4 Polymerisation assays: the effect of protein concentration on filament formation

The polymerization capacity of the different constructs was also assessed using transmission electron microscopy. Septins are able to polymerise into filaments under low ionic strength conditions (50 mM NaCl). Nevertheless, the protein concentration has been already shown to tune this polymerisation process: high septin concentration (>200 nM) have been shown to promote filament formation even at intermediate ionic strength (> 50 mM NaCl).[75]

The original samples were always at very high protein concentration (1 µM) compared to the physiological concentration (100~200 uM).[76] These samples were also purified under high salt concentration (300 mM NaCl) to hamper filament formation.

Therefore, in order to understand the protein concentration effect on filament formation, it was necessary to be very careful about the sequence of the dilutions used (the dilution of protein concentration prior to the dilution of the salt). We needed to be sure that the septin complexes were starting to polymerise under the protein concentration that we wanted to analyse, and that they were not just an artefact of filaments formed at higher protein concentration being simply diluted to this final concentration.

In order to assure this analysis was not biased by this effect, a meticulous protocol was developed to prevent filament formation under intermediate protein concentrations and low ionic strength. Firstly, the protein concentration of the samples, at high ionic strength (300 mM NaCl) was diluted. The same high salt concentration buffer was used for this first procedure, diluting the samples to intermediate concentrations, six times higher than the final protein concentration (*i.e.*, if the final protein concentration was to be 100 nM, the samples would be diluted to 600 nM initially, with high ionic strength buffer). Then, both protein and salt concentrations were diluted simultaneously to their final concentrations, six times lower

than these intermediate concentrations, achieving a low ionic strength condition (50 mM NaCl) at the desired protein concentration. Finally, the samples were incubated in ice baths for at least 30 min, and then they were applied to the TEM grids and stained, as described earlier.

3.6.5 Evaluating septin interaction with lipids via PIP Strips

In order to investigate the interaction of septins with PIPs and other related lipids, nitrocellulose membranes containing pre-immobilized lipids (PIP Strips) were incubated with septin complexes, which were later analysed using antibodies.

These PIP strips, purchased from Echelon Biosciences, were firstly blocked with TBS-T (10mM Tris-HCl, pH 7.6, 140 mM NaCl, 0.1% Tween 20) supplemented with 0.1% ovalbumin for 2 hours at 25 ºC, under constant stirring. Before incubating with septins, the strips were washed three times with TBS-T buffer for 15 minutes each time. This washing cycle was repeated after all incubation steps and before the detection. After this first washing cycle, the membranes were incubated overnight at 4 ºC, under constant shaking, with the purified septin complexes (500 nM) diluted in TBS-T supplemented with 0.5 M Dextrose (established to improve the observation of septin-lipid interactions).

Thus, after washing, the membranes were incubated with an anti-SEPT2 primary antibody purchased from Abcam (ab187654 1:1000). Following a similar washing cycle, the membrane was incubated with the secondary antibody, a rabbit anti-mouse IgG HRP-conjugated (Sigma-Aldrich) previously diluted (1:5000) in TBS-T. Both incubations last for 1 h at 25 ºC whilst stirring.

After another washing sequence, Clarity Western ECL Substrate (Bio-Rad) solution was added to the membrane case. Then following an incubation time of 2 minutes, the images were detected with ChemiDoc XRS+ (Bio-Rad) for 30 s, with a frame at every 0.5 s.

The images were finally analyzed with Image Lab 6.01 software (Bio-Rad). All 16 spots on each membrane were delimited with circles. The global background was subtracted, and the mean pixel intensity of each spot was measured. The relative intensity was calculated with reference to the blank spot (containing no immobilized lipid).

3.7 Biophysical analysis of the flaviviral proteases

3.7.1 *In vitro* protease assay

Recombinant human heterodimers SEPT2NGC-SEPT6G (more stable than the SEPT2NGC homodimer) were purified following similar protocols described by Rosa *et al.*[68] for SEPT2G-SEPT6G. Recombinant WT NS2B3 from ZIKV and YFV were purified following the same protocol as stated above for their inactive mutants.

The septins (at 15 μM) and the proteases (at 1.5 and 0.15 μM, respectively 1:10 and 1:100 enzyme/substrate ratio) were incubated in protease assay buffer (25 mM Tris-HCl pH8.5, 10% Glycerol, 0.01% Triton-X 100) at 37 ºC for 24 h. Samples, collected after 30 min, 1 h, 2 h, and 24 h, were then analyzed by SDS-PAGE.

To further confirm the cleavage, some SDS-PAGE gels were further analysed by western blotting employing an anti-SEPT2 antibody purchased from Abcam (ab187654 1:1000). To ultimately confirm these cleavage bands corresponded to SEPT2, they were extracted from the gel and a mass-spectrometer analysis was performed.

3.7.2 Quantification of proteolytic activity by fluorescent assays

To prove the effectiveness of site-directed mutations in promoting the inactivation of proteases, the proteolytic activity of mutant proteases was measured using a fluorescence assay using the fluorescent substrate Benzoyl-Norleucine-Lysine-Lysine-Arginine-7-amido-4-methylcoumarin (Bz-Nle-Lys-Lys-Arg-AMC; Genscript). For each protease, triplicates were performed monitoring the fluorescence signal of the AMC release at 460 nm with the excitation wavelength of 360 nm.

3.7.3 Oligomeric state analysis of the flaviviral proteases (SEC-MALS)

The oligomeric state plays a central role in regulating protease activities, as many proteases show enhanced activity when in specific oligomeric states.[77] Therefore, we used SEC-MALS analysis to evaluate the oligomeric state(s) of each flaviviral protease, and also to analyse the influence of the mutations introduced in these proteins.

3.7.4 Co-purification of septins and inactive proteases

The wild-type hexameric complex (SEPT267 NGC) and the SEPT2NGC-SEPT6G dimer, whose sequences contain the ZIKV protease recognition and cleavage site, were used in the co-purification assays with the inactive proteases. Thus, the purified septin complexes (containing a His-tag) were used as baits, immobilized on a nickel affinity column. The

inactive ZIKV NS2B3 protease (after cleavage of the polyhistidine tag) was loaded into the column as prey, followed by washing and elution of immobilized proteins.

Tests were performed at different ionic strengths (75, 150 and 300 mM NaCl) to assess the interaction between these proteins in more detail. These analyses were observed and compared with control samples (without septins) by SDS-PAGE.

3.7.5 Size Exclusion Chromatography Coupled to Multiple Angle Light Scattering (SEC-MALS) of septin and proteases complexes

In order to analyse the possible complexes obtained through the interaction of septins with inactive proteases, these proteins were previously incubated at a 1:1 ratio (mol/mol) for at least 30 min. Aliquots of the proteins were then applied to the SEC-MALS, as previously described.

3.7.6 Crystallisation Assays with peptides

The purified mutant proteases were concentrated (~20-30 mg/mL) and used for crystallization assays by the sitting drop vapour diffusion method, using commercial kits, such as PACT Premier™ (Molecular Dimension) and Index™ (Hampton Research); and the Gryphon Crystallization Robot (Art Robbins Instruments), with the technical support of Dr Humberto D'Muniz Pereira. The plates were then incubated in ROCKIMAGER® 1000 (Formulatrix) for crystal growth at 18 ºC. Each well was imaged after 0, 1, 2, 3, 5, 8, 13, 21, 34 and 55 days. A machine learning algorithm (provided with the equipment) selected the most favourable conditions, later manually inspected and imaged with UV light.

A peptide mimicking the SEPT2 cleavage site ($_{303}$RLKRGGRK$_{310}$) was synthesised (Genscript) and used for co-crystallisation assays. It was incubated with the proteases prior to loading onto the crystallization plates. The ratio between the protease and the peptide used was respectively 1:10 (mol/mol). In some crystallization plates, seeds of the wild-type ZIKV NS2B3 protease crystal (grown at the CIBFar), previously diluted five times in the protease buffer, were added to the drops (0.5 nL per drop), aiming for better chances of nucleation and crystal formation.

4 RESULTS: STRUCTURAL AND FUNCTIONAL RELEVANCE OF THE C-TERMINAL DOMAIN IN SEPTINS

4.1 Alignments and analyses of the sequential identities of the N, G and C domains

4.1.1 Alignment of each individual domain

Sequence alignments, combined with structural information, were successfully useful in identifying important motifs and conserved residues in the G domain, involved in the selectivity and stability of the septin interfaces within each of the four human septin groups.[68]

Even though the other two domains possess intrinsically higher sequence variability and less structural information is available, we were able to produce alignments and to annotate their sequence motifs and characteristic residues. Additionally, we also extended here the previously published alignments of the N- and G-domain,[68,78] which includes only the most common isoforms of each gene, to all the 44 humans septin isoforms in UniProt. The results are displayed in Appendix.

4.1.2 Identity between subgroup members in each domain:

Each alignment produced was employed to compute the sequence identity matrixes between the genes. The results were then averaged to compute mean percentage identity within each of the four groups and amongst all septins. The results are displayed in Figure 4.1. The division of the 13 human septin genes into the four groups is given in Figure 1.5.

It can be easily seen (Figure 4.1) that the sequence identity is higher amongst all groups in their G-domain, being around 55% amongst all septins (grey bar) and ranging from 65% to nearly 100% within each septin group (coloured bars).

On the other hand, the identity tends to be lower in the flanking domains N and C. For the N-terminal domain, the percentage identity overall is almost 35% amongst all septins, and for the C-terminal, the most variable domain between septins, it is less than 30%. This pattern could be anticipated, since both the N- and C- domains possess less structured regions compared to the G-domain.

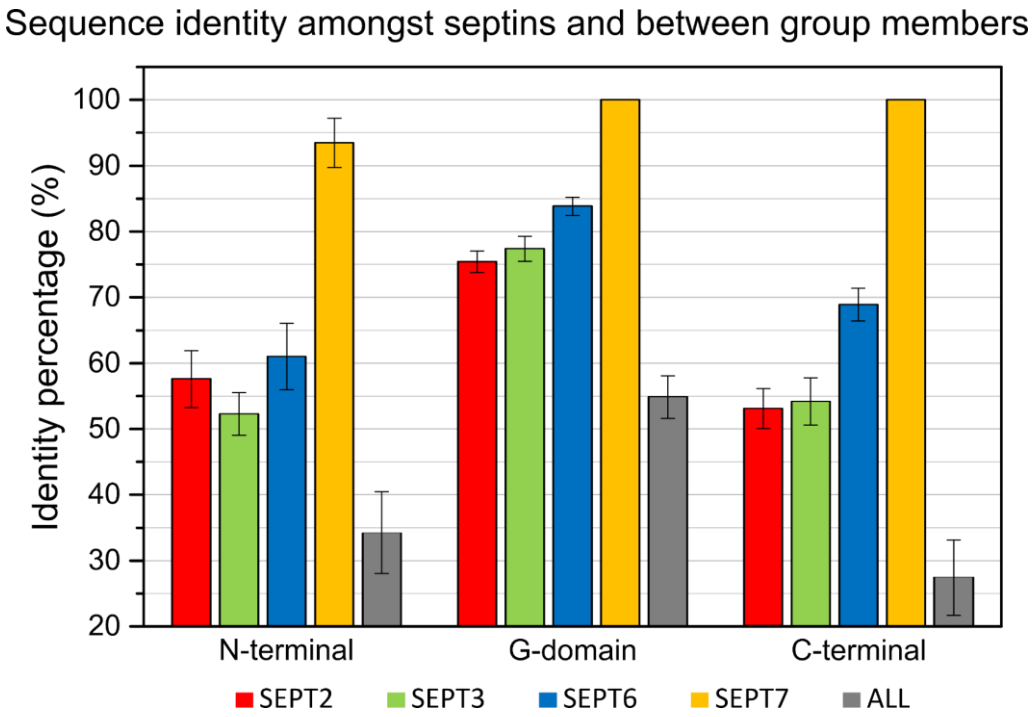

Figure 4.1 – **Sequence identity, of each domain, between members of the same human septin group.** SEPT2, SEPT3, SETPT6 and SEPT7 groups are represented in the bars coloured, respectively, in red, green, blue, and yellow. The grey bars represent the sequence identity, including all septins isoforms. The standard error estimated by Bootstrap (1000 replications) is displayed in each bar. See Figure 1.5 for the members of each of the four human septin groups.

Source: By the author.

By examining the conservation inside each septin group, it can be seen, *e.g.*, that the SEPT2 group sequence identity pattern (red) is similar to the overall trend, with higher sequence similarity in the G-domain (75%), which is decreased within the N-terminal domain (58%). As with the overall comparison, the C-terminal domain possesses the lowest sequence identity in this group (54%). Conversely, for the SEPT6 group, the trend is quite different. In this case, it is the identity within the N-terminal domain that has the lowest value (61%), which rises substantially to more than 80% (84%) within the G-domain. This is due to the higher conservation of many residues related to the lack of catalytic activity, which is a unique characteristic of this group.[68] The sequence identity decreases to 69% for the C-terminal domain. This conservation might be related to the long coiled coil region found in this domain for this group.[69] Finally, the SEPT3 group septins show a similar trend compared to the other groups, with the G-domain being the most conserved (77%).

Inspecting the C-terminal domain, which surprisingly is the most variable domain overall, the most variable group (ignoring the SEPT3 group, whose members possess very

short C-termini and are not predicted to possess coiled coil domains or other structured regions) is the SEPT2 group. This is of greatest interest in the context of the present study.

Scrutinizing the alignments of this domain and identities of these group members (see Appendix 4 and Appendix 7), we observe that the septin member with the most prominent differences (lowest identities) between all SEPT2 members is SEPT2. Firstly, observing the entire domain and highlighting the region predicted to form coiled coils[69] in this septin (Figure 4.2), it is readily noted that the linker connecting the end of the structured region of the G-domain and the beginning of the coiled coil itself is very short (less than ten residues) in this septin compared to others in the same group (20-30 residues).

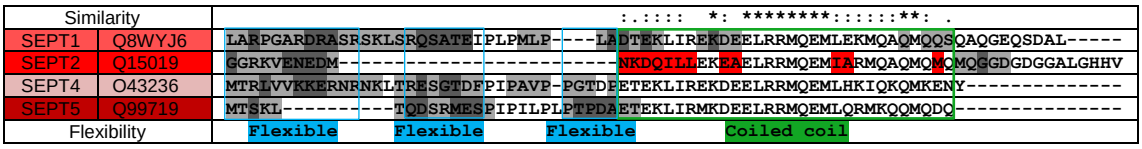

Figure 4.2 – **Alignment of the C-terminal domain sequences from the canonical isoforms of the septins from the SEPT2 group.** The alignment shows the presence of flexible regions (blue boxes) predicted before the structured coiled coil region (green box), a feature observed for all the members of the SEPT2 group. The conservation of each position is displayed in a ruler above all sequences ("*" indicates total conservation, ":" indicates high conservation and, "." indicates partial conservation). The degree of flexibility for each residue in the four sequences was calculated using PredyFlex, [79] and is represented by shades of grey (blank for rigid, light grey for intermediate and dark grey for flexible). It can be seen that there are fewer residues in this flexible region for SEPT2 compared to the other members from the same group. Another feature observed is the sequence divergency of SEPT2 (compared to these septins) in the initial residues inside of the structured coiled coil region (highlighted in red).

Source: By the author.

Despite the presence of some flexible residues (glycines), AlphaFold predictions[61] of this region (in NC-interface homodimers) show models containing a single continuous helix protruding from the final helix of the G-domain (the α6 helix) for SEPT2 forming a parallel coiled coil (with a helix from its neighbour), but not for the other group members, which displayed the presence of unstructured loops corresponding to this flexible linker. In some specific environments, this might occasionally favour the formation of a parallel coiled coil compared to the antiparallel form.[69] Additionally, changes in some residues (highlighted in red in Figure 4.2) near this coiled coil region (which are "conserved" within other group members but not in SEPT2) might also shift the equilibrium towards a specific form of interaction not observed in other septins, conferring specific functions to the isoforms from the SEPT2.[69]

Further studies might be fruitful in exploring and addressing the particularities of these variable regions and understanding the specificities of each gene (and even each isoform), ultimately verifying the extent of "Kinoshita's Rule" of exchangeability between subgroup members.[58]

4.2 Septin complexes production: from cloning to purification

4.2.1 Production of truncated constructs lacking the C-terminal domain (NG)

In order to produce truncated complexes to investigate the roles of the C-terminal domain, the NG domain regions were amplified by PCR and the products of these reactions are shown in Figure 4.3.

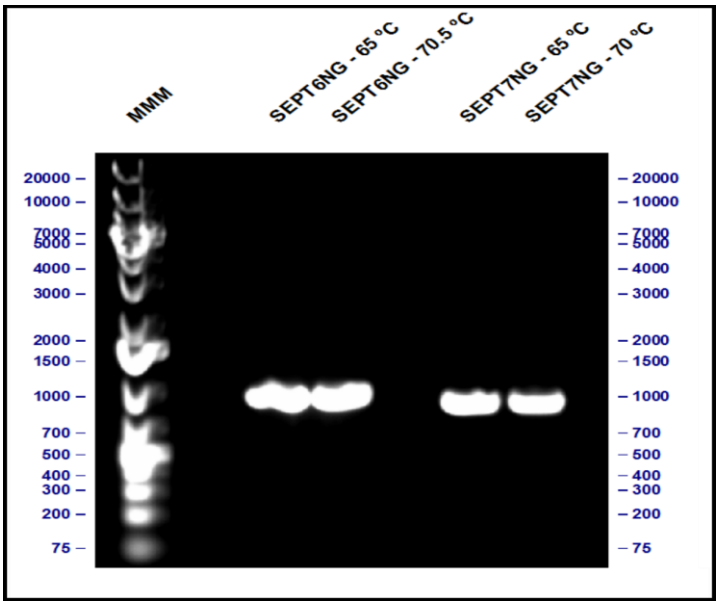

Figure 4.3 – **PCR products from the amplification of the NG domains of septins 6 and 7.** MMM – Molecular mass marker (base pairs). The temperatures indicated next to the names represent the annealing temperatures used during the amplification cycles. It can be seen that the bands were successfully amplified.
Source: By the author.

After purifying the bands of interest, we first cloned them into the replication vectors and then subcloned them into expression vectors. Three different plasmids were used. The first expression plasmid was pETDuet, digested with *BamH*I and *Pst*I enzymes, to insert the SEPT7NG sequence. The other two plasmids were plasmids pRSFDuet, digested both with *Nco*I and *Hind*III enzymes, which were used to perform the subcloning of SEPT6NG. The

main difference between the two pRSFDuet plasmids was the presence of a SEPT2NG construct in one, while the other had a full-length construct for this septin (SEPT2NGC).

Finally, for the positive clones, nucleotide sequencing analysis was performed to confirm the fidelity and integrity of the sequences. It was verified that these regions corresponded to the expected sequences. In this regard, three new plasmids with these constructs became available: pETDuet-SEPT7NG, pRSFDuet-SEPT2NGC/SEPT6NG and pRSFDuet-SEPT2NG/SEPT6NG.

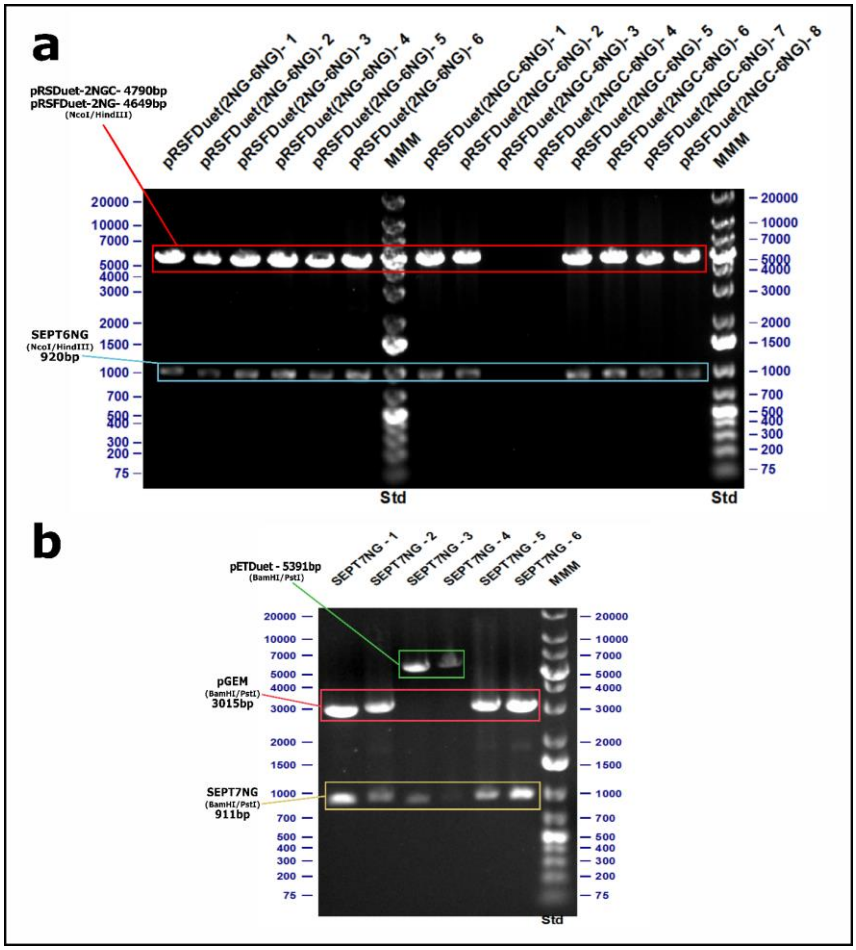

Figure 4.4 – **Restriction analyses of NG constructs (SEPT2, SEPT6, SEPT7) in the expression plasmids.** In a, restriction analyses for SEPT6NG clones inserted into pRSFDuet plasmids containing SEPT2NG and SEPT2NGC. MMM-Molecular Mass Marker (base pairs). The insertion success can be noted for the most clones (only clones 3 and 4 of the pRSFDuet construction (2NGC-6NG) did not show bands at the expected height). In b, restriction analyses of NG constructs (SEPT7) in pETDuet expression plasmids. MMM-Molecular Mass Marker (base pairs). The insertion success can be noticed only for clones 3 and 4, whose bands after digestion actually correspond to the expected sizes for the insert and the expression vector (pETDuet).

Source: By the author.

4.2.2 The rationale behind the choice of truncated complexes to be purified and studied

To study the importance of the C-terminal domains of each septin group in the structural organization of the hexamers and their influence on the polymerization of these hexamers into filaments, we used the designed constructs for assembling complexes in the absence of this specific region.

The septin 3 group is known to possess a very short C-terminal domain, and it has been recently speculated to have little influence on septin filament formation.[80] Since this group has already been analysed and seemed to exhibit only minor effects on this process, we restricted our analyses to the C-terminals of the other three groups (SEPT2, SEPT6, SEPT7). Since the SEPT3 group members only participate in the formation of octamers, this meant that our study was conveniently limited to the study of hexamers composed of SEPT2, SEPT6 and SEPT7.

It is noteworthy that, as the C-terminal domains of septins 6 and 7 interact in solution, [55] we decided to start the study by evaluating the influence of these regions together, truncating them simultaneously (reducing the number of hexameric combinations from eight to four). In addition, this was expected to reduce the chances of having significant instabilities, which might happen if, for example, one of these coiled coil regions was absent from its interaction partner.

On the other hand, the influence of the C-terminal domain of septin 2 (and the ZIKV protease cleavage) was evaluated individually, as it is predicted to interact with an identical counterpart from another septin 2 during filament polymerization.

Thus, we started the purification of hexameric complexes containing the full-length septins (2NGC-6NGC-7NGC), to use as a wild-type (WT) control. The other complexes that were evaluated were 2NG-6NGC-7NGC (also named 2ΔC), 2NGC-6NG-7NG (67ΔC) and finally removing all C-terminals, 2NG-6NG-7NG (ΔC).

4.2.3 Purification and analysis of the 2NGC-6NGC-7NGC complex

Firstly, it was possible to observe that the proteins eluted in equimolar proportions (1:1:1) on affinity purification (Figure 4.5, panel b). SEPT7NGC and SEPT6NGC have similar molecular masses and overlapping bands on the gel. The lowest molecular mass band refers to SEPT2NGC. An intermediate band (between the SEPT6NGC/SEPT7NGC band and the SEPT2NGC) can also be seen for some fractions (labelled His-SEPT7NGc), which

corresponds to cleavage within the C-terminal region of septin 7, widely described in the literature,[43,60,81] due to proteases from the expression strain.

Fractions without contamination with chaperones (DnaK) could be separated from those that were co-eluted with them during this step. These chaperones (highlighted in the purple box in Figure 4.5, panel b) are generally co-expressed with septins, interacting promiscuously with them in order to help their translation and increase their folding efficiency.[82]

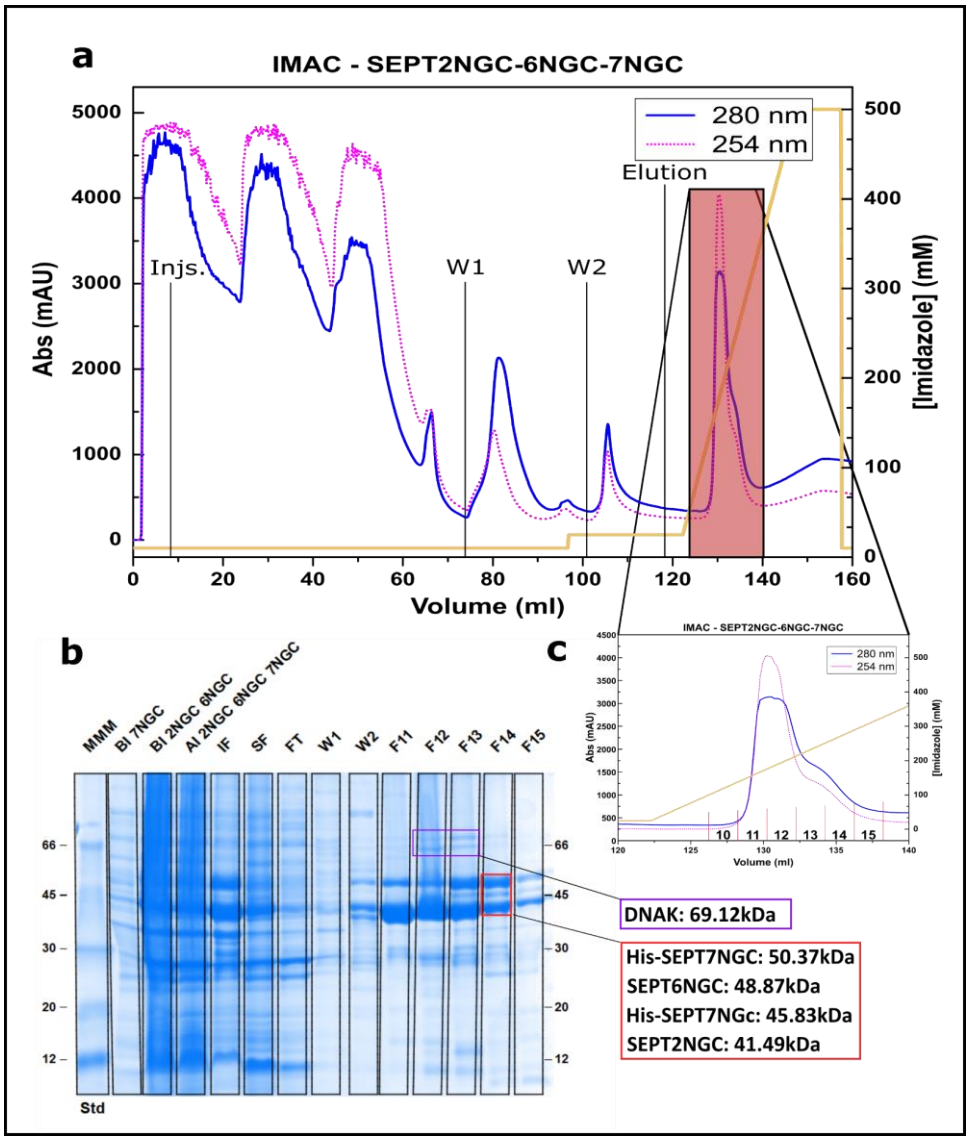

Figure 4.5 – **Affinity chromatography purification of the 2NGC-6NGC-7NGC septin complex.** In a, IMAC chromatogram shows peaks of injection (Injs.), 1st wash (W1), 2nd wash (W2) and elution (Elution). In b, SDS-PAGE shows fractions representing the main steps of the affinity chromatography (molecular mass marker - MMM, culture samples before - BI and after induction with IPTG - AI, insoluble fraction - IF, soluble fraction - SF, unbound flow-through - FT, 1st wash - W1, 2nd wash - W2, fractions along the elution peak - F11 to F15). In c, it is possible to observe in detail the elution region of the affinity chromatography, showing the positions of the fractions applied in the SDS-PAGE.

Source: By the author.

It is possible to verify by SDS-PAGE (Figure 4.5, panel b) that the fractions towards the end of the elution peak are those with fewer contaminants. These fractions were applied in the size exclusion chromatography column to evaluate their oligomeric states and remove other contaminants (Figure 4.6).

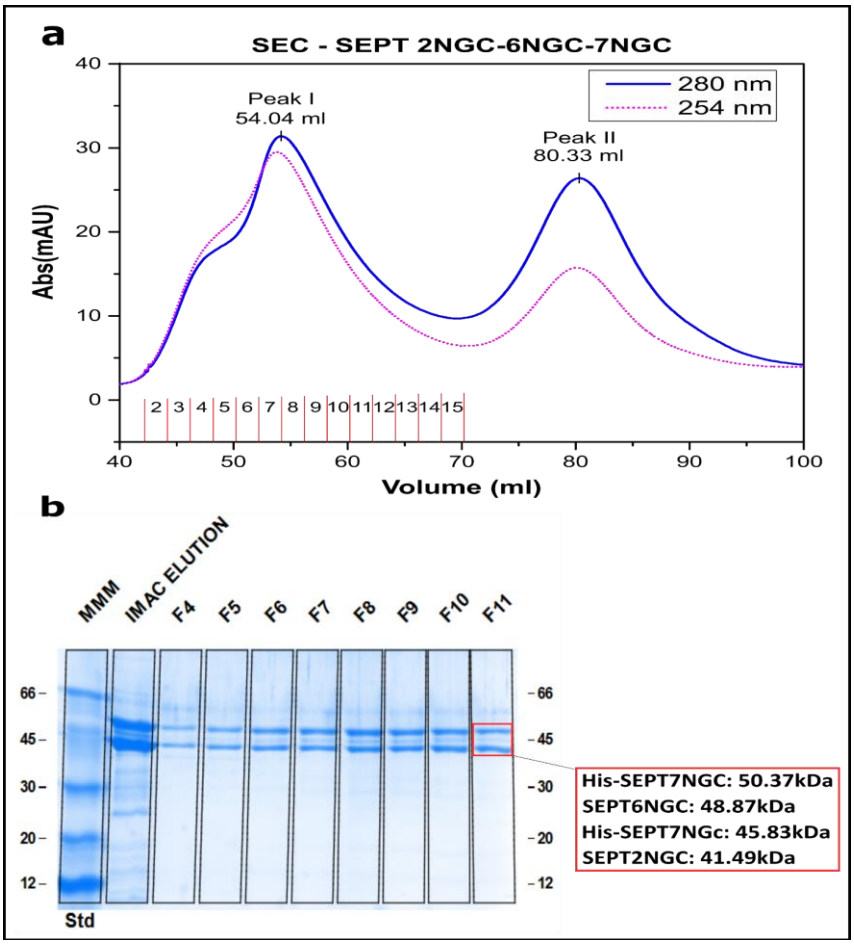

Figure 4.6 – **Size exclusion chromatography purification of the 2NGC-6NGC-7NGC septin complex.** In a, the SEC chromatogram highlights the elution peak regions of the septins hexameric complexes (Peak I) and of lower molecular weight contaminants (Peak II) and the respective collected fractions. In b, SDS-PAGE shows the fractions representing the elution peak (molecular mass marker - MMM, sample injected onto the column - IMAC Elution, fractions along the elution peak - F4 to F11).

Source: By the author.

Two elution peaks appeared on the SEC chromatogram (Figure 4.6, panel a). The first peak (Peak I) contains the full-length septins, as hexamers or larger aggregates (on the leftmost part of this peak, a shoulder can be observed, Figure 4.6, panel a). The second peak (Peak II) contains septins with lower oligomeric states (tetramers, trimers, dimers, monomers) and may contain other contaminants.

After separating the septins and their contaminants, visual inspection of the bands in the gel suggests an equimolar elution of the septin in the septin complex (Figure 4.6). Again,

the purest fractions lie in the rightmost part of the peak. These fractions were selected, concentrated and used for the following experiments (SEC-MALS, EM, PIP-Strip). This elution trend and sample selection method were shown to be similar to the all complexes purified, as it will be described in more detail for each one of the truncated complexes below.

4.2.4 Purification and analysis of the 2NG-6NGC-7NGC complex

In order to assess the effect of the loss of the C-terminal domain of septin 2, which is cleaved by the ZIKV protease, we produced a complex mimicking this loss.

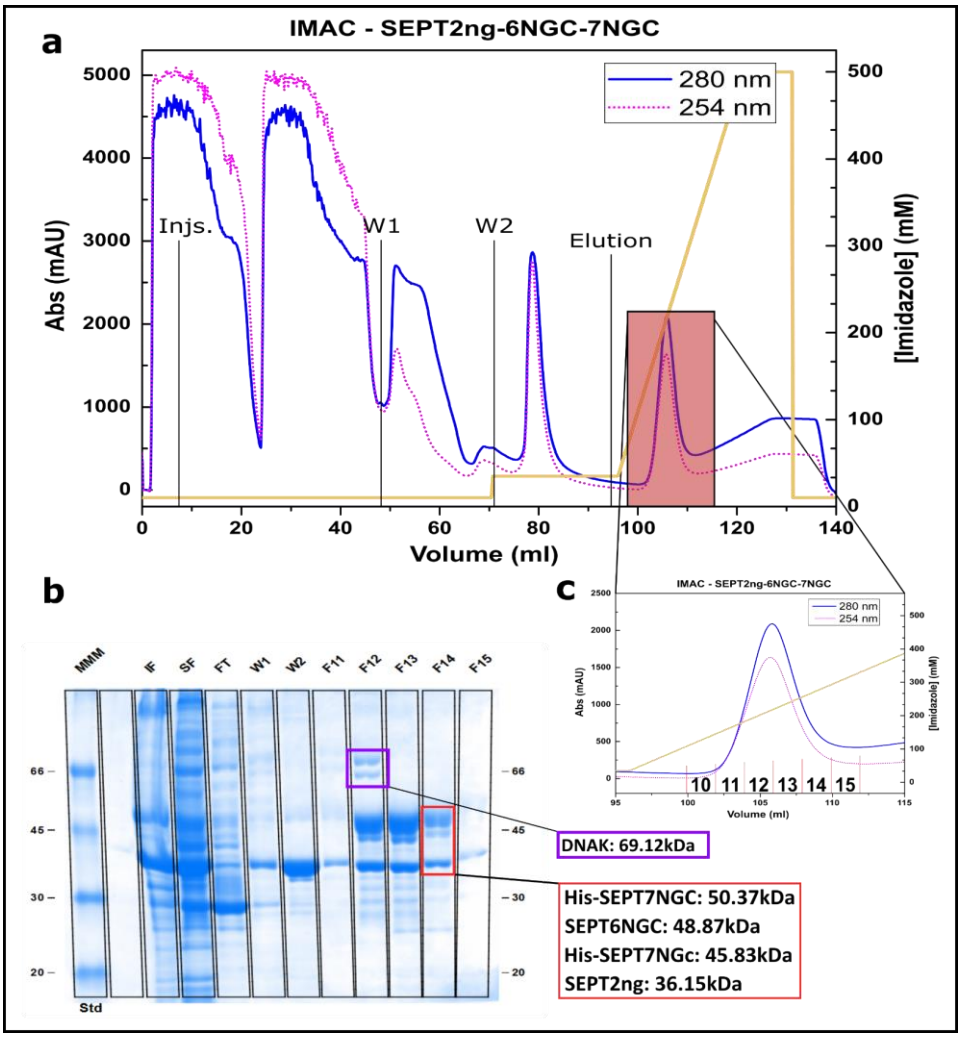

Figure 4.7 – **Affinity chromatography purification of the 2NG-6NGC-7NGC septin complex.** In **a**, IMAC chromatogram shows peaks of injection (Injs.), 1st wash (W1), 2nd wash (W2) and elution (Elution). In **b**, SDS-PAGE shows the fractions representing the main steps of affinity chromatography (molecular mass marker - MMM, insoluble fraction - IF, soluble fraction - SF, unbound - FT, wash 1 - W1, wash 2 - W2, fractions along the elution peak – F11 to F15)**.** In **c**, it is possible to observe in detail the elution region of the IMAC chromatogram showing the positions of the fractions applied to the SDS-PAGE.

Source: By the author.

By observing the shift in the position of the band of this truncated septin 2 (SEPT2NG) to a position of lower molecular mass in the SDS-PAGE analysis (comparing this SDS-PAGE shown in Figure 4.7 - panel b, to the full-length construct shown in Figure 4.5 - panel b), it was possible to validate the correct truncation in the SEPT2 C-terminal and, thus, the production of SEPT2NG.

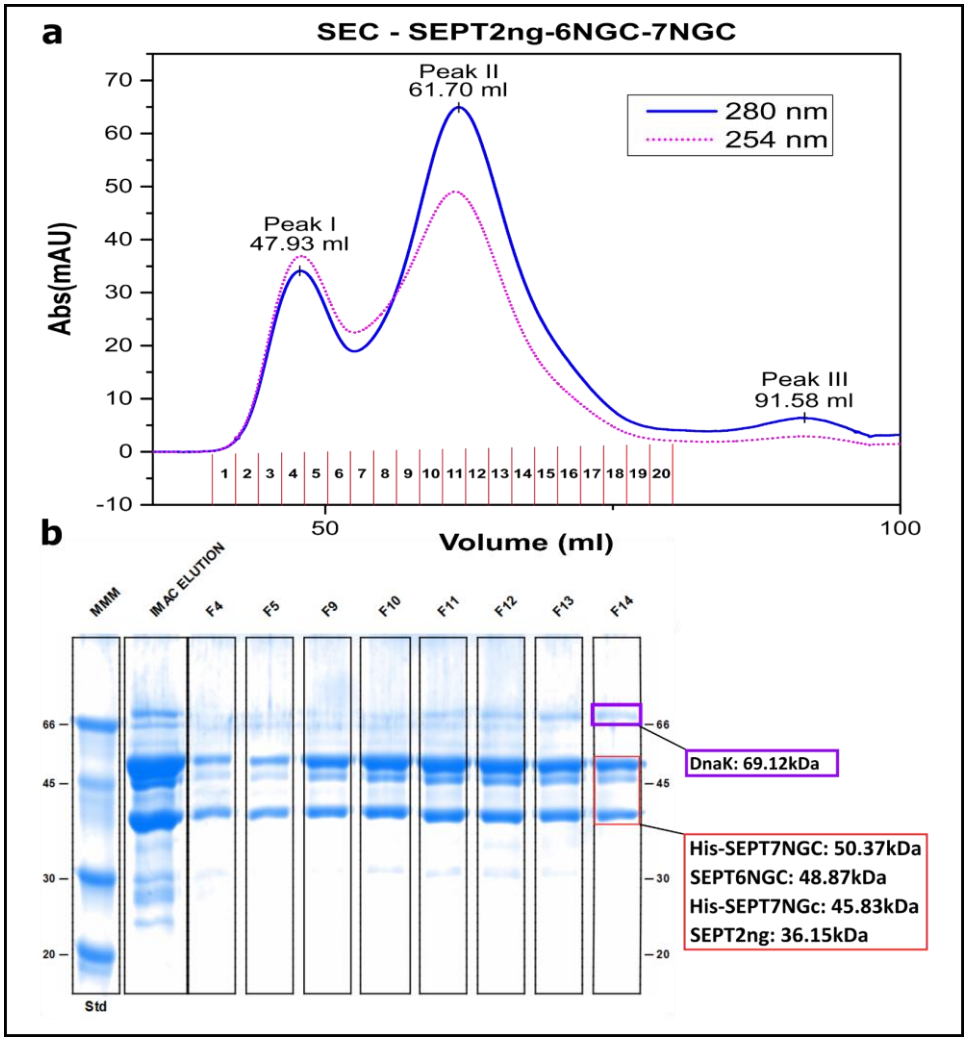

Figure 4.8 – **Size exclusion chromatography purification of the 2NG-6NGC-7NGC septin complex.** In **a**, SEC chromatogram highlights the elution peak regions of aggregates and higher oligomeric states (Peak I), hexameric septin complexes (Peak II) and lower molecular weight contaminants (Peak III) and fractions respective to each peak. In **b**, SDS-PAGE showing the fractions representing the elution peak (molecular mass marker - MMM, sample injected onto the column - IMAC Elution, fractions along the elution peak - F4 to F14).

Source: By the author.

In the SEC chromatogram for this truncated complex (Figure 4.8, panel a), an additional elution peak (Peak I) appeared before the hexameric peak (Peak II), indicating that there may be greater instability of this complex in solution, due to the removal of the C-

terminal domain of the septin 2, leading to the formation of aggregates. Alternatively, this could be just a better separation of the peak I into two different peaks, compared to the WT, whose peak I possess a shoulder. This better separation of the peaks might be a consequence of an increase in the retention time of the hexameric peak (Peak II) compared to the respective peak in the wild type complex (Peak I - Figure 4.5, panel a). This was already expected since the complex is slightly smaller in mass and volume compared to the WT.

4.2.5 Purification and analysis of the 2NGC-6NG-7NG complex

A purification to assess the importance of the C-terminal domains from the septins 6 and 7 was also performed by removing these domains concomitantly.

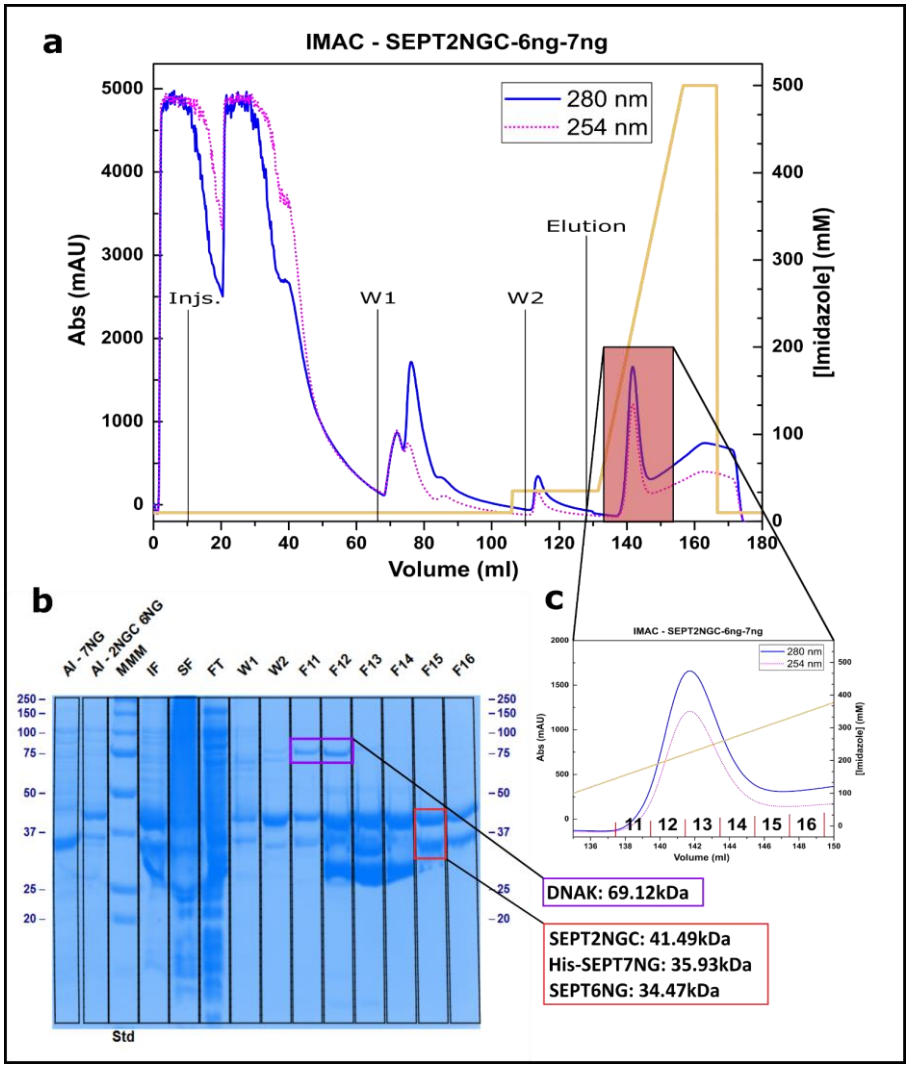

Figure 4.9 – **Affinity chromatography purification of the 2NGC-6NG-7NG septin complex.** In **a**, IMAC chromatogram shows peaks of injection (Injs.), 1st wash (W1), 2nd wash (W2) and elution (Elution). In **b**, SDS-PAGE shows fractions representing the main steps of affinity chromatography (molecular mass marker - MMM, culture medium samples after induction with IPTG - AI, insoluble fraction - IF, soluble fraction - SF, unbound - FT, wash 1 - W1, wash 2 - W2, fractions along the elution peak - F11 to F16). In **c**, it is possible to observe in detail the elution region of the affinity chromatogram showing the positions of the fractions applied in the SDS -PAGE

Source: By the author.

In accordance with what was expected, the SDS-PAGE bands for the SEPT6NG and the SEPT7NG (Figure 4.9, panel b) also showed changes in the molecular masses compared to the full-length protein bands on the WT complex (Figure 4.6, panel b). Despite these changes, the purest fractions, applied on SEC, were found at the rightmost part of the peak (F13 to F16 in Figure 4.9, panel b).

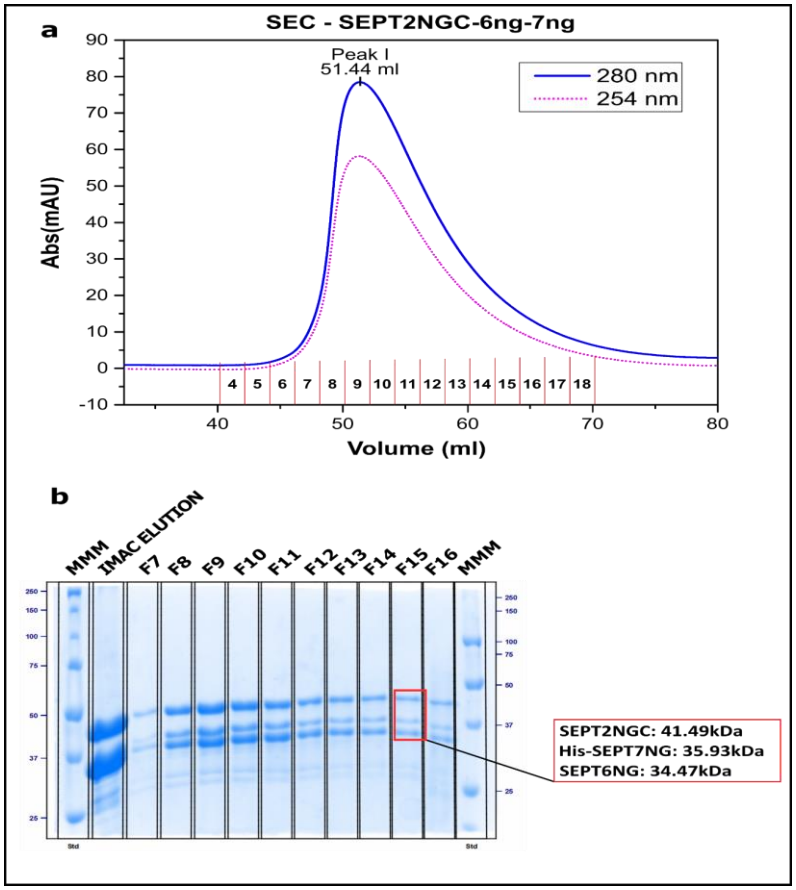

Figure 4.10 – **Size exclusion chromatography purification of the 2NGC-6NG-7NG septin complex.** In **a**, SEC chromatogram highlights the elution peak regions of the hexameric septin complexes (Peak I) and fractions respective to each peak. In **b**, SDS-PAGE shows the fractions representing the elution peak (molecular mass marker - MMM, sample injected onto the column - IMAC Elution, fractions along the elution peak – F7 to F16).

Source: By the author.

Different from what was observed in the SEC chromatograms from the previous complexes (panel a, in Figure 4.6 and Figure 4.8), when we analyse the SEC elution profile for this complex (Figure 4.10, panel a), it is clear to see that the truncation of the C-termini from SEPT6 and SEPT7 led to a single peak with a shorter retention time, earlier than expected from the expected mass of the hexamer, and with an extended tail. This may indicate greater instability and the formation of larger oligomeric states and aggregates. Maybe, a possible explanation for this is that these truncations may lead to more promiscuous interactions (probably some interactions between different hexamers), suggesting that the C-termini of SEPT6 and SEPT7 might prevent these lateral contacts, helping stabilise isolated hexameric complexes. However, it is still too early to confirm this, and more studies need to be performed to understand and better explain the phenomenon. Again, the fractions used for

the next experiments were selected from the rightmost part of the peak (F13 to F16 in Figure 4.10), aiming to reduce the influence of these larger aggregates into the following analyses.

4.2.6 Purification and analysis of the 2NG-6NG-7NG complex

Finally, the C-terminal domains of all septins were removed in order to assess whether the hexameric complex was able to assemble correctly and also to polymerize. For this, the purification of this complex was carried out like the previous ones (Figure 4.11).

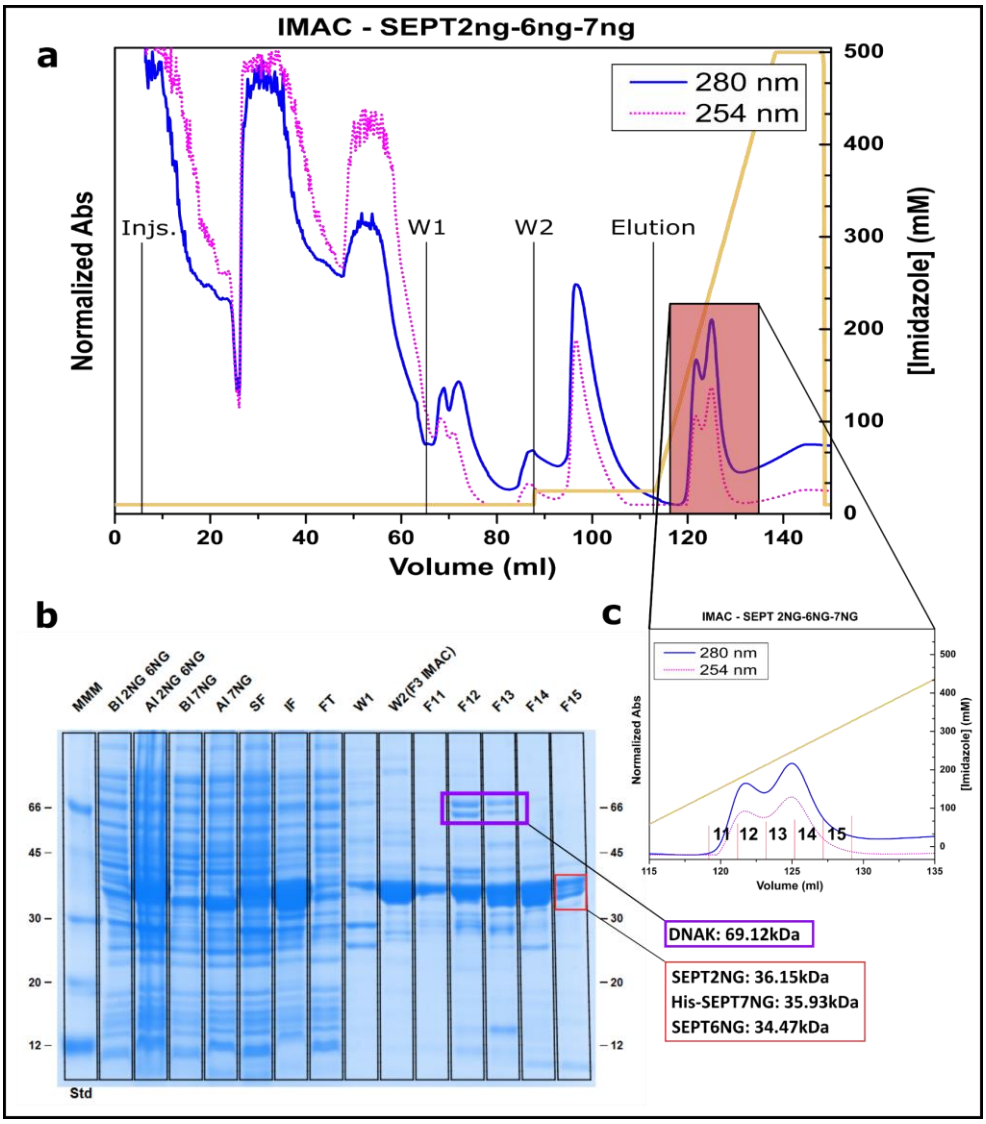

Figure 4.11 – **Affinity chromatography purification of the 2NG-6NG-7NG septin complex.** In **a**, IMAC chromatogram shows peaks of injection (Injs.), 1st wash (W1), 2nd wash (W2) and elution (Elution). In **b**, SDS-PAGE showing fractions representing the main steps of affinity chromatography (molecular mass marker – MMM, culture medium samples before induction with IPTG – BI and after – AI, insoluble fraction – IF, soluble fraction – SF, unbound – FT, wash 1 – W1, wash 2 – W2, fractions along the elution peak – F11 to F15). In **c**, it is possible to observe in detail the elution region of the affinity chromatogram showing the positions of the fractions applied in the SDS-PAGE

Source: By the author.

Again, it is possible to observe from the SDS-PAGE (Figure 4.11, panel b) that the purest and equimolar fractions are seen at the right ends of the elution peak. Furthermore, it can be seen that the bands of interest appear much closer to each other, due to the proximity of their molecular masses, also indicating the success in making these constructs (Figure 4.11, panel b).

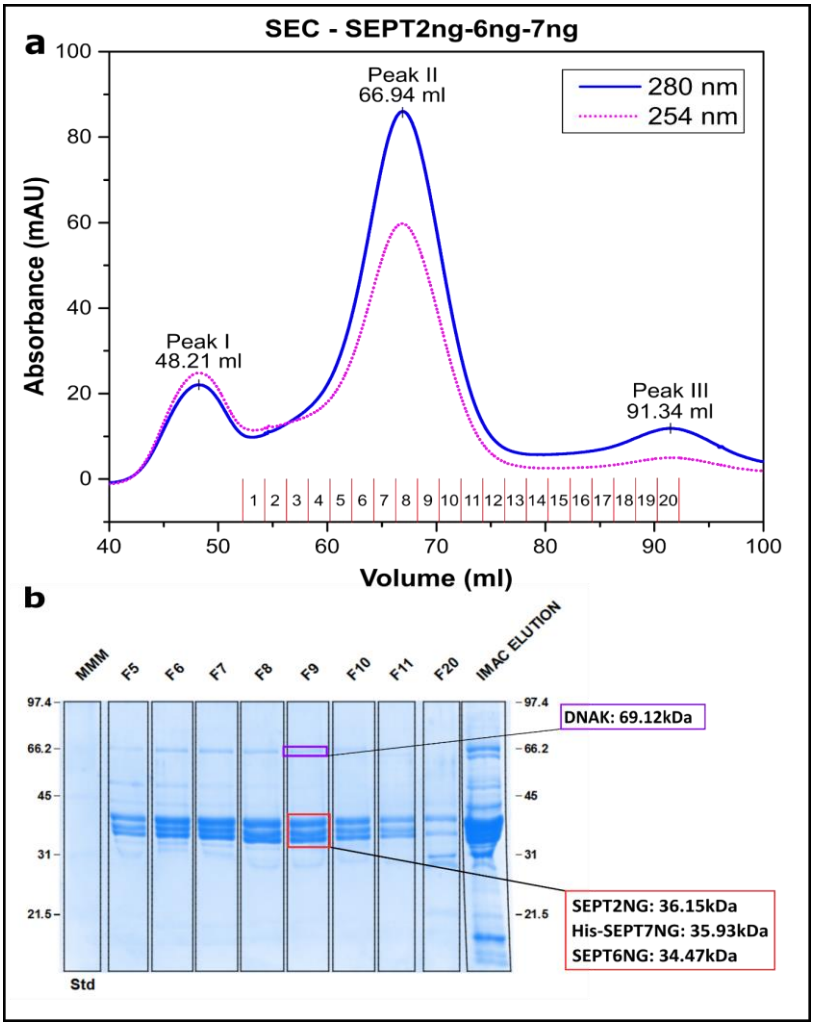

Figure 4.12 – **Size exclusion chromatography purification of the 2NG-6NG-7NG septin complex.** In **a**, SEC chromatogram, highlighting the region referring to the elution peaks of aggregates and higher oligomeric states (Peak I), hexameric septin complexes (Peak II) and lower molecular weight contaminants (Peak III) and fractions respective ones. In **b**, SDS-PAGE shows the fractions representing the elution peak (molecular mass marker - MMM, fractions along the elution peak - F5 to F20 and the sample injected onto the column - IMAC Elution).

Source: By the author.

It can be identified by the SDS-PAGE (Figure 4.12, panel b) that the septin bands, corresponding to the subunits in the hexameric complex, eluted apparently in equimolar

proportions, with a low degree of contaminants. In addition, the elution peak in size exclusion chromatography (Peak II, Figure 4.12, panel a) was the one with the longest retention time, as expected, due to the reduced mass of the complex when compared to the previous.

4.3 Analysing the influence of the C-terminal domains on the oligomeric state and the complex self-assembly (in high ionic strength conditions)

After the purification of the different complexes and selection of the best samples (the rightmost part of the elution peak for the hexamer in the SEC of each one of the complexes), we proceeded with the biophysical characterization of these complexes in order to assess the importance of the C-terminal regions of each of the groups for the formation of hexameric complexes, both by analysing the oligomeric states and molecular weight by SEC-MALS, as well as the morphological analysis of these complexes from the preparation of grids by negative staining for observation by transmission electron microscopy.

It is important to note that these tests were performed under a condition of high ionic strength (300mM NaCl), expected to disturb the stability of the NC interfaces between septins 2, required for polymerization and formation of larger oligomeric states in solution.[45]

4.3.1 Analysis of molecular masses of complexes by SEC-MALS

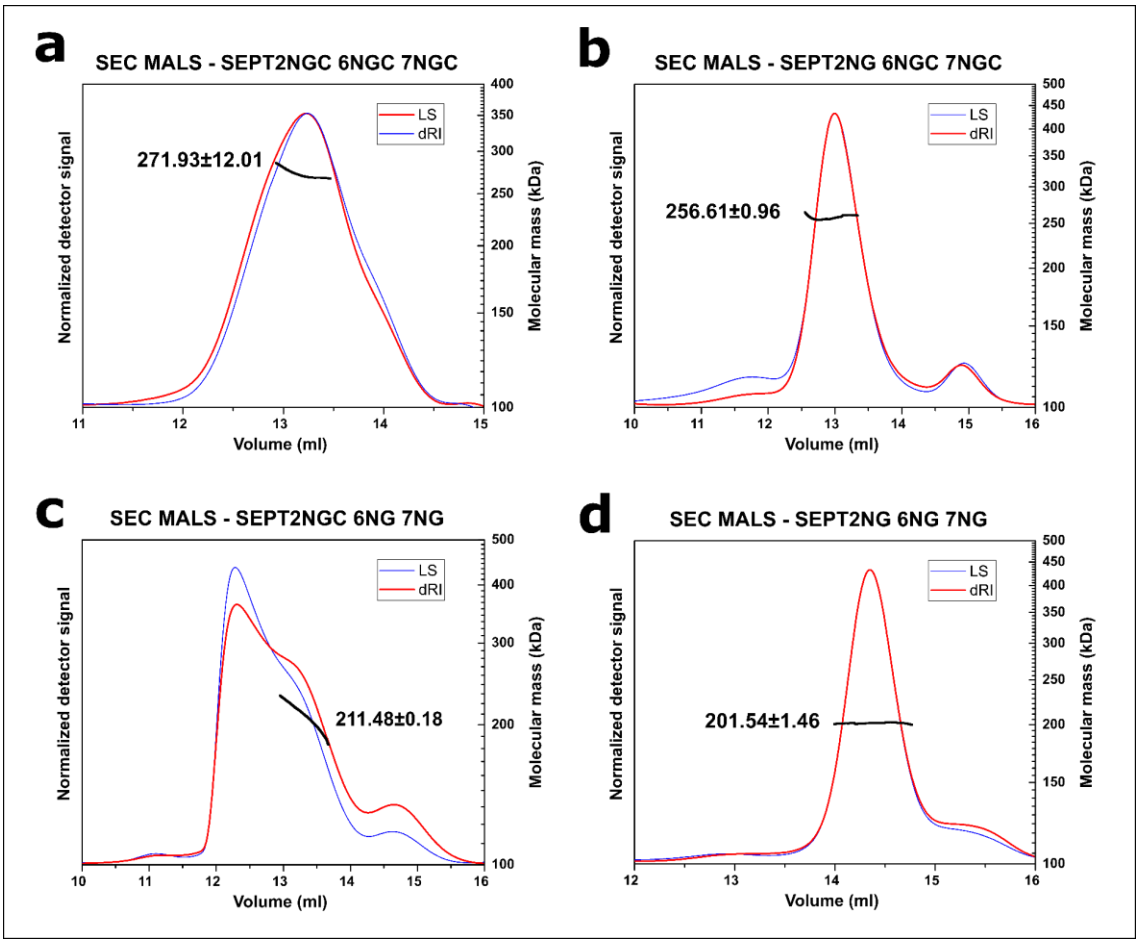

Figure 4.13 – **SEC-MALS profiles of full-length and truncated septin complexes.** In **a**, SEPT 2NGC 6NGC 7NGC complex. In **b**, SEPT 2NG 6NGC 7NGC complex. In **c**, SEPT 2NGC 6NG 7NG complex. In **d**, SEPT 2NG 6NG 7NG complex. Average values for molecular masses in kDa are shown alongside the peaks.

Source: By the author.

Based on analysis of the masses found by SEC-MALS, shown in Figure 4.13 and summarized in Table 4.1, it is possible to verify a slight difference in the expected (calculated from the sequence) and measured molecular mass values (~10kDa). This is due to problems in the sensitivity of one of the three detectors (narrow-angle), responsible for the sensitivity of molecules with high molecular mass (complexes). In addition, the presence of other peaks near the peak related to the complexes can also be noted (*e.g.*, Figure 4.13, panels b and c), which makes it difficult to determine the correct baseline, thus interfering with the correct determination of the baseline. The most difficult SEC-MALS elution profile to analyse was the 67ΔC (Figure 4.13, panel c), in which the presence of many peaks (possibly some

aggregates, as seen in the SEC Figure 4.10) may have possibly affected the measurement and determination of the correct mass.

Table 4.1 – Molecular masses of septin complexes.

Molecular Masses	**SEPT 2NGC 6NGC 7NGC**	**SEPT 2NG 6NGC 7NGC**	**SEPT 2NGC 6NG 7NG**	**SEPT 2NG 6NG 7NG**
Calculated *ExPASy* (kDa)	281.37	270.70	223.67	213.02
Measured SEC-MALS (kDa)	271.93±12	256.61±0.96	211.48±0.18	201.54±1.46

Source: By the author.

Despite these minor differences in the masses, all the masses found for the complexes are compatible with hexamers in solution, even in the absence of C-terminals, indicating that these regions are not completely essential for the assembly of hexameric complexes, although they assuredly have some influence on the complex stability.

4.3.2 Analysis of the assembly of hexameric complexes by electron microscopy (negative stain) under conditions of high ionic strength

First, we analyzed the WT complex, containing all full-length septins, under high ionic strength (300 mM NaCl) to prevent polymerization and also to use as a control for the assembly of hexameric complexes. In the raw TEM images (Figure 4.14, panel a), it was possible to observe a high concentration of proteins with the presence of some aggregates, the hexameric complexes, and other (lower and higher) oligomeric states to a small extent in the sample. Thus, following a manual inspection of the images, we analysed the sizes of these hexamers through native plugins in the software ImageJ (NIH, USA).

To facilitate the visualization of particle boundaries and determine the correct sizes, we use a low-pass filter called Gaussian blur over the raw TEM images, after setting the correct scale. After applying this filter to the images, we measured the length of 20 complexes for each studied construct, and a histogram of their size distributions was plotted.

(1) WT complex in a high-ionic strength buffer

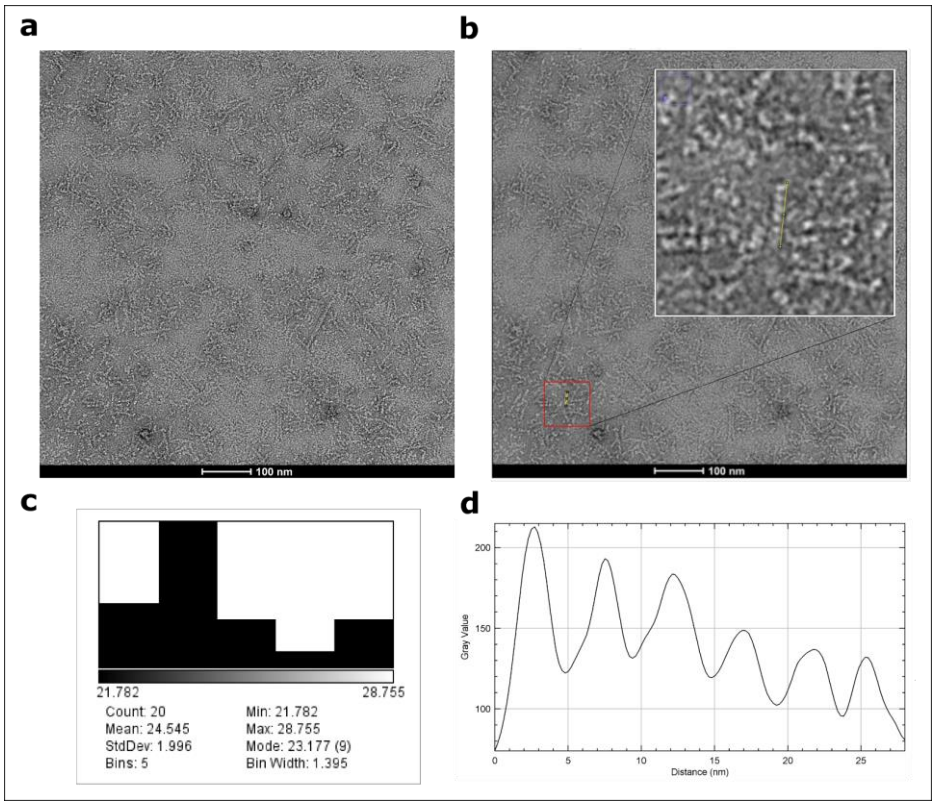

Figure 4.14 – **Micrographs of the SEPT2NGC/6NGC/7NGC hexameric complex at high ionic strength.** In **a** and **b**, TEM images of grids prepared by negative staining using purified samples (at 300 mM Septins) in buffer with a high ionic strength (300 mM NaCl), which prevents septin filament polymerization. Below each image is a nanometre scale bar. In **b**, the same micrograph as in **a** is displayed after applying a Gaussian blur filter. The insert shows a magnified area containing several particles, including one clearly visible hexamer. In the insert, it is also possible to see a yellow line on the side of the hexameric complex used to perform the intensity profile analysis, as shown in **d.** In **c,** a size distribution histogram of the lengths measured for 20 different hexameric complexes in this sample is displayed. The statistics for the histogram are shown below it.

Source: By the author.

For the wild type complex, it can be seen that the average size is ~25 nm (Figure 4.14, panel c), an expected value for hexameric septin complexes, as each monomer has an approximate size of 4~5 nm.[45,56] This is consistent with the average distance of 4-5 nm observed between the peaks in this intensity graph which can be seen in Figure 4.14, panel d. It is also worth mentioning that the number of peaks (six) proves that the complex is assembled as a hexamer. Furthermore, it is possible to observe some complexes with sizes larger than a hexameric particle, which may be interpreted as an "onset of polymerization", possibly induced by a high local protein concentration (see below in §4.5), even under a restrictive condition imposed by a high ionic strength buffer.

SEPT 2ΔC complex in a high-ionic strength buffer

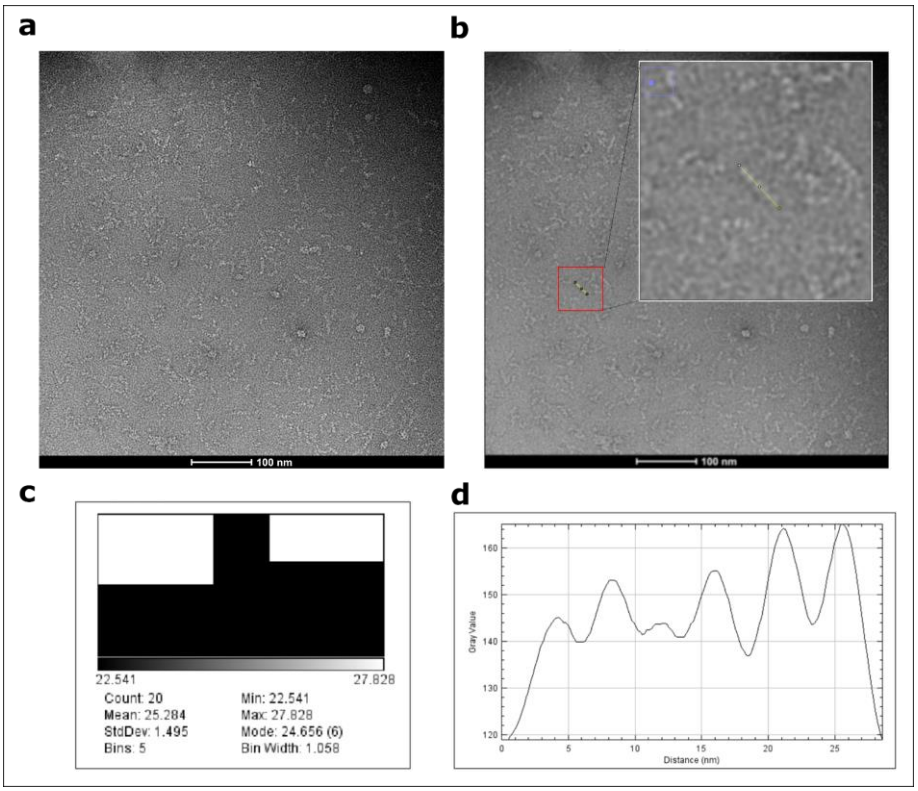

Figure 4.15 – **Micrographs of the SEPT2NG/6NGC/7NGC (2ΔC) hexameric complex at high ionic strength.** In **a** and **b**, TEM images of grids prepared by negative staining using purified samples (at 300 mM Septins) in buffer with high ionic strength (300 mM NaCl), which prevents septin filament polymerization. Below each image is a nanometre scale bar. In **b**, the same micrograph of **a** after applying a Gaussian blur filter is displayed. In the insert, a magnified area is highlighted containing a hexamer. In this insert, it is also possible to see a yellow line superimposed on the hexameric complex to perform the intensity profile analysis, as shown in **d**. In **c**, a size distribution histogram of the lengths measured for 20 different hexameric complexes on this sample is displayed. The statistics for the histogram are shown below.

Source: By the author.

By analysing the micrographs of the complex, including the truncation of the SEPT2 C-terminal domain (mimicking the protease cleavage), the ability of this construct to form hexameric complexes was evident (Figure 4.15, panels a to c). Furthermore, the spacing between the components of these complexes also remained constant (Figure 4.15, panel d). Therefore, it can be concluded that for a high salt condition, no significant differences occur for this complex, and the sample is as stable as the wild-type. This was already expected since SEPT2 occupies the terminal position in the hexameric complex,[62-63] exposing an NC interface for polymerization and filament formation. Thus, we would not expect the C-

terminal domain of this septin to be essential for the formation of complexes, but this region may be important for the formation of filaments and lateral interactions between filaments.

(2) SEPT 67ΔC complex in a high-ionic strength buffer

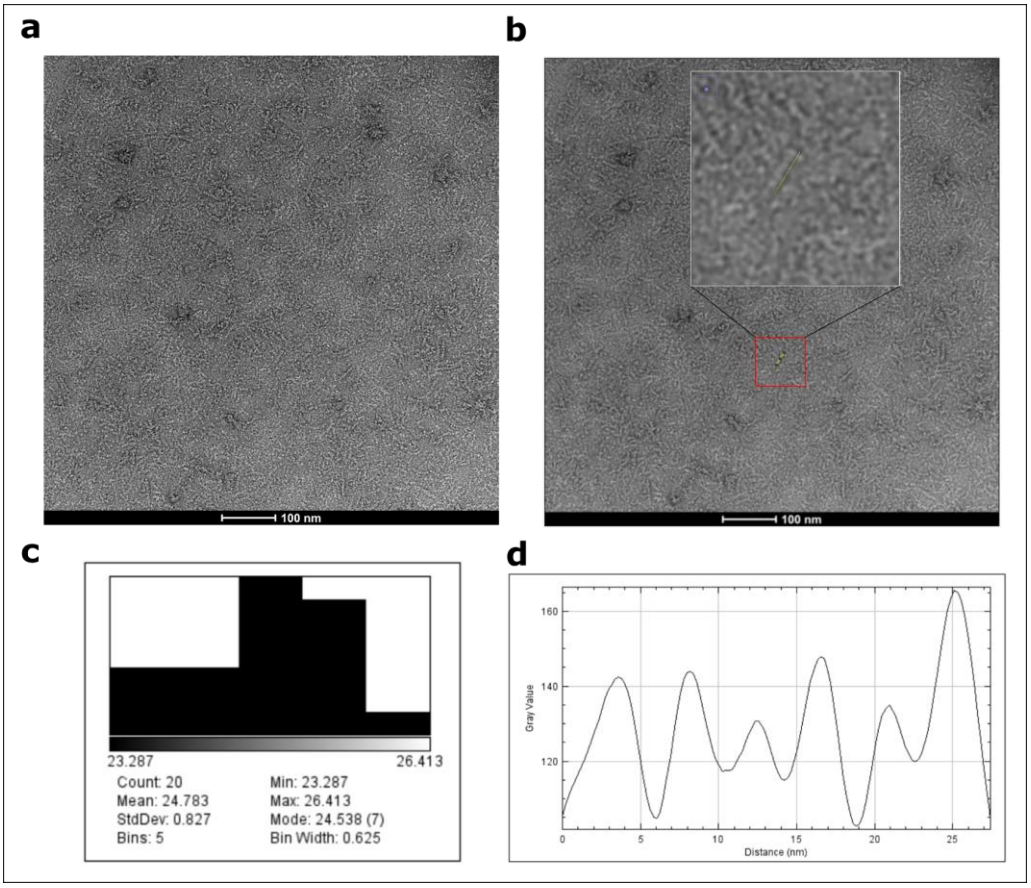

Figure 4.16 – **Micrographs of the SEPT2NGC/6NG/7NG (67ΔC) hexameric complex at high ionic strength.** In **a** and **b**, TEM images of grids prepared by negative staining using purified samples (at 300 mM Septins) in buffer with high ionic strength (300 mM NaCl), which prevents septin filament polymerization. Below each image is a nanometre scale bar. In **b**, the same micrograph as in **a** after applying a Gaussian blur filter is displayed. The insert shows a magnified area containing a hexamer. In this insert, it is also possible to see a yellow line superimposed on the hexameric complex to perform the intensity profile analysis, as shown in **d**. In **c**, a size distribution histogram of the lengths measured for 20 different hexameric complexes on this sample is displayed. The statistics for the histogram are shown below it.

Source: By the author.

Unlike the two previous complexes, the complex from which the C-termini of septin 6 and 7 were removed proved to be a little more unstable than the previous. Several aggregates and particles with other oligomeric states (*e.g.*, tetramers) were observed (Figure 4.16, panels a and b). Despite this intrinsically increased instability, the size of selected hexameric complexes and the spacing between particles within the hexameric complexes (Figure 4.16,

panels c and d) were similar to the former complexes analysed (corresponding panels in Figure 4.14 and Figure 4.15). Thus, although the truncated C-termini from SEPT6 and SEPT7 help, [55] to some extent, increase the stability of the complex, they are not essential for the selectivity of the NC interfaces between SEPT6-SEPT7, and consequently, the assembly of the hexamer.

(3) SEPT ΔC complex in a high-ionic strength buffer

Finally, we also performed the analysis of the construct in which all C-termini were absent. Firstly, the hexameric complexes can be easily observed on the raw micrographs (Figure 4.17, panels a and b). Therefore, the assembly of the hexameric complexes can occur even in the absence of all C-termini, consistent with the previous observations. [43, 83] Thus, while the presence of these C-terminal regions may help in the stability and interface selectivity within the complex, they are not essential for its self-assembly.

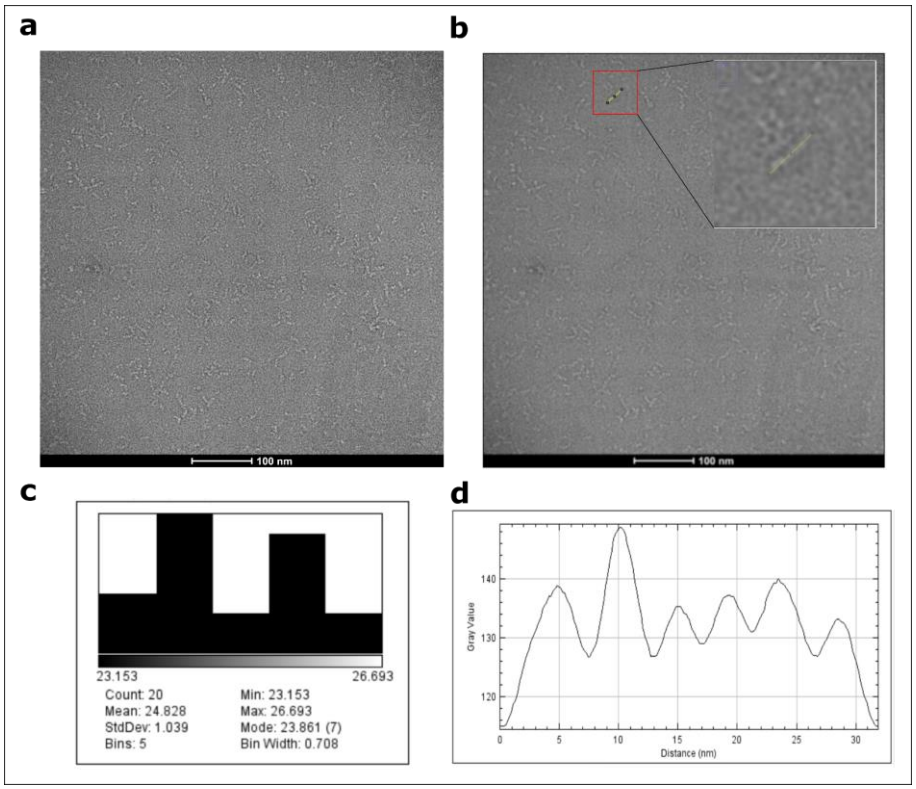

Figure 4.17 – **Micrographs of the SEPT2NG/6NG/7NG (ΔC) hexameric complex at high ionic strength.** In **a** and **b**, TEM images of grids prepared by negative staining using purified samples (at 300 mM Septins) in buffer with high ionic strength (300 mM NaCl), which prevents septin filament polymerization. Below each image is a nanometre scale bar. In **b**, the same micrograph as in **a** after applying a Gaussian blur filter is displayed. The Insert shows a magnified area containing a hexamer. In this insert, it is also possible to see a yellow line superimposed on the hexameric complex to perform the intensity profile analysis, as shown in **d**. In **c**, a size distribution histogram of the lengths measured for 20 different hexameric complexes on this sample is displayed, and the statistics for the histogram are shown below it.

Source: By the author.

Despite the absence of all C-termini, this complex (shown in Figure 4.17) was not as unstable as the previous complex (67ΔC) (Figure 4.16). The presence of the SEPT2 C-terminal, in the absence of the C-termini for SEPT6 and SEPT7, appears to generate instability in the latter complex. The same might also happen (being maybe even more intensified) by truncating the long C-terminus of either SEPT6 or SEPT7 alone (and maintaining the full-length interaction partner). Under this situation, due to the absence of the predicted heteromeric parallel coiled coil interactions with the partner, the solitary preserved C-terminus might even interfere in the complex heteromeric NC-interface, and thus, in the complex assembly itself, by triggering promiscuous homomeric interactions between others unsatisfied C-terminals in order to fulfil the lacking interactions. However, since these experiments were not performed, at present, this is merely speculative.

As demonstrated, even though the C-termini of septin 6 and 7 were not directly involved in the single filament polymerization, they were shown to be important for stabilising the isolated complexes through indirect mechanisms that need to be further investigated.

Table 4.2 – Average length for the hexameric of septin complexes.

Complex	**SEPT 2NGC 6NGC 7NGC**	**SEPT 2NG 6NGC 7NGC**	**SEPT 2NGC 6NG 7NG**	**SEPT 2NG 6NG 7NG**
Average length (nm)	25±2	25±2	25±1	25±1

Source: By the author.

Another interesting point to note is that there is no change in the overall length of the complexes (Table 4.2) nor in the spacing between monomers within the hexamers, even in the absence of C-terminals. Thus, the molecular determinants required for the specificity, selectivity and stabilisation of the interaction interfaces within the heterocomplex can be effectively provided and maintained by both the G-domain and the N-terminal domain. This observation is an important finding from the evolutionary point of view, as it enables/supports a higher sequence variation for these C-terminal domains, due to a smaller selective pressure from this so important function for septins in general (although we cannot neglect that other additional pressures, related with other functions, might also be incorporated to some of the genes in the course of the septin evolution or even before).

Thus, once the complex self-assembly has already been satisfied by the other two domains (and if there is no pre-existing function or pressure assigned to this C-terminal

domain), additional functions might be “explored and acquired” by it, like those already described for this domain: tuning morphologies and dynamics of high-order septin structures, expanding interactions with membranes and other protein partners, or even enhancing the stability and selectivity of the interface interactions that maintain the complex itself.

In summary, with morphological (TEM) and quantitative (SEC-MALS) analyses of the hexameric complexes in a condition of high ionic strength (restricting the formation of filaments), it was possible to validate that the complex self-assembly can occur independently from the presence of C-terminal domains. However, as also demonstrated, this does not exclude the possibility that these domains may have additional influences on the interface stabilities and, therefore, influences on the stabilities of septin complexes.

4.4 Analysis of the influence of C-terminal domains on the capacity of interaction with membranes (PIP-Strips)

Septins are largely known for interacting with membranes, sensing their curvatures and more recently, they have been described to actively modify them. [84-86] More specifically, septins are recognized by and associated with phosphorylated forms of phosphatidylinositol (PI), called phosphoinositides (PIP). Each type of PIP possesses binding specificities (PIP code) and is also related to specific cellular functions. As the septin C-terminal domain has been reported to be important for the interaction with membranes,[85] we evaluated the specificities in the binding of this domain by comparing the WT complex with the ΔC variants, excluding one or more of the C-domains. Additionally, we also verified the importance of polymerization for the interaction with these lipids. For this purpose, we utilized a complex containing SEPT2G, which is incapable of polymerizing. The results for these complexes are shown in Figure 4.18.

Evaluating the interactions with lipids in the WT complex (Figure 4.18, panels a and b), it is possible to observe that septins interact mainly with negative lipids such as PIPs, PA and PS. Within PIPs, the most significant interactions were found within mono-phosphorylated PIPs (PI_3P, PI_4P and in special PI_5P), albeit biphosphorylated ($PI_{3,4}P_2$, $PI_{4,5}P_2$, and specially $PI_{3,5}P_2$), and the triphosphorylated $PI_{3,4,5}P_3$ also displayed a significant interaction. Interestingly, interactions with PA and PS were also retrieved by this experiment.

The same PIP-Strip experiment examining each yeast septin specifically was not able to detect an interaction between these septins and PS. [46] However, recent studies with fruit fly and human septins[49,83,87] showed clearly an interaction with this lipid, raising the question if the interactions between septins and lipids are governed solely by electrostatic interactions

with negatively charged lipids or if septins possess a preference for specific lipids. Here we showed a slightly enhanced interaction of septins for PIPs compared to PS, specifically those phosphorylated on position 5 (PI_5P, $PI_{3,5}P_2$). In terms of levels in mammalian cells, these lipids are 20~100-fold times less abundant than PI_4P, $PI_{4,5}P_2$, being associated with vesicles (endosomes, lysosomes) and membranes. [88]

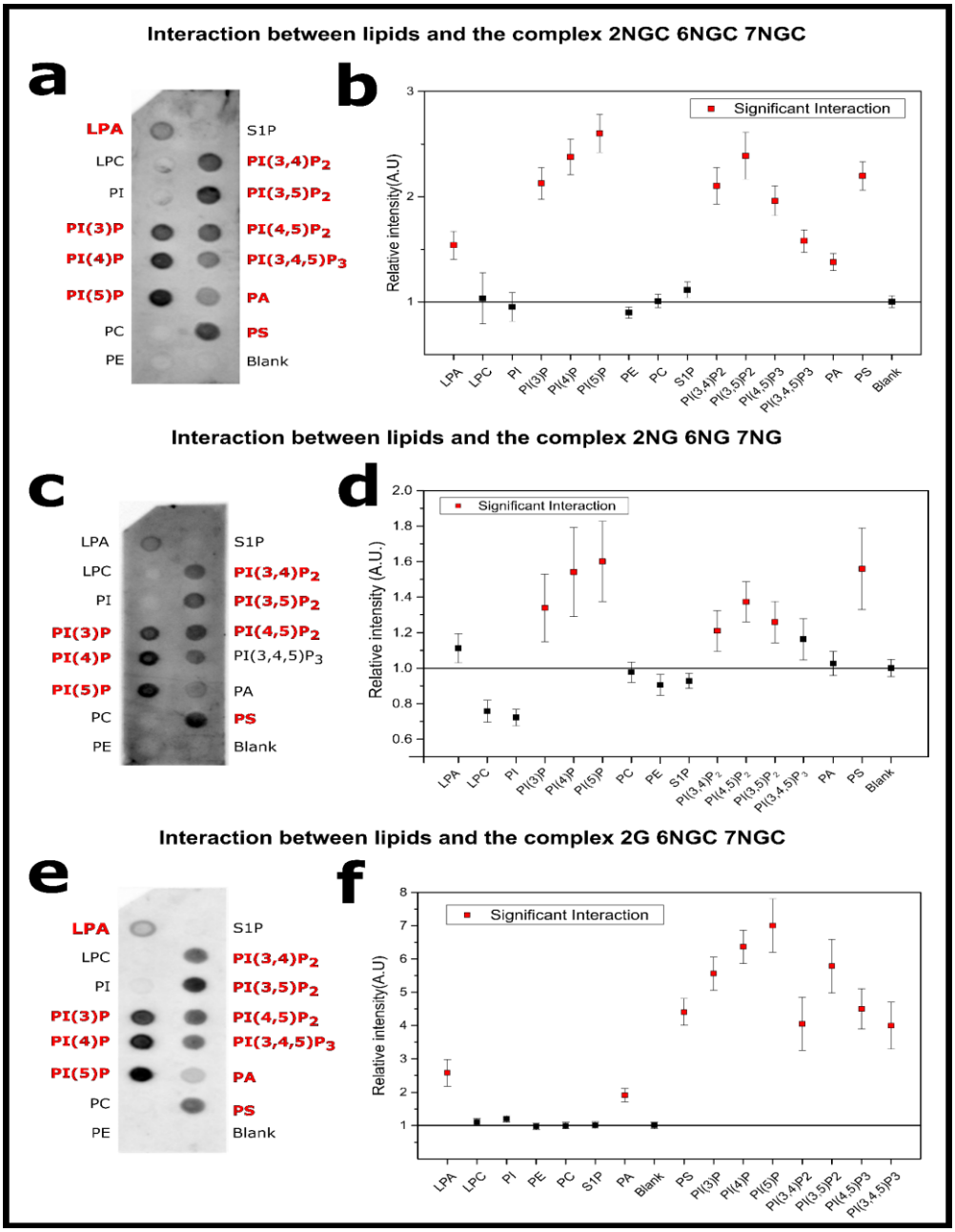

Figure 4.18 – **PIP-Strip analysis of different complexes.** In **a**, **c**, and **e**, PIP Strip membranes, after chemiluminescent detection containing, respectively, the WT complex, the ΔC complex, and the SEPT2G complex. Lipids whose spot displays significant interaction with septins are labelled in red. In **b**, **d** and **f**, quantitative analyses of the relative mean intensity at each spot are displayed.

Source: By the author.

Comparing the ΔC complex (the hexamer containing septins lacking their C-terminal domains), which is displayed on the panels c and d of Figure 4.18, with the WT complex (Figure 4.18, panels a and b), we saw no significant difference in the interaction pattern with the lipids: despite slight changes in the emission of some spots, no interacting spots disappeared, neither new one emerged. Although this observation may suggest that regions within the N and G domain possess the requirements and are sufficient for the interaction with the lipids analysed, this does not exclude the possibility that the affinity coefficients and other interactions parameters may be tuned by the presence of these C-terminal domains. Equally noteworthy is the fact that the C-terminal domains may also be important in sensing membrane curvature, as already reported for the C-terminal region of the yeast septin Cdc12.[85]

Finally, analysing the complex containing SEPT2G (Figure 4.18, panels e and f), incapable of polymerizing, we could observe that the same pattern of interactions is preserved. Therefore, these interactions between septins and lipids may not depend on initial filament formation, *i.e.*, the complex is able to interact directly with the lipids, and they may possibly polymerize into filaments after this event (even though our conditions might not be the most favourable for filament polymerization). This complex interaction and recruitment to the lipidic membrane have been shown recently to restrict the diffusion to the membrane, imposing an additional spatial restriction, in which pre-formed filaments would act as templates, favouring the polymerization of new ones.[76,89] Additionally, none of the interactions was lost by truncating the N-terminal domain of SEPT2, containing the polybasic region 1 (the PB1 region was shown to be important for membrane interaction).[46,48-49,90] This was already expected since mutations in this SEPT2 PB1 motif were shown not to affect this interaction.[91] Additional studies may be helpful in identifying other lipid-interacting regions within the septins domains analysed in these hexameric complexes.

4.5 Analysis of the influence of C-terminal domains on the polymerization process

Although no significant difference was found regarding the influence of the C-terminals on the self-assembly of the hexameric complex (Figure 4.13, Table 4.2) or on lipid binding (Figure 4.18), these domains are expected to modulate the polymerization process and the lateral interactions formed between filaments.[45,69,83,89] Thus, we evaluated the polymerization capacities of these complexes in order to evaluate the influence of the C-terminal domain on these processes. We analysed the different constructs under conditions of

low ionic strength, allowing for the maintenance of the electrostatic interactions necessary for the formation of filaments and lateral interactions.[45] The protein concentration proved to be an important factor in these processes, corroborating previous reports.[75,89]

4.5.1 WT complex under polymerising conditions: the loose and tight filament spacings

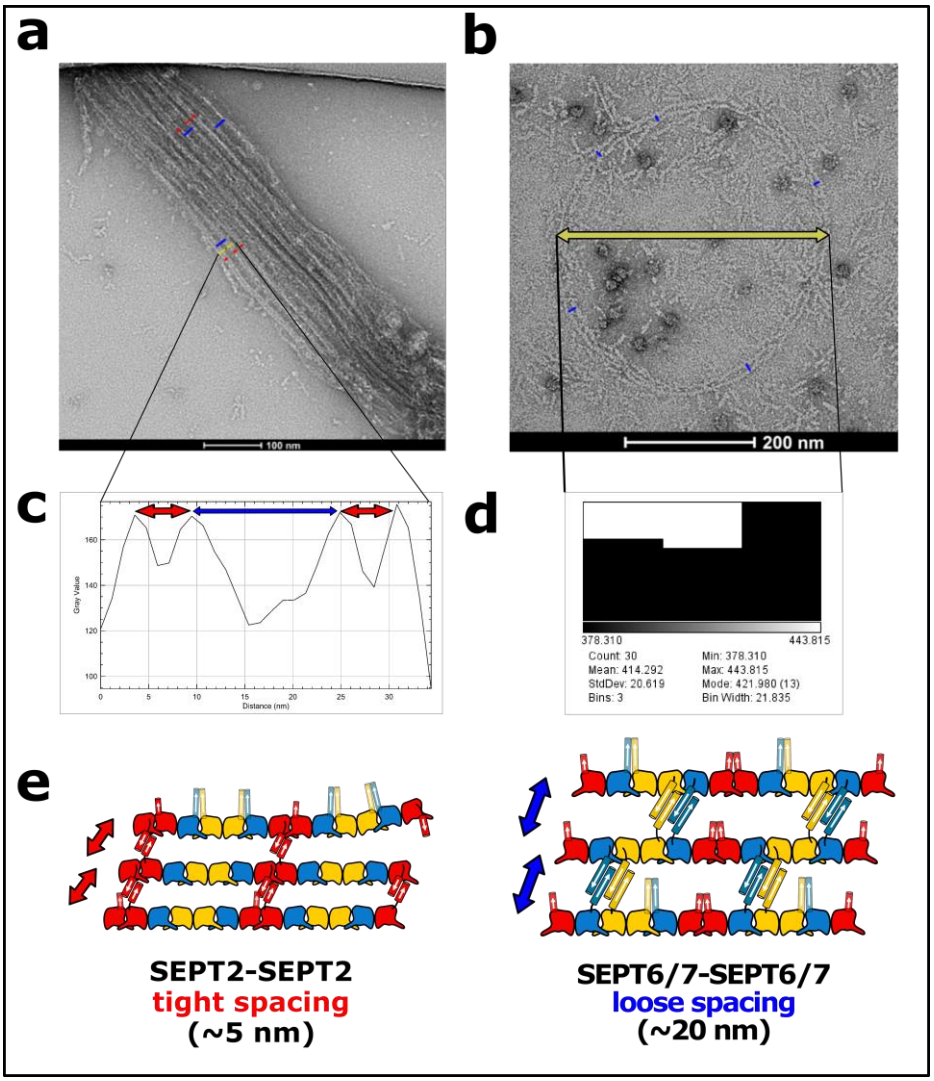

Figure 4.19 – **Micrographs of the SEPT2NGC/6NGC/7NGC hexameric complex under polymerizing conditions.** In **a,** TEM micrograph of a grid prepared by negative staining using purified samples (at 100 nM Septins) in buffer with low ionic strength (50 mM NaCl), which allows for filament polymerization. In this micrograph, it is possible to observe the tight and loose spacings (in red and blue, respectively) between filaments in a bundle. In **b**, TEM micrograph of a grid prepared by negative staining using the same purified samples (at a high protein concentration >500 nM Septins and high-salt concentration 300 mM NaCl), showing the formation of a septin ring. Below each image is a nanometre scale bar. In **c**, it is possible to observe an intensity profile corresponding to the yellow line trace shown in a., perpendicular to the filament polymerising direction, which was employed to measure the spacing between the filaments. The distances measured for the tight filament spacing were 5 nm, whereas, for the loosed, it varied more between 15~20 nm. In **d**, is displayed a size distribution histogram of the lengths measured for 30 different diameters on the ring displayed in b. The statistics for this histogram are shown below it. The main diameter for this ring was (414±20) nm. Finally, in **e**, is displayed the proposed model to explain the appearing of two different distances between filaments: the tight filament spacing is thought to be established by interactions of the C-termini of SEPT2 members, whereas the loose one is believed to be formed by the other C-termini (from SEPT6 and SEPT7 group members), whose coiled coils and thus C-termini are longer in extent than that from SEPT2 group members.

Source: Adapted from LEONARDO.[92]

Firstly, analysing the polymerisation capacities of the WT complex (SEPT267 NGC) and using it as a control for the other complexes, we were able to observe interesting morphological aspects (Figure 4.19). It was possible to observe not only filament polymerisation but also the presence of lateral interactions between these filaments and, thus, the formation of septin bundles and rings (Figure 4.19, panels a and b) under certain conditions. Interestingly, it was possible to clearly observe the emergence of two different spacing patterns between the filaments on the grids (Figure 4.19, panel c).

These two different filament spacings are presumed to be formed by interactions and distance restrictions involving mainly the C-terminal domains of the septins,[69] but they might also be similarly supported by the direct interactions of the N- and G- domains, to some extent.[83,89] The observation of an interaction via the C-terminal domain is further corroborated by the fact that the distances between these filaments are approximately equivalent to the lengths of the extended C-terminal antiparallel coiled coils present in these C-termini (Figure 4.19, panel e). The narrower spacing may correspond to interactions involving the SEPT2-SEPT2 C-terminals and its coiled coil region (shorter in length than the other two groups analysed). On the other hand, the wider spacing requires the appearance of larger C-termini, as provided by SEPT6 and SEPT7 subgroup members. In this case, not only to the coiled coil region but also part of the linkers connecting this structural element to the G domain may be important. This can be concluded from the fact that the distances found in the micrographs are larger than would be expected if they were formed only by the coiled coil region and not the entire C-domain.[69]

Another interesting feature observed was the formation of a septin ring (Figure 4.19, panel b), with an approximate diameter of (414±20) nm (Figure 4.19, panel d), under high protein concentration (> 500 nM Septins). Rings with this diameter have already been reported in the literature[91] and are possibly related to membrane curvatures, in which septins displayed enhanced affinity.[84,86]

This ring assembly, shown in Figure 4.19 (panel b), has also drawn attention since it was observed under high salt concentration (300 mM NaCl), which was thought to hamper the polymerisation.[45,93] However, not only did the filament formation occur, but also the formation of rings was observed. In addition to being surprising, this effect emphasized the impact of high protein concentration in promoting filament and septin polymerisation under restricting conditions. It may be that the increase in protein concentration can locally increase the polymerisation by "forcing" the interaction between complexes, which would be otherwise (at lower protein concentration) restricted by the difficulties in the establishment of

electrostatic interactions between these complexes, imposed by the high ionic strength buffer. Thus, high protein concentration is shown here to be as equally important as low ionic strength buffers in promoting septin polymerisation. This is something that has already been discussed in the literature[75,89] and, certainly, needs to be carefully considered, particularly when evaluating septin polymerization events. Many results and discussions may be misinterpreted if only the ionic strength of the buffer is considered, without considering the concentration of the analyzed proteins, for example. Furthermore, this effect of protein concentration on the polymerisation must be considered when evaluating the data even for the same protein, under different protein concentrations (*e.g.*, analysing different experiments requiring different concentrations).

4.5.2 **SEPT 2ΔC complex in a low ionic strength buffer:** the ZIKV protease cleavage effect on polymerization

Using the hexamer with the truncation of the C-terminal domain of SEPT2, we evaluated the influence of this domain on filament formation and its relevance to the lateral interactions. At the same time, with this trimmed construct, we mimicked the cleavage of the ZIKV protease on the SEPT2 C-terminal domain (which is intrinsically difficult to observe *in vitro*, see §5.1).

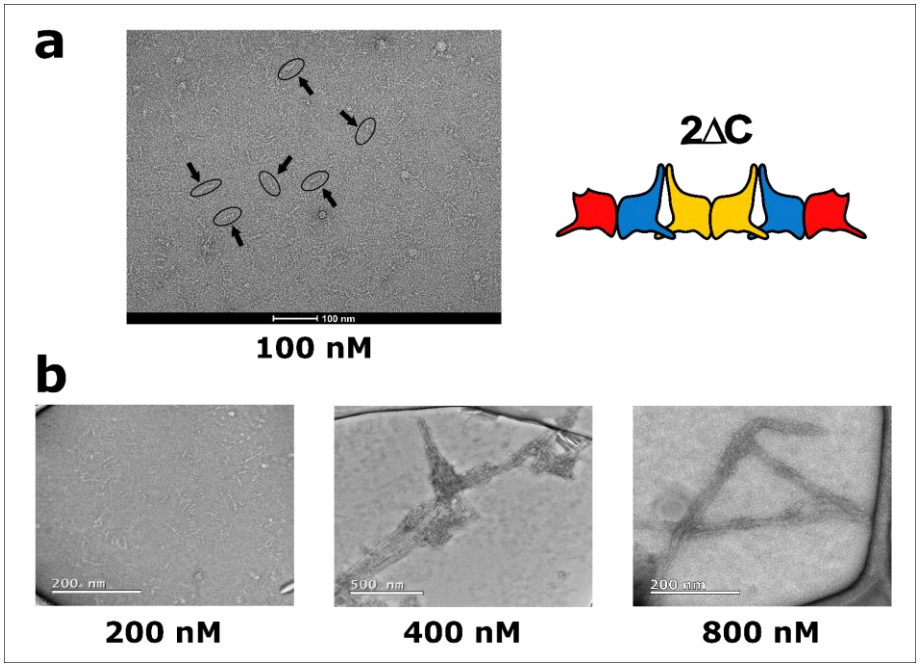

Figure 4.20 – **Micrographs of the SEPT2NG/6NGC/7NGC hexameric complex under polymerizing conditions.** In **a**, micrographs of a grid prepared by negative staining using purified samples (at 100 nM Septins) in buffer with low ionic strength (50 mM NaCl), which normally allows for filament polymerization. It is possible to observe in this micrograph only isolated complexes (possibly hexamers), circled and indicated by arrows. In **b**, **c**, and **d**, micrographs of grids prepared by negative staining using the same purified samples (at higher protein concentrations of 200, 400 and 800 mM Septins). Inside each image, a nanometre scale bar is displayed.

Source: Adapted from LEONARDO.[69]

With this approach, we were able to show the relevance of the C-terminal domain of this specific septin (and possibly its group members) to filament formation. Under physiological protein concentrations (100 - 200 nM Septins),[76] we were unable to observe any filaments for this complex (Figure 4.20, panels a and b), which was something readily seen for the wild-type hexamer, even at the lowest protein concentration of 100 nM (Figure 4.19, panel a). Only isolated complexes were observed for the concentrations of 100 and 200 nM of septins (Figure 4.20, panels a and b), which did not even form larger aggregates, as seen for the WT complex at high ionic strength (Figure 4.14). Therefore, the loss of this domain due to the action of the viral protease clearly impairs the formation of filaments at physiological septin concentrations.

Curiously, by increasing the protein concentration to higher levels (400 and 800 nM), well above the physiological concentration, the restriction of filament formation (and even bundles) is overcome (Figure 4.20, panel c and d). Nevertheless, filaments polymerised from this truncated complex appear mostly in bundles. There is no subtle transition between

isolated complexes at lower concentrations to bundles at higher concentrations, *i.e.*, single and paired filaments were not detected through a manual inspection of the grids at intermediate concentrations (Figure 4.20, panel b and c). This indicates that the bundle formation and lateral interactions, possibly facilitated by other septins (maybe the C-terminals from SETP6 or SEPT7), may support and trigger filament assembly, providing templates for the complexes to polymerise and also provide stabilisation and maintenance for the filaments once assembled, in a cooperative manner.

4.5.3 **SEPT 67ΔC complex in a low ionic strength buffer:** formation of paired filaments and only tight filament spacing

Analogously to what was observed for the WT complex (Figure 4.19), the combination with truncations of the C-terminal domains of both SEPT6 and SEPT7 (but preserving that of SEPT2) was able to form filaments under physiological concentrations (Figure 4.21, panel a and b). This further corroborates the importance of the C-terminal domain of SEPT2 for the polymerization process. However, the C-terminal domains of SEPT6 and SEPT7 do not appear to be essential for this process, consistent with the fact that they do not occupy terminal positions within the hexamer. The presence of the SEPT2 C-terminal domain also seems important in establishing lateral interactions (even at very low protein concentrations) between two filaments forming the so-called paired filaments, observed at all concentrations (Figure 4.21).

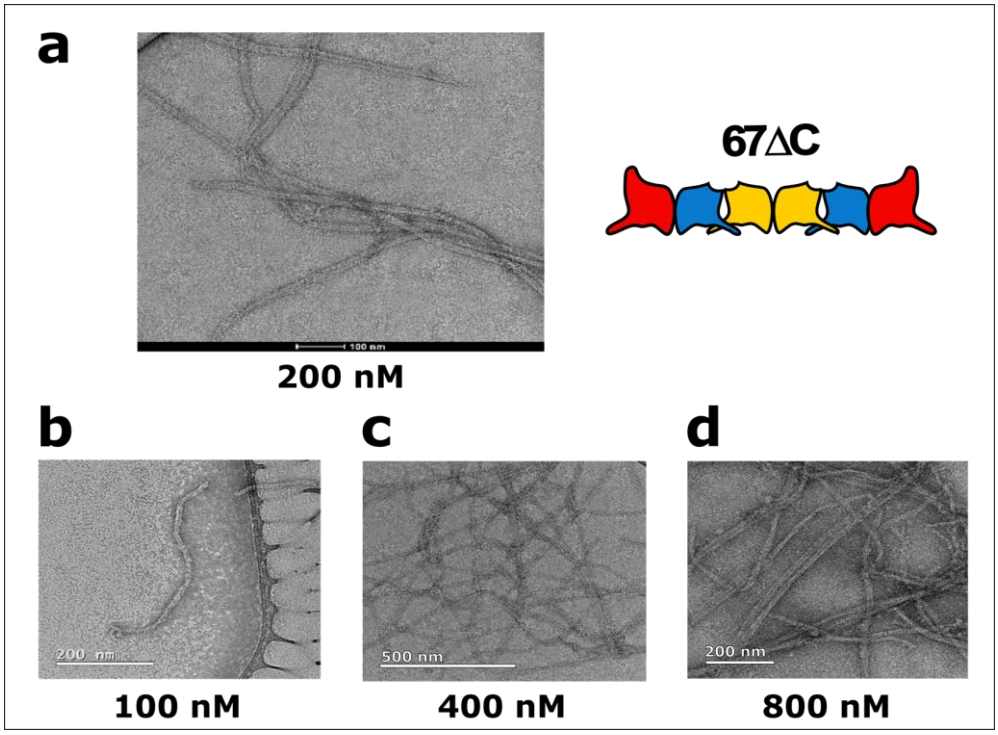

Figure 4.21 – **Micrographs of the SEPT2NGC/6NG/7NG hexameric complex under polymerizing conditions.** In **a**, micrograph of a grid prepared by negative staining using purified samples (at 200 nM Septins) $_{in}$ buffer with low ionic strength (50 mM NaCl), which allows the septin filament polymerization. It is possible to observe in this micrograph paired filaments assembling into a bundle. In **b**, **c**, and **d**, micrographs of grids prepared by negative staining using the same purified samples (at protein concentrations of 100, 400 and 800 mM Septins). Even at very high concentrations, it is not possible to observe very wide bundles, as observed for the WT complex. The "bundles" formed appear to be always formed by paired filaments. Inside each image is displayed a nanometre scale bar.

Source: By the author.

Measuring the distances between the filaments (Figure 4.21), we readily notice that the distances (typically in the order of 5 nm) are related to the tight filament spacing, which is expected to be formed by the antiparallel coiled coil interactions of the C-terminal of the SEPT2.[69] Neither the loose spacing between the filaments nor very wide bundles were observed in the grids of this construct (Figure 4.21), compared to the bundles observed in the WT (Figure 4.19, panel a) and even to those of the SEPT2ΔC complex samples at high concentrations (Figure 4.20, panels c and d). Possibly, similarly to what was observed when truncating the C-terminal domain of SEPT2, these truncations in the correspondent region in SEPT6 and SEPT7 might be crucial to stabilizing the lateral interactions, despite not being so crucial for the filament polymerization as in SEPT2, susceptible to the ZIKV protease cleavage. However, the importance, to some extent, of these C-terminal domains (from SEPT6 and SEPT7) for the filament assembly process should not be neglected, as filaments

were not as readily observed in the grids with lower protein concentration as it was for the WT complex. Indeed, similarly to the stabilisation induced by the presence of the SEPT2C-terminal (observed when we compare the WT complex in Figure 4.19 with the 2ΔC complex in Figure 4.20), which also leads to interfilament interactions and bundle formation, the presence of the C-terminal domain from these other two groups might additionally help in the stabilisation of these interfilament interactions and, thus, maintenance of the assembled filaments to serve as templates for others.

4.5.4 SEPTΔC complex in a low ionic strength buffer

The final piece of the septin ultrastructural puzzle was the complex, where all septins lacked their C-terminal domains (ΔC). This was important not only to confirm the previous observations from truncating each combination of C-termini but also to allow correlations between these secondary effects, not so clear when analysing only the previous complexes.

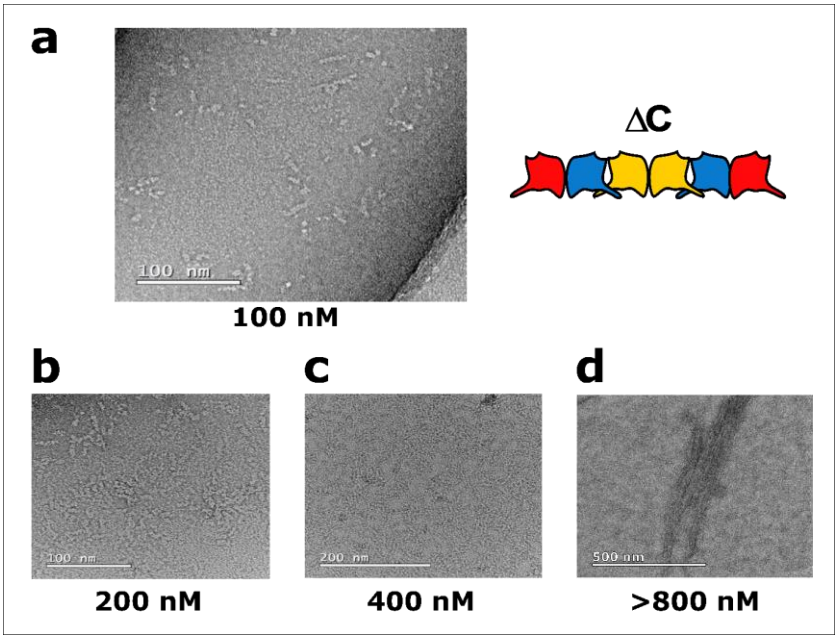

Figure 4.22 – **Micrographs of the SEPT2NG/6NG/7NG hexameric complex under polymerizing conditions.** In **a**, micrograph of a grid prepared by negative staining using purified samples (at 100 nM Septins) in buffer with low ionic strength (50 mM NaCl), which allows the septin filament polymerization. It is possible to observe in this micrograph only isolated complexes (possibly hexamers). In **b**, **c**, and **d**, micrographs of grids prepared by negative staining using the same purified samples (at protein concentrations of 200, 400 and 800 nM Septins). The filaments are observed only at 800 nM, highlighting the critical role of the C-terminal in supporting filament and bundle formation. Inside each image is displayed a nanometre scale bar.

Source: By the author.

The first major functional influence of C-terminals was observed when comparing this complex with the SEPT2ΔC complex. Whereas this latter complex (SEPT2ΔC) starts its polymerization at a septin concentration of 400 nM (Figure 4.21, panel c), the former complex lacking all C-termini was only able to form filaments in solution, at concentrations higher than 800 nM of septins (1~2 μM) (Figure 4.22, panel d). This observation is very important as it clearly demonstrates some influence of the C-termini from SEPT6 and SEPT7 in the filament polymerization process. Despite not being as impactful on the polymerization as is the SEPT2 C-terminal domain, the presence of these regions in SEPT6 and SEPT7 clearly helps the filaments to assemble at an intermediate concentration (Figure 4.21, panel c), lower than in their absence (Figure 4.22, panel d).

A recent study had already highlighted the formation of filaments using a similar construct (with truncations of the C-termini) but analysing the polymerization using lipid membrane as a scaffold for this assembly.[83] However, the septin concentrations required for polymerization (as shown in this previous study) were well above the normal physiological concentrations, emphasizing, therefore, the role of these C-termini in facilitating and supporting filament formation.

A possible explanation for this cooperative effect of the C-termini of SEPT6/SEPT7 on polymerization would be that the presence of lateral interactions between filaments, facilitated by the presence of these C-termini, can, by approximating (spatially) and aligning (in the favourable orientations for the interactions) the complexes and filaments, indirectly increasing (the collisions between SEPT2 and thus) the chances of formation and stabilization of the NC interfaces between the SEPT2 at the ends of the different complexes. These processes of pairing/aligning molecules and reducing the "dimensionality" of their diffusions have already been mentioned in the literature as being "facilitators" of polymerization and are called templating and annealing.[76,89]

Thus, by assisting in the establishment of lateral interactions, these C-termini (from SEPT6 and SEPT7) possibly indirectly help in the formation of filaments (with less impact, of course, than the C-terminal of SEPT2) as well as directly assist in the formation of bundles. In cooperation with SEPT2 C-terminal domains, these C-terminal extensions and the lateral interaction they make via their coiled coils might be the keystone to the formation of multi-layered bundles of filaments that have been recently described in the literature.[83,89]

A complete picture of this systematic study is shown in Figure 4.23. The main remark is undoubtedly the critical role of the SEPT2 C-terminal domain in filament polymerisation (*e.g.*, comparing the presence of filaments in WT and SEPT67ΔC with SEPT2ΔC and

SEPTΔC), clearly highlighting the impact of the ZIKV protease cleavage on this specific domain. In parallel, we could emphasize the importance of the C-termini of SEPT6 and SEPT7 for the formation of the loose spacing between the filaments and, hence, wide bundles (*e.g.*, comparing the width of the bundles between WT and SEPT67ΔC).

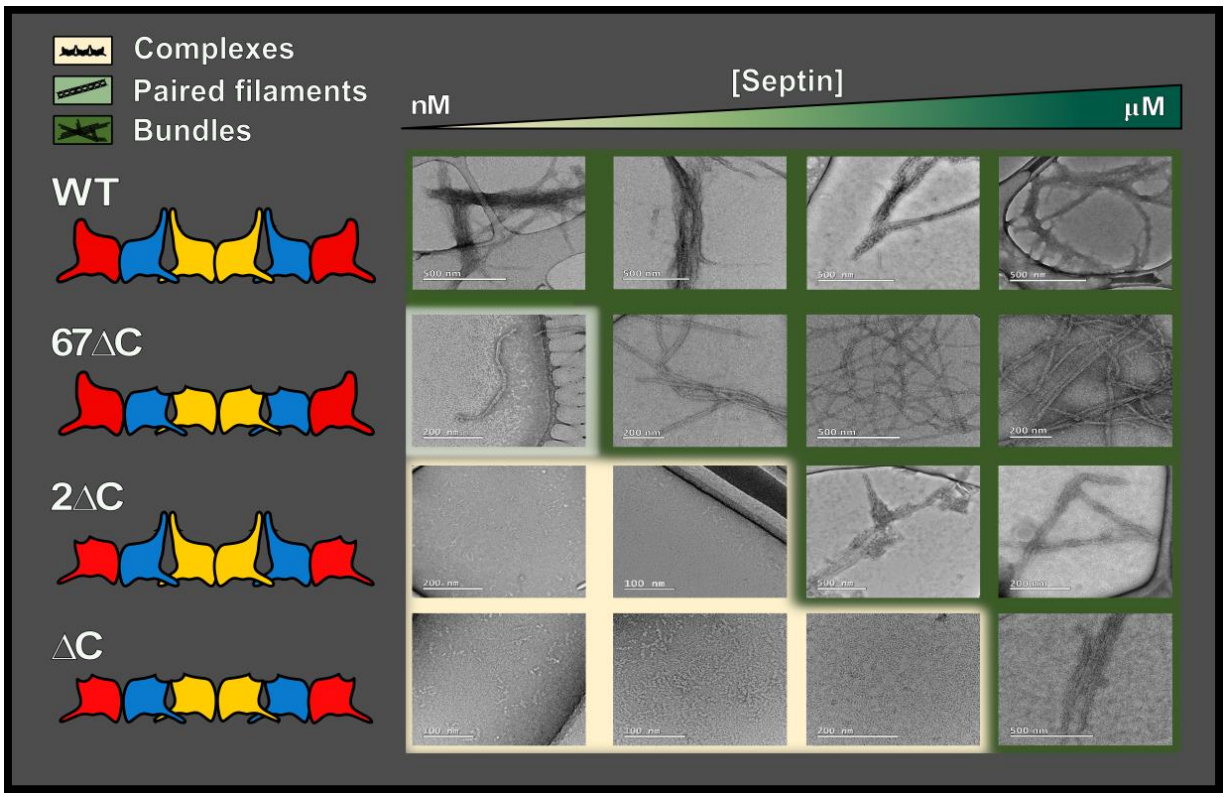

Figure 4.23 – **Systematic analysis of the polymerization capacities of wild and truncated hexameric complexes as a function of their concentrations (100, 200, 400 and 800 nM).** Grids prepared by negative staining using samples diluted in buffer with low ionic strength (50 mM NaCl) that allow polymerization. In each image, it is possible to observe the scale bar in nanometres. The influence of C-terminals for polymerization and for the formation of lateral interactions and beams is clearly identified.

Source: By the author.

4.6 Conclusion

From the data and results presented in this chapter, we are able to conclude that the septin C-terminal domains play a key role in filament polymerization and formation of lateral interactions, involved in the formation of larger and possibly multi-layered bundles. Additionally, the C-terminals were shown to provide some stability for the complex.

Although these domains emerge as being very influential in these processes, complexes lacking this region were shown to still form similar structures. Thus, albeit not completely essential for these processes, they were revealed to be crucial in tuning the concentrations in which these morphologies start to be observed. They decisively allow the assembly of filaments and bundles at physiological concentrations, possibly through cross-interactions involving equivalent regions from other septin complexes. Once they are trimmed, as observed in the ZIKV protease cleavage of SEPT2, these structures possibly collapse, impacting regular septin functions (*e.g.*, slowing cytokinesis), eventually disturbing homeostasis, causing failures and deficiencies, such as ZIKV-induced microcephaly.

5 RESULTS: FLAVIVIRAL PROTEASES AND THE INTERACTION WITH SEPTINS

5.1 *In vitro* Proteolytic Assays

A construct of the heterodimer SEPT2α0GC-SEPT6G (more stable and simpler to manipulate than the SEPT2 alone) already available in the laboratory was purified by IMAC and SEC, as well as the NS2B3 protease from Zika Virus (ZIKV), kindly provided by Dr Nathalya Mesquita (CIBFar) and, the homologous protease from Yellow Fever Virus (YFV), kindly provided by Gabriela Dias Noske (CIBFar). Thus, *in vitro* proteolytic assays (Figure 5.1) were carried out to confirm the cleavage of septin 2 by the proteases from ZIKV and YFV.

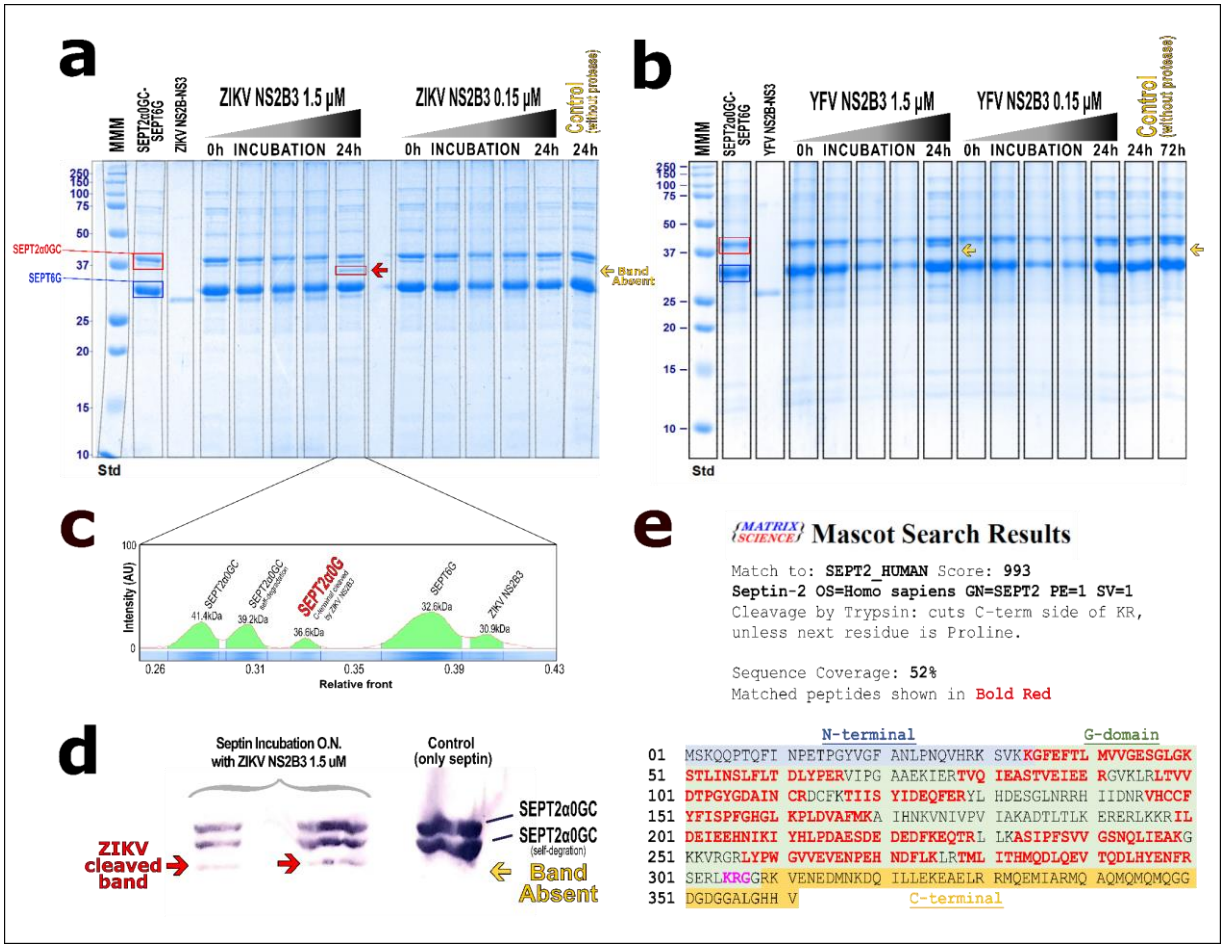

Figure 5.1 – ***In vitro* proteolytic assays**. In **a**, SDS-PAGE (12%) analysis of the protease cleavage of septins (heterodimer SEPT2α0GC-SEPT6G in lane 2) with ZIKV NS2B3 (lane 3). In lane 1, molecular mass marker (MMM) and in the other lanes, the result of the incubation of septins with the protease at high concentration (lanes 4 to 8 - 1.50 µM NS2B3) and low concentration (ranges 10 to 14 - 0.15 µM NS2B3). The control (containing only septins, without any protease) is displayed in lane 15. The septins were incubated for varying periods of 0 h (lanes 4 and 10), 1/2h (lanes 5 and 11), 1h (lanes 6 and 12), 2h (lanes 7 and 13), and overnight - 24 h (lanes 8 and 1). The red arrow indicates the protease cleavage band of septin 2 (lane 8). The yellow arrow indicates that the same behaviour was not observed in the control after overnight incubation (lane 15), as expected. In **b**, the same analysis was performed for the YFV NS2B3. However, it was not possible to observe a band corresponding to cleaved SEPT2 in this case. In **c**, analysis of the intensity profile of the bands in the 8th lane of **a** (overnight incubation with 1.5 µM of ZIKV NS2B-NS3), and the calculated molecular mass (values in kDa above the peaks) for each of these bands. The same 36.6 kDa band for cleaved septin 2 is seen. In **d**, Western Blot analysis (using a SEPT2 antibody) of the *in vitro* cleavage assay with NS2B3. The band of cleaved septin 2 is indicated by the red arrow. The yellow arrow indicates that the same behaviour was not observed in the control (without protease), as expected. In **e**, mass spectrometry analysis of the cleaved band after extraction from the gel and trypsinisation. Identified peptides are shown in red. It is possible to observe that no peptide was found encompassing the SEPT2 C-terminal region (after the cleavage site, whose residues are displayed in magenta) as expected after the protease cleavage.

Source: By the author.

It is possible to observe in the SDS-PAGE (Figure 5.1, panel a) the presence of a band (indicated by a red arrow) after the incubation with the ZIKV protease, which is 5 kDa smaller than the initial band of septin 2, being coherent with the expected size for the cleavage of its C-terminal domain. Later, this band was confirmed as being from septin 2, both by Western Blot with an antibody specific for the G domain of this septin (Figure 5.1, panel d) and also by mass spectrometry (Figure 5.1, panel e). The degraded form with the highest molecular mass of septin 2 appears naturally, even in the control. Even though we could detect and validate this cleavage by many techniques, its efficiency was a lot lower than we expected, restricting further experiments using this WT protease planned to observe effects of this cleavage directly on septins.

Interestingly, the same protocol was performed with the protease from the Yellow Fever Virus (YFV). However, it was not possible to observe any band (with a similar intensity of the cleaved band on SEPT2 induced by ZIKV NS2B3) at the expected region in the SDS-PAGE (Figure 5.1, panel b).

The ZIKV NS2B3 catalytic activity over SEPT2 has been shown to be intrinsically greater than the counterpart enzymes from other flaviviruses.[65] This could be a straightforward explanation for the presence of a cleavage band on the ZIKV assay but not on the YFV. Despite this, inspecting in more detail the substrate preferences of the NS2B3 proteases from ZIKV and YFV and comparing them with the SEPT2 sequence recognized prior to cleavage, one can also observe that the specificities of residues at the P1 (Arg) and P2 (Lys) position for ZIKV protease are fulfilled by SEPT2 ($_{305}$KRGGRK$_{310}$).[94] However, these residues are not the preferred ones required for the cleavage of the YFV protease (Arg on both P1 and P2). [95] Therefore, even though the cleavage might happen at the molecular level for YFV, it might not be possible to observe this effect directly by SDS-PAGE, as clearly as we observed for the ZIKV.

This ZIKV NS2B3 increased preference for the SEPT2 sequence, resulting in an enhanced cleavage activity of this protease over this septin, compared with YFV and possibly other flaviviral proteases (with the similar sequence preference as the YFV protease), might be one of the explanations of an enriched appearance of microcephaly cases related to ZIKV. This, of course, might not be the leading cause of a more significant number of cases by this specific flavivirus compared to others but might play a role in boosting this off-target cleavage effect, ultimately leading to the ZIKV-related microcephaly cases.

5.2 Production of catalytically inactive mutant flaviviral NS2B3 proteases

The plasmids containing the wild-type NS2B3 flaviviral proteases were amplified by oligonucleotides containing the mutations on the bases in order to change the codons from serine to alanine, abolishing the catalytic activity of these proteases. After the PCR amplification, the methylated template was digested with *Dpn* I, leaving only the amplified vector. With the restriction analysis (with enzymes flanking the desired region), it was possible to confirm the amplification of the gene and the plasmid itself (Figure 5.2, panel a). The mutation was confirmed by sequencing, as shown in Figure 5.2, panel b. The same process was successfully repeated for the yellow fever virus protease (YFV NS2B3^{S138A}).

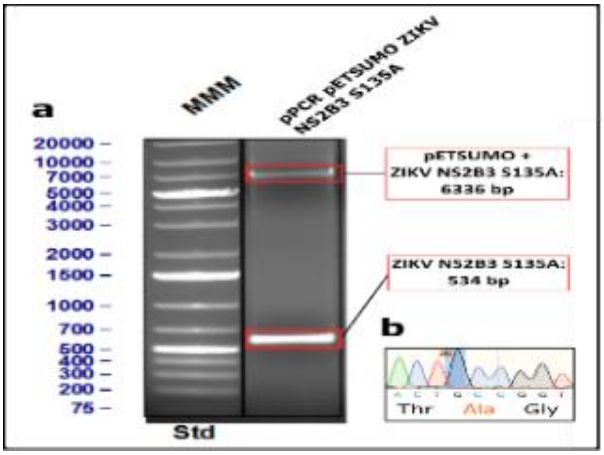

Figure 5.2 – **Cloning of the ZIKV NS2B3S135A. a**. ZIKV NS2B3S135A restriction analysis. MMM – Molecular Mass Marker (base pairs). **b**. Sequencing chromatogram showing the mutation region, highlighting the mutated base with an asterisk.

Source: By the author.

5.3 Purification of inactive flaviviral proteases and proteolytic activity assays

In order to characterize the activity of flaviviral proteases, as well as to analyse their oligomeric state, the flaviviral proteases were first expressed and purified (Figure 5.3 and Figure 5.4).

Soluble protein was submitted to affinity chromatography (IMAC) (panels a and b, in Figure 5.3 and Figure 5.4). TEV protease was added to the eluted fractions (for cleavage of the SUMO fusion protein), and this solution remained under dialysis for 16 hours. With the cleavage of the fusion protein, the uncleaved fractions could be separated by a second affinity chromatography (panel c, in Figure 5.3 and Figure 5.4).

Finally, it was possible to observe, after application of size exclusion chromatography to the cleaved and eluted samples (panel d, in Figure 5.3 and Figure 5.4), the presence of two peaks that refer to the dimeric (peak I) and monomeric (peak II) states of the NS2B3 proteases of the two flaviviruses (ZIKV and YFV).

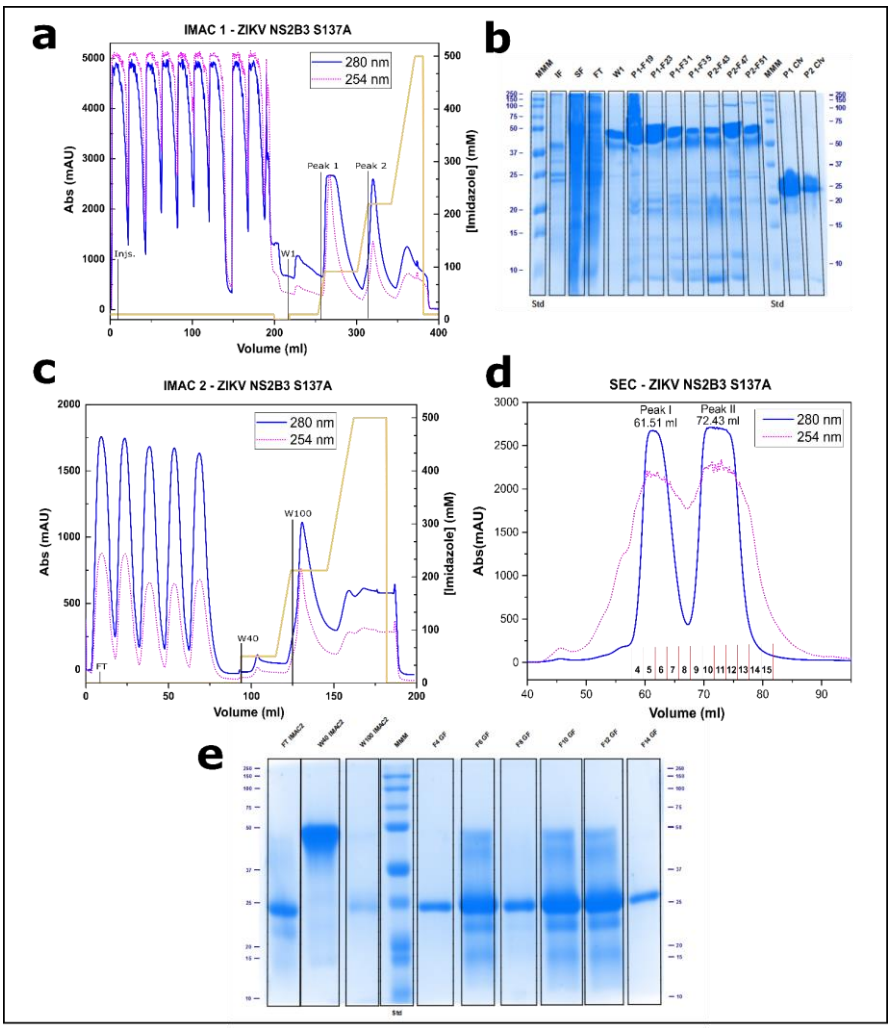

Figure 5.3 – **Purification of ZIKV NS2B3^{S135A} protease.** In **a**. IMAC 1 chromatogram shows peaks of injection (Injs.), wash (W1) and elution (Peak 1 and Peak 2). In **b**. SDS-PAGE shows fractions representing the main steps of the IMAC 1 chromatogram (molecular mass marker -MMM, culture medium samples before induction with IPTG -BI and after -AI, insoluble fraction -IF, soluble fraction -SF, unbound flow-through -FT, wash -W1, fractions along elution peak 1 -P1, and elution peak 2 -P2, fraction of peak 1 after dialysis and cleavage with TEV protease -P1-Clv, and the fraction of peak 2 after dialysis and cleavage with TEV protease P2-Clv). In **c**. IMAC 2 chromatogram shows injection and unbound flow-through (FT) peaks, wash 1 (W40) and wash 2 (W100). The **d**. SEC chromatogram shows peaks I and II, referring to the dimeric and monomeric states. In **e**. SDS-PAGE shows the fractions displayed in the chromatograms in **c**. and **d**.

Source: By the author.

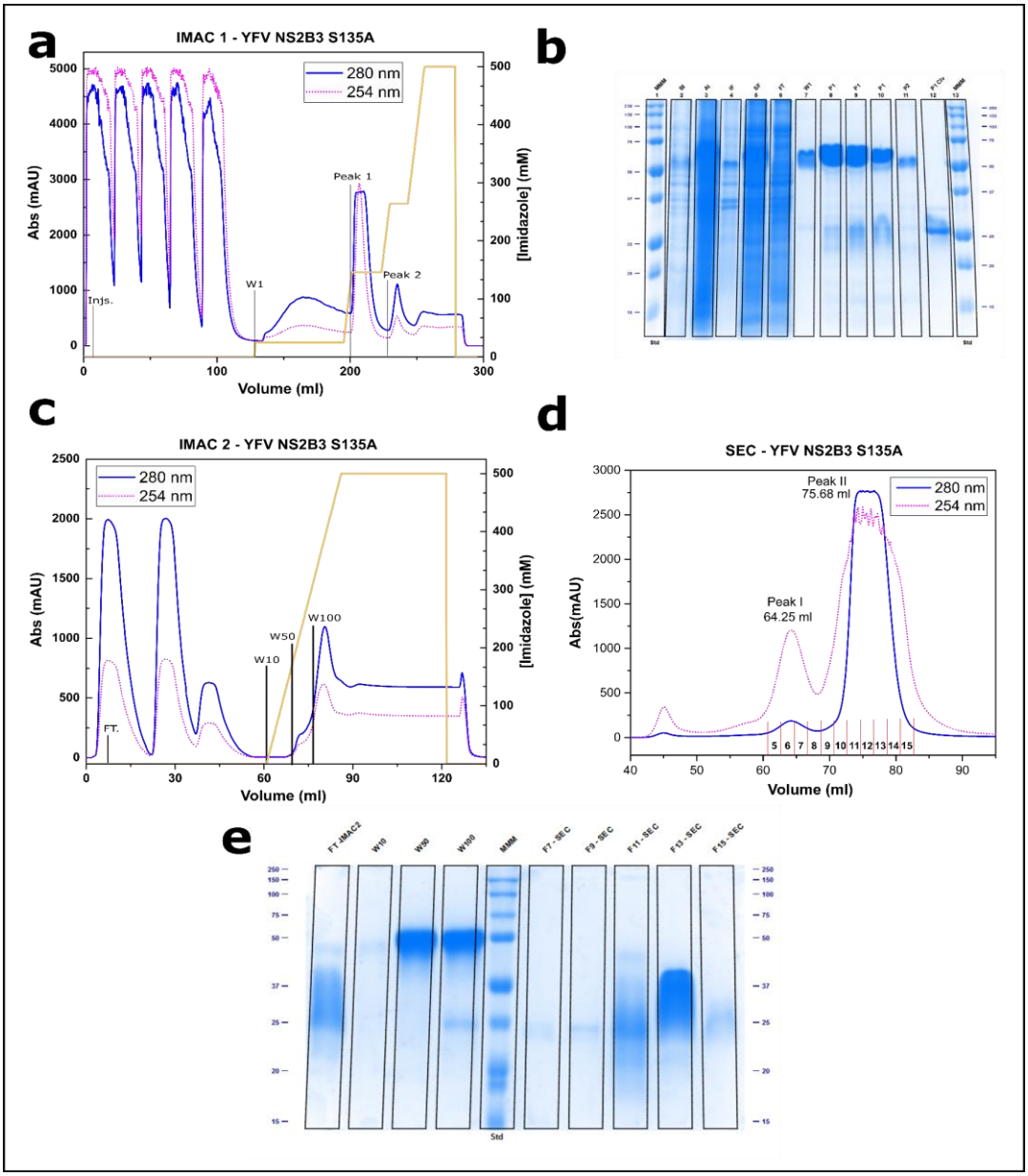

Figure 5.4 – **Purification of YFV NS2B3^{S138A} protease.** In **a**, IMAC 1 chromatogram shows peaks of injection (Injs.), wash (W1) and elution (Peak 1 and Peak 2). In **b**, SDS-PAGE showing fractions representing the main steps of IMAC 1 (molecular mass marker -MMM, culture medium samples before induction with IPTG - BI and after - AI, insoluble fraction - IF, soluble fraction - SF, unbound flow-through - FT, wash 1 - W1, fractions along elution peak 1 - P1, and elution peak 2 - P2, fraction of peak 1 after dialysis and cleavage with TEV protease - P1-Clv). In **c**, IMAC 2 chromatogram shows the injection and unbound flow-through (FT) peaks, wash 1 (W50) and wash 2 (W100). In **d**, SEC chromatogram shows peaks I and II, referring to the dimeric and monomeric states. In **e**, SDS-PAGE showing the main fractions displayed in the chromatograms in c. and d.

Source: By the author.

By inspecting the chromatograms and the polyacrylamide gels (Figure 5.3 and Figure 5.4), it can be seen that the proteins were purified in a soluble form and with a satisfactory degree of purity. Furthermore, there is a particular difference in the elution pattern of the two samples in size exclusion chromatography. While the YFV protease NS2B3^{S138A} has a major

monomeric peak II and a small dimeric peak I (panel d in Figure 5.4), the ZIKV protease peaks I and II have the same intensity, indicating a larger population of dimers in solution (peak I) (panel d in Figure 5.3). Moreover, the presence of an additional small peak on the leading edge of peak I in the ZIKV SEC chromatogram can be observed, suggesting that even higher oligomeric states (trimers, tetramers) might be present, depending on the concentration of the samples.

5.3.1 An oligomeric state analysis of the flaviviral proteases (SEC-MALS)

SEC-MALS analyses (Figure 5.5) were done to confirm the oligomeric states of the flaviviral proteases observed in the SEC purifications described previously. Therefore, we quantitatively assessed their molecular weight and further explored the dependence of these oligomeric states upon variation of the protein concentration. For both ZIKV and YFV, these samples represented the fractions obtained from peak II, predicted to have the lowest oligomeric state (panel d, in Figure 5.3 and Figure 5.4). The corresponding eluted fractions (peak II) from the wild type versions of these proteases (kindly provided by CIBFar) were also analysed.

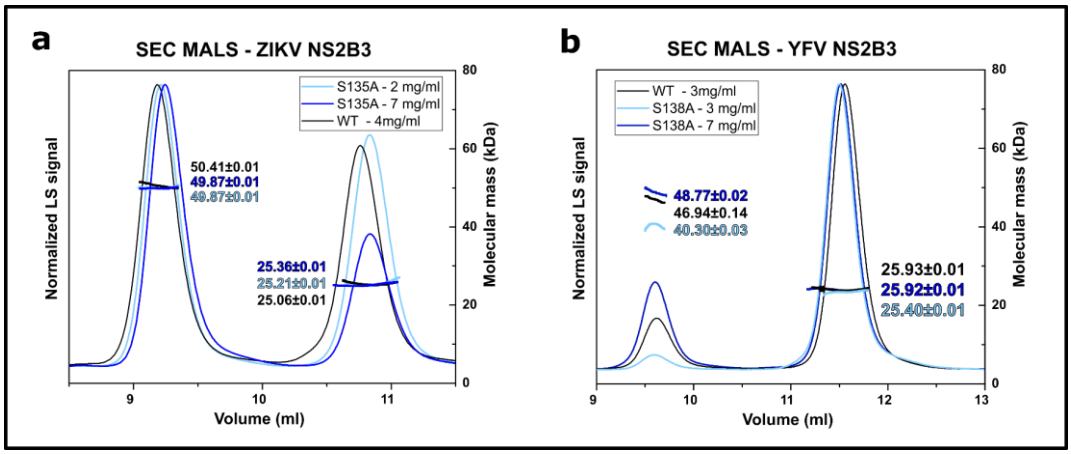

Figure 5.5 – **SEC-MALS profiles of ZIKV and YFV NS2B3 proteases (natives WT and inactive mutants).** In **a**, SEC-MALS profile of ZIKV NS2B3 protease (native version – WT and mutant – S135A) and in **b**, similar data for YFV NS2B3 protease (native version – WT and mutant – S138A). In light blue, the chromatograms and mass distributions across the dimeric and monomeric peaks for the ZIKV mutant protease, at a concentration of 2 mg/ml (in **a**), and for the YFV mutant at 3 mg/ml (displayed in **b**), are shown. The same parameters are shown in dark blue for higher concentrations (7 mg/ml) of these inactive proteases. In black, the elution profiles of the native proteases are represented; these proteins were injected at 4 mg/ml for ZIKV and 3 mg/ml for YFV. Average values for molecular masses in kDa are shown alongside the peaks.

Source: By the author.

Firstly, we do not observe any significant difference in the elution profile (Figure 5.5) resulting from the introduction of mutations on these proteases. In other words, comparing the

wild type versions with the mutants, both showed a monomer-dimer equilibrium, which seems to be influenced by the protein concentration in the sample, also noticed in different runs during SEC purifications, varying the concentrations of the injected samples.

Analysing the ZIKV NS2B3 protease in solution (Figure 5.5, panel a), a slightly higher percentage of dimers in solution than monomers was detected, directly dependent on the protein concentration (the relative height of the monomeric peak decreases on increasing the concentration, which is the opposite to the behaviour of the dimeric fraction, which grows). However, there is no significant change in the molecular mass values upon variations of the protein concentration, as expected.

From the analysis of the SEC-MALS profile for the YFV protease (Figure 5.5, panel b), it can be seen that an equilibrium of monomers and dimers in solution also occurs. On the other hand, differently from what was observed for the ZIKV protease, the samples containing the YFV proteases are composed of a more significant fraction of monomers in solution and, even increasing the protein concentrations, the predominance of dimers in solution could not be accomplished, as observed in the case of the protease from ZIKV. Changes in the profile of the oligomeric state are shown to have a considerable impact on the catalytic activity of some viral proteases. [77] The predominance of dimers in solution for the ZIKV protease might, thus, help and have some influence, in addition to other factors, on the intrinsically enhanced catalytic activity of this protease, compared to other flaviviral proteases.

5.3.2 Confirming the loss of catalytic activity in the mutant flaviviral proteases through *in vitro* proteolytic assays

After confirming the oligomeric states, we used the same fractions to test the effectiveness of the site-directed mutation in removing the catalytic activity of the flaviviral proteases. For this purpose, we compared the proteolytic activity of the mutants to the wild-type proteases measured by the cleavage of the fluorescent substrate (Bz-Nle-Lys-Lys-Arg-AMC). The results are shown below in Table 5.1.

Table 5.1 – Proteolytic activity assay with flaviviral proteases.

	ZIKV NS2B3 WT	**ZIKV NS2B3 S135A**	**YFV NSB3 WT**	**YFV NS2B3 S138A**	**Blank (buffer)**
Fluorescence after cleavage assay (AU)	$(9.16\pm0.08)10^6$	$(1.22\pm0.02)10^5$	$(1.81\pm0.08)10^6$	$(1.21\pm0.01)10^5$	$(1.25\pm0.01)10^5$
Relative activity (%) compared to the WT*	100%	0% (-3.35%)	100%	0% (-21.11%)	-

*Relative activity formula: [(Value-Blank)/WT].

Source: By the author.

It is possible to observe from Table 5.1 that the mutations from serines to alanines in the proteases were effective in removing the catalytic activities, as expected. Negative percentage values occurred due to measurements being taken at the lower sensitivity limit of the equipment. Additionally, it is possible to observe that the ZIKV protease is almost five times more effective in cleaving this specific fluorescent substrate (Bz-Nle-Lys-Lys-Arg-AMC) than the YFV protease.

5.4 Interaction and complex formation between septins and ZIKV inactive protease

5.4.1 Pull-down assay with septins and ZIKV inactive protease

After standardizing the expression and purification protocols for the inactive proteases and validating the mutations and inactivation of their catalytic activity through proteolytic assays, we started the co-purification assays with septins containing the cleavage site, aiming to obtain a stable complex between these proteins, which would enable further studies.

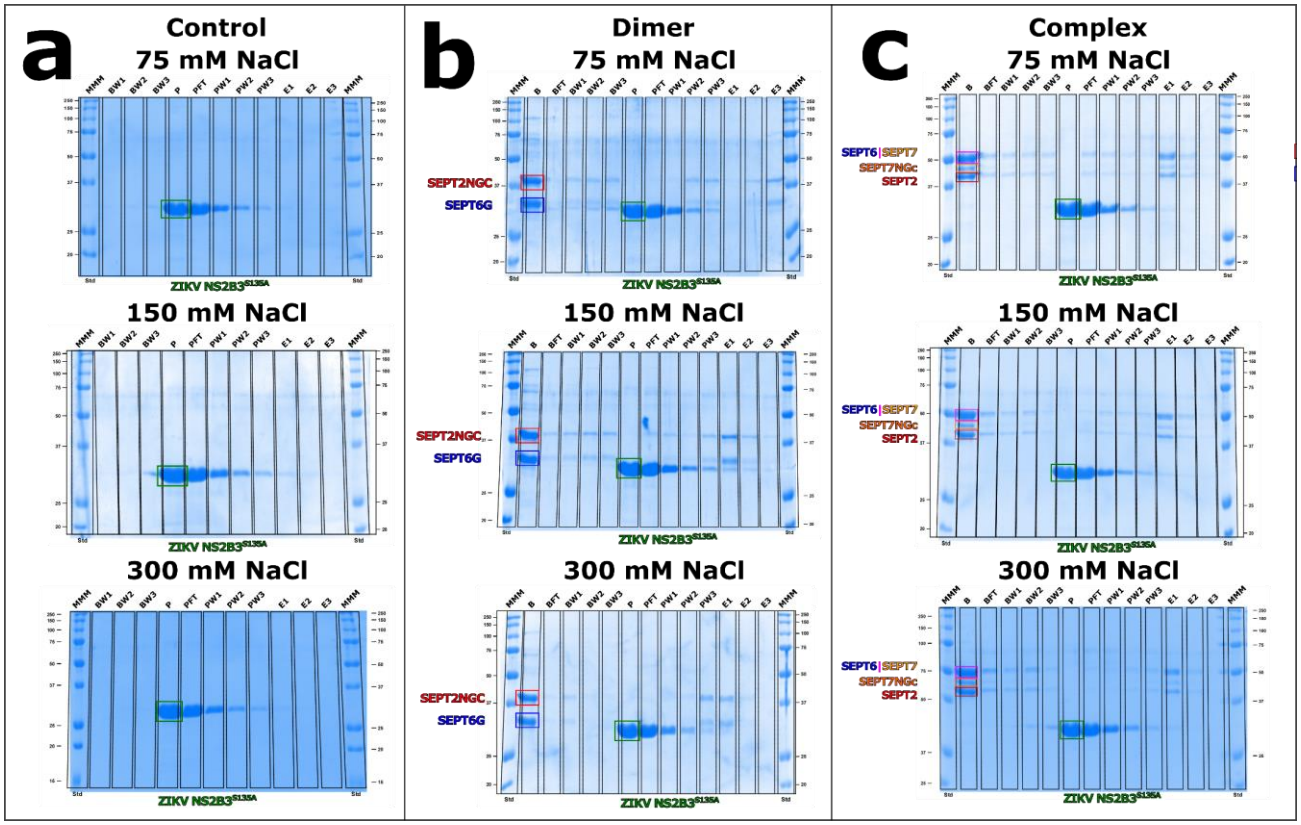

Figure 5.6 – **Co-purification of septins and ZIKV inactive protease.** SDS-PAGE of the affinity chromatography co-purification assay using ZIKV NS2B3^{S135A} (as prey) and different baits. Proteins used as baits: in **a** - control (without septins), in **b** - Dimer (2NGC-6G), and in **c** - Complex (2NGC-6NGC-7NGC). The main steps are shown for each SDS-PAGE (molecular mass marker -MMM, septins used as bait -B, unbound flowthrough after loading the bait –BFT, washes after loading the bait -BW1/BW2, inactive ZIKV protease used as prey -P, unbound flowthrough after loading the prey - PFT, washes after loading the prey -PW1 to PW3, protein elution -E1 to E3.

Source: By the author.

Evaluating the elution profile (Figure 5.6) of the pull-downs using the inactive ZIKV NS2B3 protease as prey (whose His-tag had been previously cleaved) and the septins as bait (containing His-tag and therefore enable to bind the IMAC column), and comparing it with the control samples (without the septin as bait), it can be seen that for both the SEPT2NGC-6G heterodimer and the WT hexameric complex (SEPT2NGC-6NGC-7NGC) there is no significant co-elution of the proteases and septins, which would characterize the formation of a stable complex between them.

Under some conditions (mainly in assays with the SEPT2NGC-6G heterodimer), it is possible to see a small band in the elution fraction, which might correspond to the inactive protease band co-eluted with these septins. However, the protease band is not equimolar (in intensity) with the septin bands on the same lane, and this protease is also observed in the control sample without any septin. New assays with more extensive washes were performed, but it was not possible to observe a significant co-elution of the proteins, characterising the formation of a stable complex. Different buffers varying the ionic strength concentration were also tested in order to assess their effects on the interaction; nevertheless, no significant differences were observed in the elution profile during the co-purification assay.

5.4.2 SEC-MALS analysis of the incubation between septins and ZIKV inactive protease

Additionally, the formation of a stable complex between the inactive ZIKV protease and the septins was evaluated by SEC-MALS (Figure 5.7). The inactive protease and the septin heterodimer (2NGC-6G) were incubated to allow the formation of the complex, and after some time, the oligomeric states present in the solution were analysed.

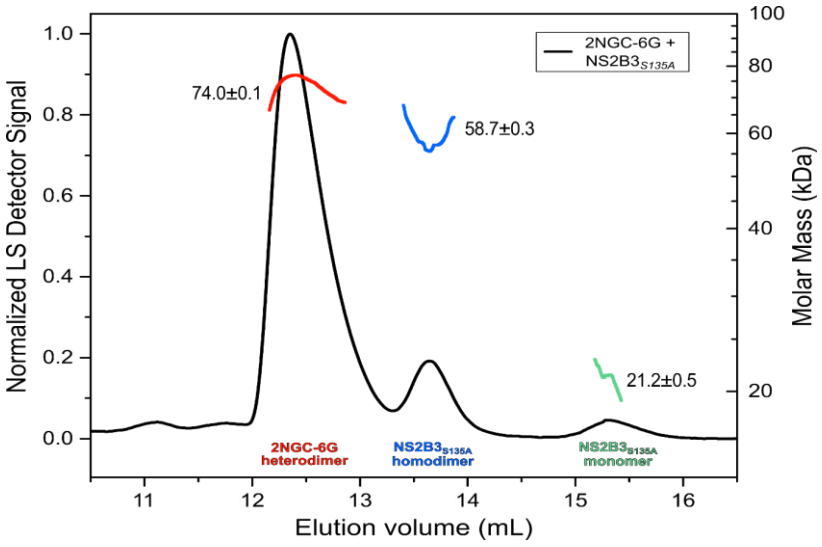

Figure 5.7 – **SEC-MALS profile of 2NGC-6G dimer incubated with ZIKV NS2B3^{S135A} protease.** Values for the molecular masses are shown beside the peaks.

Source: By the author.

Supporting the data obtained by the co-purification assay (Figure 5.6), it was not possible to observe any significant fraction of complexes formed between these proteins (Figure 5.7). Possibly, the interaction may have a transient nature, being therefore not very stable in solution, or it is also possible that the interaction site is not so accessible on the conditions of the experiment.

Moreover, as a large part of the sample in solution is dissociated from a possible complex between the proteins, the degree of heterogeneity in this sample was very high, making it difficult to attempt crystallization assays using these full-length septin constructions.

5.4.3 Co-crystallization assays with SEPT2 peptides containing the cleavage residues

Therefore, in order to increase the chances of obtaining a crystal from a complex involving the inactive protease and septins, we order a synthetic peptide covering the cleavage region on the SEPT2 ($_{303}$RLKRGGRK$_{310}$) in order to try to perform co-crystallization experiments with the apo inactive protease.

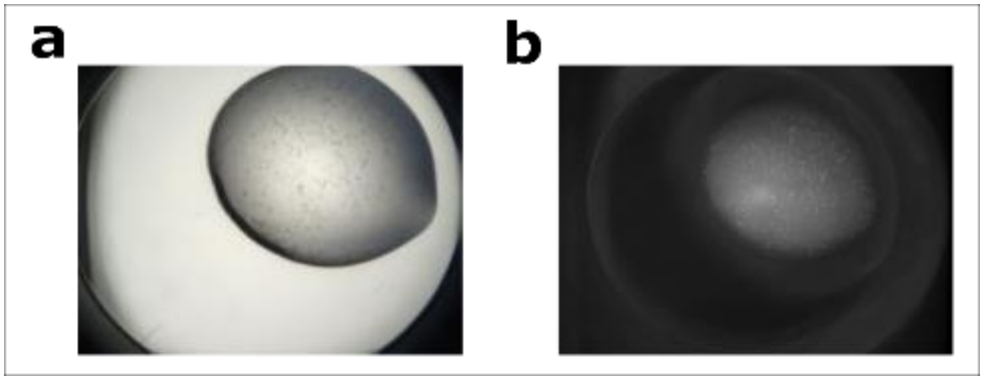

Figure 5.8 – **Microcrystals observed in the crystallization assays of the ZIKV NS2B3^{S135A} protease incubated with a peptide covering the cleavage region on the SEPT2.** In **a**, it is shown a drop containing microcrystals on the condition D10 of the crystallization kit PACT Premier™ (0.2 M $MgCl_2$, 0.1 M Tris pH 8.0 and 20 % w/v Polyethylene Glycol 6000). In **b**, the same region was illuminated with UV highlighting the microcrystals.

Source: By the author.

Many microcrystals were observed in these assays, as shown in Figure 5.8, validating the purpose of this experiment. New crystallization assays, expanding the conditions and increasing the initial protein concentration utilized for this experiment may be the key to getting and increasing the chances of larger diffracting crystals. Thus far, none of these microcrystals has been harvested, or diffraction tested. If successful in the future, it is expected to shed light on the understanding of the critical interactions involving the protease

and the septin. This may possibly help in designing inhibitors and drugs to fight ZIKV/YFV infections, as viral proteases are known to be excellent targets for antivirals. [96]

5.5 Conclusion

By analysing the interactions involving septins and flaviviral proteases, we were able to demonstrate an increased specificity of the ZIKV NS2B3 protease for SEPT2 compared to its YFV counterpart, allowing us to observe a more pronounced cleavage activity through a more intense band. The primary explanation for this effect may possibly be related to the higher correspondence between the preferential residues (Arg in P1 and Lys in P2) in the cleavage sites recognized by ZIKV NS2B3 protease and the SEPT2 sequence ($_{305}$KRGGRK$_{310}$), compared to those of YFV (which prefers Arg in both positions). Likewise, an additional justification for this effect might come from the intrinsically higher catalytic activity of the ZIKV NS2B3 compared to the YFV counterpart. In this regard, we also noticed a substantial difference in the oligomeric state profile and in the equilibrium dimer-monomer of these two proteases in solution: whereas the YFV protease dimer-monomer equilibrium is shifted towards monomers, the ZIKV NS2B3 protease was found to be encountered mainly as a dimer in solution. This change in the oligomerization profile in solution might help and have some influence on the intrinsically enhanced catalytic activity of ZIKV, in addition to other factors (*e.g.*, modification in the residues in the sequence). Finally, we were not able to observe a stable complex between full-length septin and the mutant ZIKV protease, indicating that the cleavage might occur through a transient interaction between the proteins (corroborating the low efficiency observed *in vitro*). Further studies employing short peptides concerning the cleavage site of SEPT2, aiming at obtaining structural information of this interaction, should be encouraged.

6 FINAL REMARKS AND FUTURE PERSPECTIVES

With these studies, we were able to show the importance and the influence of the C-terminal domains of septins on heterocomplex stability, filament polymerization, and morphology of high-order structures. Although some of these functions were shown to be accomplished even in the absence of this domain, it was shown that do they play a central role in tuning the septin concentrations required for the formation of filaments and bundles and also on the stability of all structures analysed (from complexes to bundles). More interestingly, with these experiments, we showed the direct influence of the ZIKV protease cleavage on the SEPT2 by mimicking this with a truncated version of SEPT2, which was shown to abrogate the filament polymerization under physiological concentrations. Substantial differences were also found at a sequence level for this cleavage region on SEPT2, compared to the other members of the same group. These differences might be important for some specific functions performed by SEPT2 but not its counterparts, but further studies are needed to address these specificities, both at the molecular and cellular levels.

Moreover, we were able to show an enhanced activity of ZIKV NS2B3 protease on SEPT2 compared with the protease from YFV. This greater efficiency was not only due to an intrinsic higher activity of the wild-type ZIKV protease, but also a higher degree of similarity between the preferred residues of this protease and the sequence of SEPT2, something not observed when the same SEPT2 sequence is compared with the preferred residues of the YFV protease. Nevertheless, even this more specific interaction between SEPT2 and the ZIKV protease was shown to be possibly transient during the cleavage. Further attempts are encouraged in order to get a stable intermediate complex between a synthesized peptide (encompassing this cleavage region on SEPT2) and the catalytically inactive ZIKV protease, which in case of success can possibly be convenient for the development of new compounds to stop the protease cleavage of the SEPT2 and, therefore, possibly, hampering the development of the microcephaly.

REFERENCES

1 SEVER, J. L. Viruses as teratogens. *In*: JOHNSON, E.; MARSHALLAND KOCHHAR, D. M. (ed.). **Teratogenesis and reproductive toxicology**. Berlin, Heidelberg: Springer, 1983. p. 65–73.

2 WEBSTER, W. S. Teratogen update: congenital rubella. **Teratology**, v. 58, n. 1, p. 13–23, July 1998.

3 AHLFORS, K.; IVARSSON, S. A.; HARRIS, S. Report on a long-term study of maternal and congenital cytomegalovirus infection in Sweden. review of prospective studies available in the literature. **Scandinavian Journal of Infectious Diseases**, v. 31, n. 5, p. 443–457, 1999.

4 BUTLER, D. Zika virus: Brazil's surge in small-headed babies questioned by report. **Nature**, v. 530, n. 7588, p. 13–14, Jan. 2016.

5 WORLD HEALTH ORGANIZATION **(WHO)**. Global overview - Zika epidemiology update. July 2019. Available from: https://www.who.int/emergencies/diseases/zika/zika-epidemiology-update-july-2019.pdf. Accessible at: 23 Jan. 2021.

6 GUTIÉRREZ, L. **PAHO/WHO Data**. Available from: http://www.paho.org/data/index.php/en/?option=com_content&view=article&id=524&Itemid=352.Accessible at: 3 Sept. 2019.

7 HEYMANN, D. L. *et al.* Zika virus and microcephaly: why is this situation a PHEIC? **Lancet**, v. 387, n. 10020, p. 719–721, Feb. 2016.

8 MLAKAR, J. *et al.* Zika virus associated with microcephaly. **New England Journal of Medicine**, v. 374, n. 10, p. 951–958, Mar. 2016.

9 ARAGAO, M. F. V. *et al.* Clinical features and neuroimaging (CT and MRI) findings in presumed Zika virus related congenital infection and microcephaly: retrospective case series study. **BMJ**, v. 353, Apr. 2016. DOI: 10.1136/bmj.i3182.

10 ZARE MEHRJARDI, M. *et al.* Neuroimaging findings of postnatally acquired Zika virus infection: a pictorial essay. **Japanese Journal of Radiology**, v. 35, n. 7, p. 341–349, July 2017.

11 WEN, Z.; SONG, H.; MING, G. L. How does Zika virus cause microcephaly? **Genes and Development**, v. 31, n. 9, p. 849–861, 2017.

12 TANG, H. *et al.* Zika virus infects human cortical neural progenitors and attenuates their growth. **Cell Stem Cell**, v. 18, n. 5, p. 587–590, May 2016.

13 LI, H. *et al.* The neurobiology of Zika Virus. **Neuron**, v. 92, n. 5, p. 949–958, Dec. 2016.

14 LIANG, Q. *et al.* Zika Virus NS4A and NS4B proteins deregulate Akt-mTOR signaling in human fetal neural stem cells to inhibit neurogenesis and induce autophagy. **Cell Stem Cell**, v. 19, n. 5, p. 663–671, 2016.

15 LINDENBACH, B. D. *et al.* Flaviviridae. *In*: KNIPE, D. M.; HOWLEY, P. M. (ed.). **Fields virology**. 6th ed. Philadelphia: LWW, 2013. p. 712–746.

16 PIERSON, T. C.; DIAMOND, M. S. Flaviviruses. *In*: KNIPE, D. M.; HOWLEY, P. M. (ed.). **Fields virology**. 6th ed. Philidelphia: LWW, 2013. p. 747–794.

17 YOON, K.-J. *et al.* Zika-Virus-Encoded NS2A disrupts mammalian cortical neurogenesis by degrading adherens junction proteins. **Cell Stem Cell**, v. 21, n. 3, p. 349-358.e6, 2017.

18 HILL, M. E. *et al.* The unique cofactor region of Zika Virus NS2B-NS3 protease facilitates cleavage of key host proteins. **ACS Chemical Biology**, v. 13, n. 9, p. 2398–2405, Sept. 2018.

19 LI, H. *et al.* Zika Virus protease cleavage of host protein septin-2 mediates mitotic defects in neural progenitors. **Neuron**, v. 101, n. 6, p. 1089- 1098.e4, Mar. 2019.

20 HARTWELL, L. H.; CULOTTI, J.; REID, B. Genetic control of the cell-division cycle in yeast. I. detection of mutants. **Proceedings of the National Academy of Sciences**, v. 66, n. 2, p. 352–359, June 1970.

21 HARTWELL, L. H. Genetic control of the cell division cycle in yeast: IV. genes controlling bud emergence and cytokinesis. **Experimental Cell Research**, v. 69, n. 2, p. 265–276, Dec. 1971.

22 HARTWELL, L. H. *et al.* Genetic control of the cell division cycle in yeast. **Science**, v. 183, n. 4120, p. 46 LP – 51, Jan. 1974.

23 BYERS, B.; GOETSCH, L. A highly ordered ring of membrane-associated filaments in budding yeast. **Journal of Cell Biology**, v. 69, n. 3, p. 717–21, June 1976.

24 HAARER, B. K.; PRINGLE, J. R. Immunofluorescence localization of the Saccharomyces cerevisiae CDC12 gene product to the vicinity of the 10-nm filaments in the mother-bud neck. **Molecular and Cellular Biology**, v. 7, n. 10, p. 3678 LP – 3687, Oct. 1987.

25 FORD, S. K.; PRINGLE, J. R. Cellular morphogenesis in the Saccharomyces cerevisiae cell cycle: localization of the CDC11 gene product and the timing of events at the budding site. **Developmental Genetics**, v. 12, n. 4, p. 281–292, 1991.

26 KIM, H. B.; HAARER, B. K.; PRINGLE, J. R. Cellular morphogenesis in the Saccharomyces cerevisiae cell cycle: localization of the CDC3 gene product and the timing of events at the budding site. **Journal of Cell Biology**, v. 112, n. 4, p. 535–44, Feb. 1991.

27 DIDOMENICO, B. J. *et al.* Homologs of the yeast neck filament associated genes: isolation and sequence analysis of Candida albicans CDC3 and CDC10. **Molecular and General Genetics MGG**, v. 242, n. 6, p. 689–698, Mar. 1994.

28 HARRIS, S. D.; MORRELL, J. L.; HAMER, J. E. Identification and characterization of Aspergillus nidulans mutants defective in cytokinesis. **Genetics**, v. 136, n. 2, p. 517–532, Feb. 1994.

29 NGUYEN, T. Q. *et al.* The C. elegans septin genes, unc-59 and unc-61, are required for normal postembryonic cytokineses and morphogenesis but have no essential function in embryogenesis. **Journal of Cell Science**, v. 113, n. 21, p. 3825 LP – 3837, Nov. 2000.

30 FIELD, C. M. *et al.* A purified Drosophila septin complex forms filaments and exhibits GTPase activity. **Journal of Cell Biology**, v. 133, n. 3, p. 605–616, May 1996.

31 WLOGA, D. *et al.* Septins stabilize mitochondria in Tetrahymena thermophila.

Eukaryotic Cell, v. 7, n. 8, p. 1373–1386, Aug. 2008.

32 NISHIHAMA, R.; ONISHI, M.; PRINGLE, J. R. New insights into the phylogenetic distribution and evolutionary origins of the septins. **Biological Chemistry**, v. 392, n. 8–9, p. 681–687, Aug. 2011.

33 PINTO, A. P. A. *et al.* Filaments and fingers: novel structural aspects of the single septin from Chlamydomonas reinhardtii. **Journal of Biological Chemistry** , v. 292, n. 26, p. 10899–10911, June 2017.

34 SPILIOTIS, E. T.; KINOSHITA, M.; NELSON, W. J. A Mitotic septin scaffold required for mammalian chromosome congression and segregation. **Science**, v. 307, n. 5716, p. 1781 LP – 1785, Mar. 2005.

35 SURKA, M. C.; TSANG, C. W.; TRIMBLE, W. S. The mammalian septin MSF localizes with microtubules and is required for completion of cytokinesis. **Molecular Biology of the Cell**, v. 13, n. 10, p. 3532–3545, Oct. 2002.

36 NAGATA, K. *et al.* Filament formation of MSF-A, a mammalian septin, in human mammary epithelial cells depends on interactions with microtubules. **Journal of Biological Chemistry**, v. 278, n. 20, p. 18538–18543, May 2003.

37 MOSTOWY, S.; COSSART, P. Septins: the fourth component of the cytoskeleton. **Nature Reviews Molecular Cell Biology**, v. 13, n. 3, p. 183–194, Mar. 2012.

38 KARTMANN, B.; ROTH, D. Novel roles for mammalian septins: from vesicle trafficking to oncogenesis. **Journal of Cell Science**, v. 114, n. 5, p. 839 LP – 844, Mar. 2001.

39 KINOSHITA, M. Diversity of septin scaffolds. **Current Opinion in Cell Biology**, v. 18, n. 1, p. 54–60, Feb. 2006.

40 FINGER, F. P.; KOPISH, K. R.; WHITE, J. G. A role for septins in cellular and axonal migration in C. elegans. **Developmental Biology**, v. 261, n. 1, p. 220–234, Sept. 2003.

41 BEITES, C. L. *et al.* The septin CDCrel-1 binds syntaxin and inhibits exocytosis. **Nature Neuroscience**, v. 2, n. 5, p. 434–439, 1999.

42 LARISCH, S. *et al.* A novel mitochondrial septin-like protein, ARTS, mediates apoptosis dependent on its P-loop motif. **Nature Cell Biology**, v. 2, n. 12, p. 915–921, 2000.

43 SIRAJUDDIN, M. *et al.* Structural insight into filament formation by mammalian septins. **Nature**, v. 449, n. 7160, p. 311–315, Sept. 2007.

44 JOHN, C. M. *et al.* The Caenorhabditis elegans septin complex is nonpolar. **EMBO Journal**, v. 26, n. 14, p. 3296–3307, 2007.

45 BERTIN, A. *et al.* Saccharomyces cerevisiae septins: supramolecular organization of heterooligomers and the mechanism of filament assembly. **Proceedings of the National Academy of Sciences**, v. 105, n. 24, p. 8274–8279, June 2008.

46 CASAMAYOR, A.; SNYDER, M. Molecular dissection of a yeast septin: distinct domains are required for septin interaction, localization, and function. **Molecular and Cellular Biology**, v. 23, n. 8, p. 2762–2777, Apr. 2003.

47 GARCIA, W. *et al.* Dissection of a human septin: definition and characterization of

distinct domains within human SEPT4. **Biochemistry**, v. 45, n. 46, p. 13918–13931, Nov. 2006.

48 ZHANG, J. *et al.* Phosphatidylinositol polyphosphate binding to the mammalian septin H5 is modulated by GTP. **Current Biology**, v. 9, n. 24, p. 1458–1467, Dec. 1999.

49 OMRANE, M. *et al.* Septin 9 has Two polybasic domains critical to septin filament assembly and golgi integrity. **iScience**, v. 13, p. 138–153, Mar. 2019. DOI: 10.1016/j.isci.2019.02.015.

50 KREMER, B. E.; HAYSTEAD, T.; MACARA, I. G. Mammalian septins regulate microtubule stability through interaction with the microtubule-binding protein MAP4. **Molecular Biology of the Cell**, v. 16, n. 10, p. 4648–4659, Oct. 2005.

51 KAY, B. K.; WILLIAMSON, M. P.; SUDOL, M. The importance of being proline: the interaction of proline-rich motifs in signaling proteins with their cognate domains. **FASEB Journal**, v. 14, n. 2, p. 231–241, Feb. 2000.

52 CAO, L. *et al.* Phylogenetic and evolutionary analysis of the septin protein family in metazoan. **FEBS Letters**, v. 581, n. 28, p. 5526–5532, Nov. 2007.

53 VERSELE, M. *et al.* Protein–protein interactions governing septin heteropentamer assembly and septin filament organization in saccharomyces cerevisiae. **Molecular Biology of the Cell**, v. 15, n. 10, p. 4568–4583, July 2004.

54 MARQUES, I. A. *et al.* Septin C-terminal domain interactions: implications for filament stability and assembly. **Cell Biochemistry and Biophysics**, v. 62, n. 2, p. 317–328, Mar. 2012.

55 SALA, F. A. *et al.* Heterotypic coiled-coil formation is essential for the correct assembly of the septin heterofilament. **Biophysical Journal**, v. 111, n. 12, p. 2608–2619, Dec. 2016.

56 BERTIN, A. *et al.* Phosphatidylinositol-4,5-bisphosphate Promotes Budding Yeast Septin Filament Assembly and Organization. **Journal of Molecular Biology**, v. 404, n. 4, p. 711–731, Dec. 2010.

57 RUSSELL, S. E. H.; HALL, P. A. Septin genomics: a road less travelled. **Biological Chemistry**, v. 392, n. 8–9, p. 763–767, Aug. 2011.

58 KINOSHITA, M. Assembly of mammalian septins. **Journal of Biochemistry**, v. 134, n. 4, p. 491–496, Oct. 2003.

59 MACARA, I. G. *et al.* Mammalian septins nomenclature. **Molecular Biology of the Cell**, v. 13, n. 12, p. 4111–4113, Dec. 2002.

60 MENDONÇA, D. C. *et al.* An atomic model for the human septin hexamer by cryo-EM. **Journal of Molecular Biology**, v. 433, n. 15, p. 167096, July 2021.

61 JUMPER, J. *et al.* Highly accurate protein structure prediction with AlphaFold. **Nature**, v. 596, n. 7873, p. 583–589, July 2021.

62 MENDONCA, D. C. *et al.* A revised order of subunits in mammalian septin complexes. **Cytoskeleton**, v. 76, n. 9–10, p. 457–466, 2019.

63 SOROOR, F. *et al.* Revised subunit order of mammalian septin complexes explains their

in vitro polymerization properties. **Molecular Biology of the Cell**, v. 32, n. 3, p. 289–300, Feb. 2021.

64 DEROSE, B. T. *et al.* Production and analysis of a mammalian septin hetero-octamer complex. **Cytoskeleton**, v. 77, n. 11, p. 485–499, Nov. 2020.

65 LEI, J. *et al.* Crystal structure of zika virus ns2b-ns3 protease in complex with a boronate inhibitor. **Science**, v. 353, n. 6298, p. 503–505, July 2016.

66 CALVET, G. *et al.* Detection and sequencing of Zika virus from amniotic fluid of fetuses with microcephaly in Brazil: a case study. **Lancet Infectious Diseases**, v. 16, n. 6, p. 653–660, June 2016.

67 MYSOREKAR, I. U. Zika Virus takes a transplacental route to infect fetuses: insights from an animal model. **Missouri Medicine**, v. 114, n. 3, p. 168, 2017.

68 ROSA, H. V. D. *et al.* Molecular recognition at septin interfaces: the switches hold the key. **Journal of Molecular Biology**, v. 432, n. 21, p. 5784–5801, Oct. 2020.

69 LEONARDO, D. A. *et al.* Orientational ambiguity in septin coiled coils and its structural basis. **Journal of Molecular Biology**, v. 433, n. 9, p. 166889, Apr. 2021.

70 KUMAR, S. *et al.* MEGA X: molecular evolutionary genetics analysis across computing platforms. **Molecular Biology and Evolution**, v. 35, n. 6, p. 1547–1549, June 2018.

71 EDGAR, R. C. MUSCLE: multiple sequence alignment with high accuracy and high throughput. **Nucleic Acids Research**, v. 32, n. 5, p. 1792, 2004.

72 SANGER, F.; NICKLEN, S.; COULSON, A. R. DNA sequencing with chain-terminating inhibitors. **Proceedings of the National Academy of Sciences**, v. 74, n. 12, p. 5463–5467, Dec. 1977.

73 MAVRAKIS, M.; TSAI, F. C.; KOENDERINK, G. H. Purification of recombinant human and Drosophila septin hexamers for TIRF assays of actin–septin filament assembly. **Methods in Cell Biology**, v. 136, p. 199–220, Jan. 2016.

74 NOSKE, G. D. *et al.* Structural characterization and polymorphism analysis of the NS2B-NS3 protease from the 2017 Brazilian circulating strain of yellow fever virus. **Biochimica et Biophysica Acta (BBA) -** general subjects, v. 1864, n. 4, p. 129521, Apr. 2020.

75 NAKOS, K.; RADLER, M. R.; SPILIOTIS, E. T. Septin 2/6/7 complexes tune microtubule plus-end growth and EB1 binding in a concentration- And filament-dependent manner. **Molecular Biology of the Cell**, v. 30, n. 23, p. 2913–2928, Nov. 2019.

76 BRIDGES, A. A. *et al.* Septin assemblies form by diffusion-driven annealing on membranes. **Proceedings of the National Academy of Sciences**, v. 111, n. 6, p. 2146–2151, Feb. 2014.

77 NOSKE, G. D. *et al.* A Crystallographic snapshot of SARS-CoV-2 main protease maturation process. **Journal of Molecular Biology**, v. 433, n. 18, p. 167118, Sept. 2021.

78 CAVINI, I. A. *et al.* The structural biology of septins and their filaments: an update. **Frontiers in Cell and Developmental Biology**, v. 9, p. 3246, 19 nov. 2021.

79 DE BREVERN, A. G. *et al.* PredyFlexy: flexibility and local structure prediction from

sequence. **Nucleic Acids Research**, v. 40, n. W1, p. W317–W322, July 2012.

80 FISCHER, M. *et al.* Biochemical characterization of a human septin octamer. **bioRxiv**, p. 2021.09.06.459054, Sept. 2021.

81 IV, F. *et al.* Insights into animal septins using recombinant human septin octamers with distinct SEPT9 isoforms. **Journal of Cell Science**, v. 134, n. 15, Aug. 2021.

82 JOHNSON, C. R. *et al.* Cytosolic chaperones mediate quality control of higher-order septin assembly in budding yeast. **Molecular Biology of the Cell**, v. 26, n. 7, p. 1323–1344, Apr. 2015.

83 SZUBA, A. *et al.* Membrane binding controls ordered self-assembly of animal septins. **eLife**, v. 10, 2021.

84 BRIDGES, A. A. *et al.* Micron-scale plasma membrane curvature is recognized by the septin cytoskeleton. **Journal of Cell Biology**, v. 213, n. 1, p. 23–32, Apr. 2016.

85 CANNON, K. S. *et al.* An amphipathic helix enables septins to sense micrometer-scale membrane curvature. **Journal of Cell Biology**, v. 218, n. 4, p. 1128–1137, 2019.

86 BEBER, A. *et al.* Membrane reshaping by micrometric curvature sensitive septin filaments. **Nature Communications**, v. 10, n. 1, p. 1–12, Dec. 2019.

87 KROKOWSKI, S. *et al.* Septins recognize and entrap dividing bacterial cells for delivery to lysosomes. **Cell Host and Microbe**, v. 24, n. 6, p. 866- 874.e4, Dec. 2018.

88 HASEGAWA, J.; STRUNK, B. S.; WEISMAN, L. S. PI5P and PI(3,5)P2: minor, but essential phosphoinositides. **Cell Structure and Function**, v. 42, n. 1, p. 49, 2017.

89 JIAO, F. *et al.* The hierarchical assembly of septins revealed by high-speed AFM. **Nature Communications**, v. 11, n. 1, p. 1–13, Dec. 2020.

90 TAVENEAU, C. *et al.* Synergistic role of nucleotides and lipids for the self-assembly of Shs1 septin oligomers. **Biochemical Journal**, v. 477, n. 14, p. 2697–2714, July 2020.

91 TANAKA-TAKIGUCHI, Y.; KINOSHITA, M.; TAKIGUCHI, K. Septin-mediated uniform bracing of phospholipid membranes. **Current Biology**, v. 19, n. 2, p. 140–145, Jan. 2009.

92 LEONARDO, D. A. *et al.* Orientational ambiguity in septin coiled coils and its structural basis. **Journal of Molecular Biology**, v. 433, n. 9, p. 166889, Feb. 2021.

93 FRAZIER, J. A. *et al.* Polymerization of purified yeast septins: evidence that organized filament arrays may not be required for septin function. **Journal of Cell Biology**, v. 143, n. 3, p. 737–749, Nov. 1998.

94 GRUBA, N. *et al.* Substrate profiling of Zika virus NS2B-NS3 protease. **FEBS Letters**, v. 590, n. 20, p. 3459–3468, Oct. 2016.

95 KONDO, M. Y. *et al.* Yellow fever virus NS2B/NS3 protease: hydrolytic properties and substrate specificity. **Biochemical and Biophysical Research Communications**, v. 407, n. 4, p. 640–644, Apr. 2011.

96 ZHANG, L. *et al.* Crystal structure of SARS-CoV-2 main protease provides a basis for

design of improved a-ketoamide inhibitors. **Science**, v. 368, n. 6489, p. 409–412, Apr. 2020.

APPENDIX – Alignments and Identity Matrixes

Alignment of the N-terminal elongations from some SEPT4 and SEPT9 isoforms

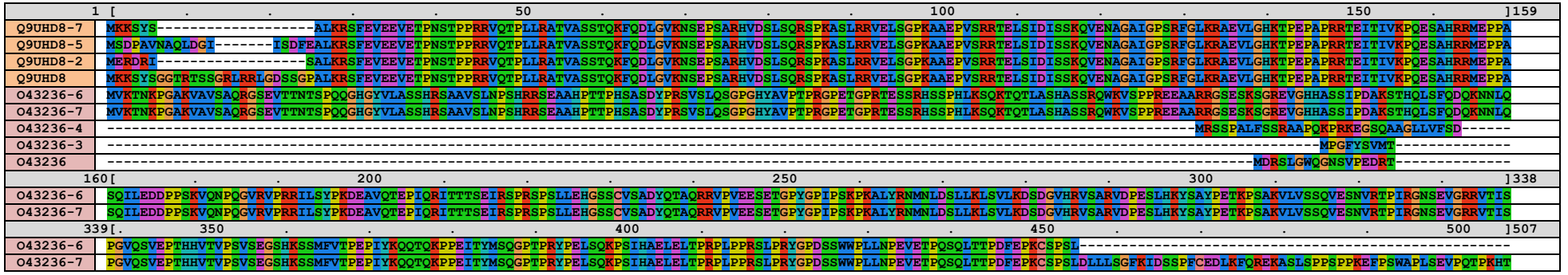

Appendix 1 **Alignment of the N-terminal elongations from the N-terminal domain of the septins 4 and 9.** This table shows the N-terminal elongations of some isoforms from SEPT4 and SEPT9. Amino acids were coloured based on their physicochemical properties. The Uniprot code for each isoform is displayed on the column on the left of the respective sequence. A ruler is also displayed on the top of each column but does not indicate the coordinate of any specific sequence. These N-terminal elongations were displayed here separately from the other parts (shown below in Appendix 2) just to facilitate the visualization.

Source: By the author.

Alignment of the N-terminal domain of all human septin isoforms

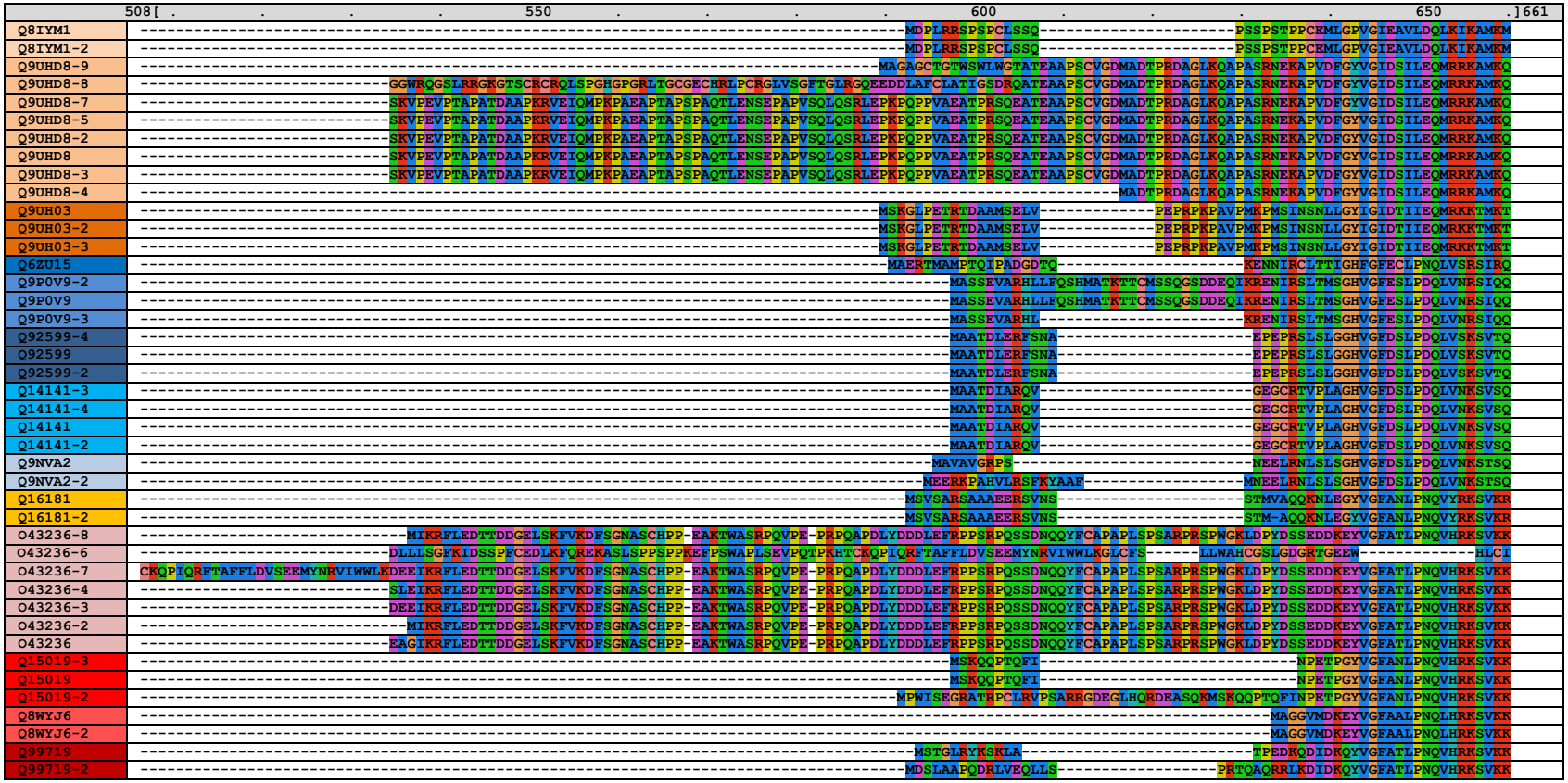

Appendix 2- **Alignment of the sequences from the N-terminal domain of all human septin isoforms.** The table shows the sequence of the N-terminal domain from all human septins isoforms (the downstream part of the sequences displayed in Appendix 1 and the full-length sequence for the other isoforms). Amino acids were coloured based on their physicochemical properties. The Uniprot code for each isoform is displayed on the column on the left of the respective sequence. A ruler is also displayed on the top of each column but does not indicate the coordinate of any specific sequence. The isoform sequences Q92599-2 and O43236-5 were omitted, as they do not possess amino acids within the N-terminal domain.

Source: By the Author.

Alignment of the G-domain of all human septin isoforms

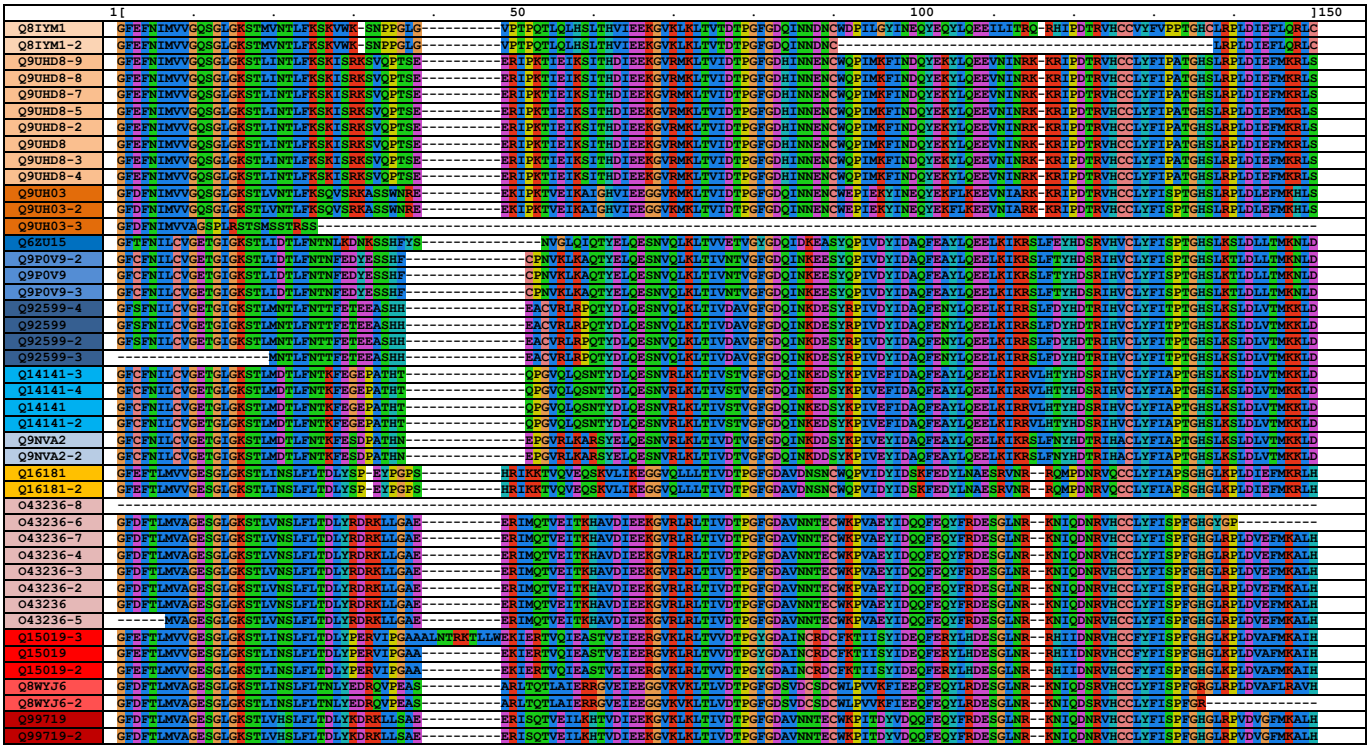

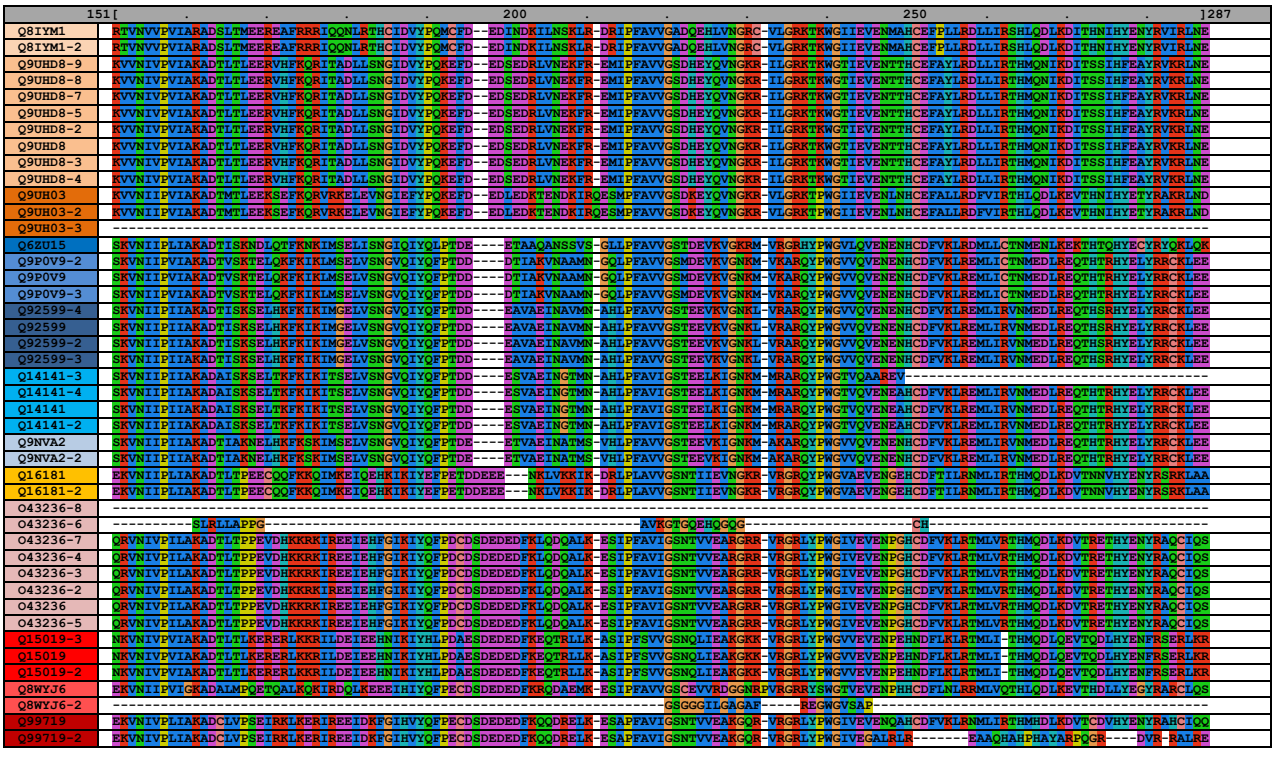

Appendix 3 - **Alignment of the sequences from the G-domain of all human septin isoforms.** The tables show the sequences from the G-domain of all human septin isoforms. Amino acids were coloured based on their physicochemical properties. The Uniprot code for each isoform is displayed on the column on the left of the respective sequence. A ruler is displayed on the top of each table but does not indicate the coordinate of any specific sequence

Source: By the author.

Alignment of the C-terminal domain of all human septin isoforms

Appendix 4 - **Alignment of the sequences from the C-terminal domain of all human septin isoforms.** The table shows the sequences from the C-terminal domain of all human septin isoforms. Amino acids were coloured based on their physicochemical properties. The Uniprot code for each isoform is displayed on the column on the left of the respective sequence. A ruler is displayed on the top but does not indicate the coordinate of any specific sequence.

Source: By the author

Identity matrix of the N-terminal domain sequences from all human septin isoforms

	1	2	3	4	5	6	7	8	9	10	11	12	13	14	15	16	17	18	19	20	21	22	23	24	25	26	27	28	29	30	31	32	33	34	35	36	37	38	39	40	41	42	43	44
1 - Q8IYM1 (1-46)		0.00	0.07	0.07	0.07	0.07	0.07	0.07	0.07	0.09	0.06	0.06	0.06	0.05	0.06	0.06	0.07	0.06	0.06	0.06	n/c	0.06	0.06	0.06	0.06	0.06	0.07	0.06	0.07	0.07	0.00	0.07	0.07	0.07	0.07	0.07	n/c	0.07	0.07	0.05	0.09	0.09	0.07	0.06
2 - Q8IYM1-2 (1-46)	0.00		0.07	0.07	0.07	0.07	0.07	0.07	0.07	0.09	0.06	0.06	0.06	0.05	0.06	0.06	0.07	0.06	0.06	0.06	n/c	0.06	0.06	0.06	0.06	0.06	0.07	0.06	0.07	0.07	0.00	0.07	0.07	0.07	0.07	0.07	n/c	0.07	0.07	0.05	0.09	0.09	0.07	0.06
3 - Q9UHD8-9 (1-71)	0.74	0.74		0.05	0.05	0.05	0.05	0.05	0.05	0.00	0.06	0.06	0.06	0.04	0.04	0.04	0.07	0.07	0.07	0.07	n/c	0.07	0.07	0.07	0.07	0.07	0.06	0.05	0.06	0.04	0.03	0.04	0.04	0.04	0.04	0.04	n/c	0.08	0.08	0.04	0.09	0.09	0.06	0.06
4 - Q9UHD8-8 (1-183)	0.74	0.74	0.23		0.03	0.03	0.03	0.03	0.04	0.00	0.06	0.06	0.06	0.04	0.04	0.04	0.06	0.07	0.07	0.07	n/c	0.07	0.07	0.07	0.07	0.07	0.06	0.05	0.06	0.03	0.02	0.02	0.02	0.03	0.03	0.03	n/c	0.08	0.08	0.04	0.09	0.09	0.07	0.06
5 - Q9UHD8-7 (1-276)	0.72	0.72	0.23	0.64		0.01	0.01	0.00	0.00	0.00	0.06	0.06	0.06	0.05	0.04	0.04	0.06	0.07	0.07	0.07	n/c	0.07	0.07	0.07	0.07	0.07	0.06	0.06	0.06	0.03	0.01	0.02	0.03	0.03	0.03	0.03	n/c	0.08	0.08	0.04	0.09	0.09	0.06	0.06
6 - Q9UHD8-5 (1-288)	0.72	0.72	0.23	0.64	0.02		0.01	0.01	0.00	0.00	0.06	0.06	0.06	0.05	0.04	0.04	0.06	0.07	0.07	0.07	n/c	0.07	0.07	0.07	0.07	0.07	0.06	0.06	0.06	0.03	0.01	0.02	0.03	0.03	0.03	0.03	n/c	0.08	0.08	0.04	0.09	0.09	0.06	0.06
7 - Q9UHD8-2 (1-277)	0.72	0.72	0.23	0.64	0.02	0.02		0.01	0.00	0.00	0.06	0.06	0.06	0.05	0.04	0.04	0.06	0.07	0.07	0.07	n/c	0.07	0.07	0.07	0.07	0.07	0.06	0.06	0.06	0.03	0.01	0.02	0.03	0.03	0.03	0.03	n/c	0.08	0.08	0.04	0.09	0.09	0.06	0.06
8 - Q9UHD8 (1-295)	0.72	0.72	0.23	0.64	0.00	0.06	0.02		0.00	0.00	0.06	0.06	0.06	0.05	0.04	0.04	0.06	0.07	0.07	0.07	n/c	0.07	0.07	0.07	0.07	0.07	0.06	0.06	0.06	0.03	0.01	0.02	0.03	0.03	0.03	0.03	n/c	0.08	0.08	0.04	0.09	0.09	0.06	0.06
9 - Q9UHD8-3 (1-131)	0.72	0.72	0.23	0.56	0.00	0.00	0.00	0.00		0.00	0.06	0.06	0.06	0.05	0.04	0.04	0.06	0.07	0.07	0.07	n/c	0.07	0.07	0.07	0.07	0.07	0.06	0.06	0.06	0.03	0.02	0.03	0.03	0.03	0.03	0.03	n/c	0.08	0.08	0.04	0.09	0.09	0.06	0.06
10 - Q9UHD8-4 (1-44)	0.61	0.61	0.00	0.00	0.00	0.00	0.00	0.00	0.00		0.08	0.08	0.08	0.07	0.06	0.06	0.08	0.09	0.09	0.09	n/c	0.09	0.09	0.09	0.09	0.09	0.08	0.08	0.08	0.06	0.06	0.06	0.06	0.06	0.06	0.06	n/c	0.10	0.10	0.06	0.09	0.09	0.08	0.08
11 - Q9UH03 (1-58)	0.74	0.74	0.72	0.72	0.71	0.71	0.71	0.71	0.71	0.63		0.00	0.00	0.04	0.03	0.03	0.04	0.06	0.06	0.06	n/c	0.06	0.06	0.06	0.06	0.07	0.07	0.07	0.07	0.05	0.02	0.05	0.05	0.05	0.05	0.05	n/c	0.07	0.07	0.05	0.08	0.08	0.06	0.06
12 - Q9UH03-2 (1-58)	0.74	0.74	0.72	0.72	0.71	0.71	0.71	0.71	0.71	0.63	0.00		0.00	0.04	0.03	0.03	0.04	0.06	0.06	0.06	n/c	0.06	0.06	0.06	0.06	0.07	0.07	0.07	0.07	0.05	0.02	0.05	0.05	0.05	0.05	0.05	n/c	0.07	0.07	0.05	0.08	0.08	0.06	0.06
13 - Q9UH03-3 (1-58)	0.74	0.74	0.72	0.72	0.71	0.71	0.71	0.71	0.71	0.63	0.00	0.00		0.04	0.03	0.03	0.04	0.06	0.06	0.06	n/c	0.06	0.06	0.06	0.06	0.07	0.07	0.07	0.07	0.05	0.02	0.05	0.05	0.05	0.05	0.05	n/c	0.07	0.07	0.05	0.08	0.08	0.06	0.06
14 - Q6ZU15 (1-49)	0.89	0.89	0.90	0.90	0.86	0.86	0.86	0.86	0.86	0.83	0.94	0.94	0.94		0.08	0.08	0.08	0.08	0.08	0.08	n/c	0.08	0.08	0.08	0.08	0.08	0.07	0.06	0.06	0.06	0.04	0.06	0.06	0.06	0.06	0.06	n/c	0.08	0.08	0.06	0.09	0.09	0.06	0.06
15 - Q9P0V9-2 (1-63)	0.78	0.78	0.87	0.89	0.87	0.87	0.87	0.87	0.87	0.84	0.94	0.94	0.94	0.48		0.00	0.00	0.08	0.08	0.08	n/c	0.08	0.08	0.08	0.08	0.08	0.07	0.06	0.07	0.05	0.02	0.05	0.05	0.05	0.05	0.05	n/c	0.08	0.08	0.04	0.09	0.09	0.07	0.07
16 - Q9P0V9 (1-63)	0.78	0.78	0.87	0.89	0.87	0.87	0.87	0.87	0.87	0.84	0.94	0.94	0.94	0.48	0.00		0.00	0.08	0.08	0.08	n/c	0.08	0.08	0.08	0.08	0.08	0.07	0.06	0.07	0.05	0.02	0.05	0.05	0.05	0.05	0.05	n/c	0.08	0.08	0.04	0.09	0.09	0.07	0.07
17 - Q9P0V9-3 (1-40)	0.78	0.78	0.80	0.83	0.80	0.80	0.80	0.80	0.80	0.77	0.93	0.93	0.93	0.45	0.00	0.00		0.08	0.08	0.08	n/c	0.08	0.08	0.08	0.08	0.08	0.08	0.07	0.07	0.06	0.04	0.06	0.06	0.06	0.06	0.06	n/c	0.08	0.08	0.06	0.09	0.09	0.07	0.07
18 - Q92599-4 (1-41)	0.79	0.79	0.78	0.78	0.76	0.76	0.76	0.76	0.76	0.72	0.82	0.82	0.82	0.61	0.51	0.51	0.51	0.49		0.00	0.00	n/c	0.08	0.08	0.08	0.08	0.08	0.08	0.08	0.08	0.07	0.04	0.07	0.07	0.07	0.07	0.07	n/c	0.08	0.08	0.07	0.09	0.09	0.08	0.07
19 - Q92599 (1-41)	0.79	0.79	0.78	0.78	0.76	0.76	0.76	0.76	0.76	0.72	0.82	0.82	0.82	0.61	0.51	0.51	0.49	0.00		0.00	n/c	0.08	0.08	0.08	0.08	0.08	0.08	0.08	0.08	0.07	0.04	0.07	0.07	0.07	0.07	0.07	n/c	0.08	0.08	0.07	0.09	0.09	0.08	0.07
20 - Q92599-2 (1-41)	0.79	0.79	0.78	0.78	0.76	0.76	0.76	0.76	0.76	0.72	0.82	0.82	0.82	0.61	0.51	0.51	0.49	0.00	0.00		n/c	0.08	0.08	0.08	0.08	0.08	0.08	0.08	0.08	0.07	0.04	0.07	0.07	0.07	0.07	0.07	n/c	0.08	0.08	0.07	0.09	0.09	0.08	0.07
21 - Q92599-3 ()	n/c	n/c	n/c	n/c	n/c	n/c	n/c	n/c	n/c	n/c	n/c	n/c	n/c	n/c	n/c	n/c	n/c	n/c	n/c	n/c	n/c	n/c	n/c	n/c	n/c	n/c	n/c	n/c	n/c	n/c	n/c	n/c	n/c	n/c	n/c	n/c	n/c	n/c	n/c	n/c	n/c	n/c	n/c	n/c
22 - Q14141-3 (1-39)	0.82	0.82	0.79	0.79	0.77	0.77	0.77	0.77	0.77	0.72	0.82	0.82	0.82	0.64	0.46	0.46	0.46	0.36	0.36	0.36	n/c		0.00	0.00	0.00	0.08	0.08	0.08	0.08	0.07	0.04	0.07	0.07	0.07	0.07	0.07	n/c	0.08	0.08	0.08	0.09	0.09	0.07	0.07
23 - Q14141-4 (1-39)	0.82	0.82	0.79	0.79	0.77	0.77	0.77	0.77	0.77	0.72	0.82	0.82	0.82	0.64	0.46	0.46	0.46	0.36	0.36	0.36	n/c	0.00		0.00	0.00	0.08	0.08	0.08	0.08	0.07	0.04	0.07	0.07	0.07	0.07	0.07	n/c	0.08	0.08	0.08	0.09	0.09	0.07	0.07
24 - Q14141 (1-39)	0.82	0.82	0.79	0.79	0.77	0.77	0.77	0.77	0.77	0.72	0.82	0.82	0.82	0.64	0.46	0.46	0.46	0.36	0.36	0.36	n/c	0.00	0.00		0.00	0.08	0.08	0.08	0.08	0.07	0.04	0.07	0.07	0.07	0.07	0.07	n/c	0.08	0.08	0.08	0.09	0.09	0.07	0.07
25 - Q14141-2 (1-39)	0.82	0.82	0.79	0.79	0.77	0.77	0.77	0.77	0.77	0.72	0.82	0.82	0.82	0.64	0.46	0.46	0.46	0.36	0.36	0.36	n/c	0.00	0.00	0.00		0.08	0.08	0.08	0.08	0.07	0.04	0.07	0.07	0.07	0.07	0.07	n/c	0.08	0.08	0.08	0.09	0.09	0.07	0.07
26 - Q9NVA2 (1-38)	0.82	0.82	0.79	0.76	0.71	0.71	0.71	0.71	0.71	0.72	0.79	0.79	0.79	0.58	0.44	0.44	0.44	0.39	0.39	0.39	n/c	0.39	0.39	0.39	0.39		0.07	0.07	0.07	0.07	0.00	0.07	0.07	0.07	0.07	0.07	n/c	0.08	0.08	0.08	0.09	0.09	0.07	0.06
27 - Q9NVA2-2 (1-48)	0.74	0.74	0.81	0.81	0.81	0.81	0.81	0.81	0.81	0.73	0.74	0.74	0.74	0.71	0.53	0.53	0.48	0.46	0.46	0.46	n/c	0.44	0.44	0.44	0.44	0.24		0.07	0.07	0.06	0.00	0.06	0.06	0.06	0.06	0.06	n/c	0.08	0.08	0.06	0.09	0.09	0.07	0.06
28 - Q16181 (1-47)	0.76	0.76	0.83	0.83	0.81	0.81	0.81	0.81	0.81	0.73	0.73	0.73	0.73	0.81	0.79	0.79	0.78	0.63	0.63	0.63	n/c	0.64	0.64	0.64	0.64	0.71	0.69		0.04	0.07	0.05	0.07	0.07	0.07	0.07	0.07	n/c	0.08	0.08	0.07	0.10	0.10	0.08	0.07
29 - Q16181-2 (1-46)	0.75	0.75	0.80	0.80	0.78	0.78	0.78	0.78	0.78	0.69	0.70	0.70	0.70	0.80	0.78	0.78	0.77	0.63	0.63	0.63	n/c	0.64	0.64	0.64	0.64	0.71	0.68	0.07		0.07	0.05	0.07	0.07	0.07	0.07	0.07	n/c	0.08	0.08	0.07	0.09	0.09	0.08	0.07
30 - O43236-6 (1-122)	0.74	0.74	0.87	0.88	0.86	0.86	0.86	0.86	0.86	0.82	0.83	0.83	0.83	0.78	0.81	0.81	0.78	0.71	0.71	0.71	n/c	0.77	0.77	0.77	0.77	0.74	0.73	0.62	0.61		0.04	0.01	0.01	0.01	0.00	0.01	n/c	0.08	0.08	0.05	0.09	0.09	0.08	0.07
31 - O43236-8 (1-562)	1.00	1.00	0.94	0.93	0.94	0.95	0.95	0.94	0.94	0.92	0.98	0.98	0.98	0.94	0.98	0.98	0.96	0.96	0.96	0.96	n/c	0.96	0.96	0.96	0.96	1.00	1.00	0.91	0.91	0.83		0.02	0.03	0.03	0.04	0.03	n/c	0.00	0.00	0.00	0.10	0.10	0.03	0.00
32 - O43236-7 (1-659)	0.74	0.74	0.87	0.89	0.91	0.92	0.91	0.91	0.87	0.82	0.83	0.83	0.83	0.78	0.81	0.81	0.78	0.71	0.71	0.71	n/c	0.77	0.77	0.77	0.77	0.74	0.73	0.62	0.61	0.01	0.16		0.03	0.02	0.01	0.03	n/c	0.08	0.08	0.05	0.09	0.09	0.08	0.07
33 - O43236-4 (1-156)	0.74	0.74	0.87	0.90	0.86	0.86	0.86	0.86	0.85	0.82	0.83	0.83	0.83	0.78	0.81	0.81	0.78	0.71	0.71	0.71	n/c	0.77	0.77	0.77	0.77	0.74	0.73	0.62	0.61	0.01	0.83	0.19		0.02	0.01	0.03	n/c	0.08	0.08	0.05	0.09	0.09	0.08	0.07
34 - O43236-3 (1-133)	0.74	0.74	0.87	0.89	0.87	0.87	0.87	0.87	0.86	0.82	0.83	0.83	0.83	0.78	0.81	0.81	0.78	0.71	0.71	0.71	n/c	0.77	0.77	0.77	0.77	0.74	0.73	0.62	0.61	0.01	0.84	0.07	0.08		0.01	0.02	n/c	0.08	0.08	0.05	0.09	0.09	0.08	0.07
35 - O43236-2 (1-122)	0.74	0.74	0.87	0.88	0.86	0.86	0.86	0.86	0.86	0.82	0.83	0.83	0.83	0.78	0.81	0.81	0.78	0.71	0.71	0.71	n/c	0.77	0.77	0.77	0.77	0.74	0.73	0.62	0.61	0.00	0.83	0.01	0.01	0.01		0.01	n/c	0.08	0.08	0.05	0.09	0.09	0.08	0.07
36 - O43236 (1-141)	0.74	0.74	0.87	0.87	0.88	0.88	0.88	0.86	0.82	0.83	0.83	0.83	0.83	0.78	0.81	0.81	0.78	0.71	0.71	0.71	n/c	0.77	0.77	0.77	0.77	0.74	0.73	0.62	0.61	0.01	0.83	0.11	0.13	0.08	0.01		n/c	0.08	0.08	0.05	0.09	0.09	0.08	0.07
37 - O43236-5 ()	n/c	n/c	n/c	n/c	n/c	n/c	n/c	n/c	n/c	n/c	n/c	n/c	n/c	n/c	n/c	n/c	n/c	n/c	n/c	n/c	n/c	n/c	n/c	n/c	n/c	n/c	n/c	n/c	n/c	n/c	n/c	n/c	n/c	n/c	n/c	n/c	n/c	n/c	n/c	n/c	n/c	n/c	n/c	n/c
38 - Q15019-3 (1-34)	0.76	0.76	0.74	0.71	0.74	0.74	0.74	0.74	0.74	0.63	0.79	0.79	0.79	0.65	0.74	0.74	0.74	0.65	0.65	0.65	n/c	0.68	0.68	0.68	0.68	0.65	0.71	0.47	0.47	0.47	1.00	0.47	0.47	0.47	0.47	0.47	n/c		0.00	0.07	0.10	0.10	0.09	0.08
39 - Q15019 (1-34)	0.76	0.76	0.74	0.71	0.74	0.74	0.74	0.74	0.74	0.63	0.79	0.79	0.79	0.65	0.74	0.74	0.74	0.65	0.65	0.65	n/c	0.68	0.68	0.68	0.68	0.65	0.71	0.47	0.47	0.47	1.00	0.47	0.47	0.47	0.47	0.47	n/c	0.00		0.07	0.10	0.10	0.09	0.08
40 - Q15019-2 (1-69)	0.85	0.85	0.86	0.86	0.84	0.84	0.84	0.84	0.84	0.80	0.80	0.80	0.80	0.79	0.87	0.87	0.80	0.71	0.71	0.71	n/c	0.67	0.67	0.67	0.67	0.68	0.75	0.55	0.52	0.72	1.00	0.72	0.72	0.72	0.72	0.72	n/c	0.26	0.26		0.10	0.10	0.08	0.07
41 - Q8WYJ6 (1-27)	0.74	0.74	0.70	0.70	0.70	0.70	0.70	0.70	0.70	0.70	0.78	0.78	0.78	0.70	0.70	0.70	0.70	0.63	0.63	0.63	n/c	0.59	0.59	0.59	0.59	0.67	0.67	0.44	0.41	0.30	0.86	0.30	0.30	0.30	0.30	0.30	n/c	0.33	0.33	0.41		0.00	0.09	0.09
42 - Q8WYJ6-2 (1-27)	0.74	0.74	0.70	0.70	0.70	0.70	0.70	0.70	0.70	0.70	0.78	0.78	0.78	0.70	0.70	0.70	0.70	0.63	0.63	0.63	n/c	0.59	0.59	0.59	0.59	0.67	0.67	0.44	0.41	0.30	0.86	0.30	0.30	0.30	0.30	0.30	n/c	0.33	0.33	0.41	0.00		0.09	0.09
43 - Q99719 (1-41)	0.78	0.78	0.78	0.76	0.78	0.78	0.78	0.78	0.78	0.69	0.80	0.80	0.80	0.78	0.75	0.75	0.75	0.67	0.67	0.67	n/c	0.72	0.72	0.72	0.72	0.76	0.74	0.51	0.54	0.41	0.96	0.41	0.41	0.41	0.41	0.41	n/c	0.42	0.42	0.59	0.33	0.33		0.08
44 - Q99719-2 (1-50)	0.80	0.80	0.81	0.79	0.75	0.75	0.75	0.75	0.75	0.71	0.83	0.83	0.83	0.74	0.74	0.74	0.75	0.71	0.71	0.71	n/c	0.72	0.72	0.72	0.72	0.68	0.78	0.60	0.61	0.54	1.00	0.54	0.54	0.54	0.54	0.54	n/c	0.50	0.50	0.60	0.37	0.37	0.46	

Appendix 5 - **Identity matrix of the N-terminal domain sequences from all human septin isoforms.** The number of amino acid differences per site from between sequences are shown (obtained by dividing the number of amino acid differences by the total number of sites compared between the two sequences). Standard error estimates are shown above the diagonal. This analysis involved 44 amino acid sequences. All ambiguous positions were removed for each sequence pair (pairwise deletion option). There was a total of 663 positions in the final dataset. Evolutionary analyses were conducted in MEGA11. The presence of n/c in the results denotes cases in which it was not possible to estimate evolutionary distances.

Source: By the author.

Identity matrix of the G- domain sequences from all human septin isoforms

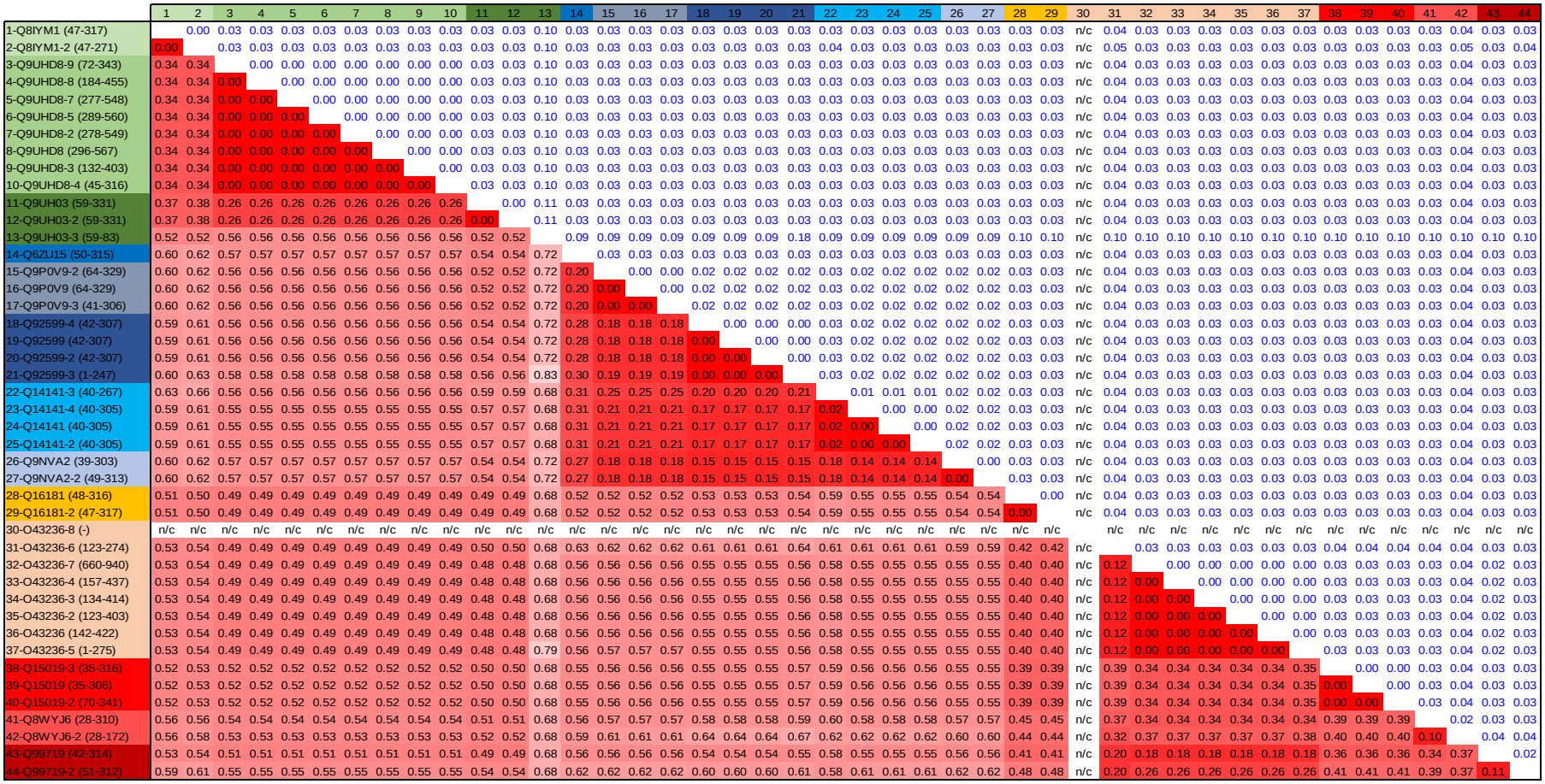

	1	2	3	4	5	6	7	8	9	10	11	12	13	14	15	16	17	18	19	20	21	22	23	24	25	26	27	28	29	30	31	32	33	34	35	36	37	38	39	40	41	42	43	44
1-Q8IYM1 (47-317)		0.00	0.03	0.03	0.03	0.03	0.03	0.03	0.03	0.03	0.03	0.03	0.10	0.03	0.03	0.03	0.03	0.03	0.03	0.03	0.03	0.03	0.03	0.03	0.03	0.03	0.03	0.03	0.03	n/c	0.04	0.03	0.03	0.03	0.03	0.03	0.03	0.03	0.03	0.03	0.04	0.03	0.03
2-Q8IYM1-2 (47-271)	0.00		0.03	0.03	0.03	0.03	0.03	0.03	0.03	0.03	0.03	0.03	0.10	0.03	0.03	0.03	0.03	0.03	0.03	0.03	0.03	0.04	0.03	0.03	0.03	0.03	0.03	0.03	0.03	n/c	0.05	0.03	0.03	0.03	0.03	0.03	0.03	0.03	0.03	0.03	0.05	0.03	0.04
3-Q9UHD8-9 (72-343)	0.34	0.34		0.00	0.00	0.00	0.00	0.00	0.00	0.00	0.03	0.03	0.10	0.03	0.03	0.03	0.03	0.03	0.03	0.03	0.03	0.03	0.03	0.03	0.03	0.03	0.03	0.03	0.03	n/c	0.04	0.03	0.03	0.03	0.03	0.03	0.03	0.03	0.03	0.03	0.04	0.03	0.03
4-Q9UHD8-8 (184-455)	0.34	0.34	0.00		0.00	0.00	0.00	0.00	0.00	0.00	0.03	0.03	0.10	0.03	0.03	0.03	0.03	0.03	0.03	0.03	0.03	0.03	0.03	0.03	0.03	0.03	0.03	0.03	0.03	n/c	0.04	0.03	0.03	0.03	0.03	0.03	0.03	0.03	0.03	0.03	0.04	0.03	0.03
5-Q9UHD8-7 (277-548)	0.34	0.34	0.00	0.00		0.00	0.00	0.00	0.00	0.00	0.03	0.03	0.10	0.03	0.03	0.03	0.03	0.03	0.03	0.03	0.03	0.03	0.03	0.03	0.03	0.03	0.03	0.03	0.03	n/c	0.04	0.03	0.03	0.03	0.03	0.03	0.03	0.03	0.03	0.03	0.04	0.03	0.03
6-Q9UHD8-5 (289-560)	0.34	0.34	0.00	0.00	0.00		0.00	0.00	0.00	0.00	0.03	0.03	0.10	0.03	0.03	0.03	0.03	0.03	0.03	0.03	0.03	0.03	0.03	0.03	0.03	0.03	0.03	0.03	0.03	n/c	0.04	0.03	0.03	0.03	0.03	0.03	0.03	0.03	0.03	0.03	0.04	0.03	0.03
7-Q9UHD8-2 (278-549)	0.34	0.34	0.00	0.00	0.00	0.00		0.00	0.00	0.00	0.03	0.03	0.10	0.03	0.03	0.03	0.03	0.03	0.03	0.03	0.03	0.03	0.03	0.03	0.03	0.03	0.03	0.03	0.03	n/c	0.04	0.03	0.03	0.03	0.03	0.03	0.03	0.03	0.03	0.03	0.04	0.03	0.03
8-Q9UHD8 (296-567)	0.34	0.34	0.00	0.00	0.00	0.00	0.00		0.00	0.00	0.03	0.03	0.10	0.03	0.03	0.03	0.03	0.03	0.03	0.03	0.03	0.03	0.03	0.03	0.03	0.03	0.03	0.03	0.03	n/c	0.04	0.03	0.03	0.03	0.03	0.03	0.03	0.03	0.03	0.03	0.04	0.03	0.03
9-Q9UHD8-3 (132-403)	0.34	0.34	0.00	0.00	0.00	0.00	0.00	0.00		0.00	0.03	0.03	0.10	0.03	0.03	0.03	0.03	0.03	0.03	0.03	0.03	0.03	0.03	0.03	0.03	0.03	0.03	0.03	0.03	n/c	0.04	0.03	0.03	0.03	0.03	0.03	0.03	0.03	0.03	0.03	0.04	0.03	0.03
10-Q9UHD8-4 (45-316)	0.34	0.34	0.00	0.00	0.00	0.00	0.00	0.00	0.00		0.03	0.03	0.10	0.03	0.03	0.03	0.03	0.03	0.03	0.03	0.03	0.03	0.03	0.03	0.03	0.03	0.03	0.03	0.03	n/c	0.04	0.03	0.03	0.03	0.03	0.03	0.03	0.03	0.03	0.03	0.04	0.03	0.03
11-Q9UH03 (59-331)	0.37	0.38	0.26	0.26	0.26	0.26	0.26	0.26	0.26	0.26		0.00	0.11	0.03	0.03	0.03	0.03	0.03	0.03	0.03	0.03	0.03	0.03	0.03	0.03	0.03	0.03	0.03	0.03	n/c	0.04	0.03	0.03	0.03	0.03	0.03	0.03	0.03	0.03	0.03	0.04	0.03	0.03
12-Q9UH03-2 (59-331)	0.37	0.38	0.26	0.26	0.26	0.26	0.26	0.26	0.26	0.26	0.00		0.11	0.03	0.03	0.03	0.03	0.03	0.03	0.03	0.03	0.03	0.03	0.03	0.03	0.03	0.03	0.03	0.03	n/c	0.04	0.03	0.03	0.03	0.03	0.03	0.03	0.03	0.03	0.03	0.04	0.03	0.03
13-Q9UH03-3 (59-83)	0.52	0.52	0.56	0.56	0.56	0.56	0.56	0.56	0.56	0.56	0.52	0.52		0.09	0.09	0.09	0.09	0.09	0.09	0.09	0.18	0.09	0.09	0.09	0.09	0.09	0.09	0.10	0.10	n/c	0.10	0.10	0.10	0.10	0.10	0.10	0.10	0.10	0.10	0.10	0.10	0.10	0.10
14-Q6ZU15 (50-315)	0.60	0.62	0.57	0.57	0.57	0.57	0.57	0.57	0.57	0.57	0.54	0.54	0.72		0.03	0.03	0.03	0.03	0.03	0.03	0.03	0.03	0.03	0.03	0.03	0.03	0.03	0.03	0.03	n/c	0.04	0.03	0.03	0.03	0.03	0.03	0.03	0.03	0.03	0.03	0.04	0.03	0.03
15-Q9P0V9-2 (64-329)	0.60	0.62	0.56	0.56	0.56	0.56	0.56	0.56	0.56	0.56	0.52	0.52	0.72	0.20		0.00	0.00	0.02	0.02	0.02	0.02	0.03	0.02	0.02	0.02	0.02	0.02	0.03	0.03	n/c	0.04	0.03	0.03	0.03	0.03	0.03	0.03	0.03	0.03	0.03	0.04	0.03	0.03
16-Q9P0V9 (64-329)	0.60	0.62	0.56	0.56	0.56	0.56	0.56	0.56	0.56	0.56	0.52	0.52	0.72	0.20	0.00		0.00	0.02	0.02	0.02	0.02	0.03	0.02	0.02	0.02	0.02	0.02	0.03	0.03	n/c	0.04	0.03	0.03	0.03	0.03	0.03	0.03	0.03	0.03	0.03	0.04	0.03	0.03
17-Q9P0V9-3 (41-306)	0.60	0.62	0.56	0.56	0.56	0.56	0.56	0.56	0.56	0.56	0.52	0.52	0.72	0.20	0.00	0.00		0.02	0.02	0.02	0.02	0.03	0.02	0.02	0.02	0.02	0.02	0.03	0.03	n/c	0.04	0.03	0.03	0.03	0.03	0.03	0.03	0.03	0.03	0.03	0.04	0.03	0.03
18-Q92599-4 (42-307)	0.59	0.61	0.56	0.56	0.56	0.56	0.56	0.56	0.56	0.56	0.54	0.54	0.72	0.28	0.18	0.18	0.18		0.00	0.00	0.00	0.03	0.02	0.02	0.02	0.02	0.02	0.03	0.03	n/c	0.04	0.03	0.03	0.03	0.03	0.03	0.03	0.03	0.03	0.03	0.04	0.03	0.03
19-Q92599 (42-307)	0.59	0.61	0.56	0.56	0.56	0.56	0.56	0.56	0.56	0.56	0.54	0.54	0.72	0.28	0.18	0.18	0.18	0.00		0.00	0.00	0.03	0.02	0.02	0.02	0.02	0.02	0.03	0.03	n/c	0.04	0.03	0.03	0.03	0.03	0.03	0.03	0.03	0.03	0.03	0.04	0.03	0.03
20-Q92599-2 (42-307)	0.59	0.61	0.56	0.56	0.56	0.56	0.56	0.56	0.56	0.56	0.54	0.54	0.72	0.28	0.18	0.18	0.18	0.00	0.00		0.00	0.03	0.02	0.02	0.02	0.02	0.02	0.03	0.03	n/c	0.04	0.03	0.03	0.03	0.03	0.03	0.03	0.03	0.03	0.03	0.04	0.03	0.03
21-Q92599-3 (1-247)	0.60	0.63	0.58	0.58	0.58	0.58	0.58	0.58	0.58	0.58	0.56	0.56	0.83	0.30	0.19	0.19	0.19	0.00	0.00	0.00		0.03	0.02	0.02	0.02	0.02	0.02	0.03	0.03	n/c	0.04	0.03	0.03	0.03	0.03	0.03	0.03	0.03	0.03	0.03	0.04	0.03	0.03
22-Q14141-3 (40-267)	0.63	0.66	0.56	0.56	0.56	0.56	0.56	0.56	0.56	0.56	0.59	0.59	0.68	0.31	0.25	0.25	0.25	0.20	0.20	0.20	0.21		0.01	0.01	0.01	0.02	0.02	0.03	0.03	n/c	0.04	0.03	0.03	0.03	0.03	0.03	0.03	0.03	0.03	0.03	0.04	0.03	0.03
23-Q14141-4 (40-305)	0.59	0.61	0.55	0.55	0.55	0.55	0.55	0.55	0.55	0.55	0.57	0.57	0.68	0.31	0.21	0.21	0.21	0.17	0.17	0.17	0.17	0.02		0.00	0.00	0.02	0.02	0.03	0.03	n/c	0.04	0.03	0.03	0.03	0.03	0.03	0.03	0.03	0.03	0.03	0.04	0.03	0.03
24-Q14141 (40-305)	0.59	0.61	0.55	0.55	0.55	0.55	0.55	0.55	0.55	0.55	0.57	0.57	0.68	0.31	0.21	0.21	0.21	0.17	0.17	0.17	0.17	0.02	0.00		0.00	0.02	0.02	0.03	0.03	n/c	0.04	0.03	0.03	0.03	0.03	0.03	0.03	0.03	0.03	0.03	0.04	0.03	0.03
25-Q14141-2 (40-305)	0.59	0.61	0.55	0.55	0.55	0.55	0.55	0.55	0.55	0.55	0.57	0.57	0.68	0.31	0.21	0.21	0.21	0.17	0.17	0.17	0.17	0.02	0.00	0.00		0.02	0.02	0.03	0.03	n/c	0.04	0.03	0.03	0.03	0.03	0.03	0.03	0.03	0.03	0.03	0.04	0.03	0.03
26-Q9NVA2 (39-303)	0.60	0.62	0.57	0.57	0.57	0.57	0.57	0.57	0.57	0.57	0.54	0.54	0.72	0.27	0.18	0.18	0.18	0.15	0.15	0.15	0.15	0.18	0.14	0.14	0.14		0.00	0.03	0.03	n/c	0.04	0.03	0.03	0.03	0.03	0.03	0.03	0.03	0.03	0.03	0.04	0.03	0.03
27-Q9NVA2-2 (49-313)	0.60	0.62	0.57	0.57	0.57	0.57	0.57	0.57	0.57	0.57	0.54	0.54	0.72	0.27	0.18	0.18	0.18	0.15	0.15	0.15	0.15	0.18	0.14	0.14	0.14	0.00		0.03	0.03	n/c	0.04	0.03	0.03	0.03	0.03	0.03	0.03	0.03	0.03	0.03	0.04	0.03	0.03
28-Q16181 (48-316)	0.51	0.50	0.49	0.49	0.49	0.49	0.49	0.49	0.49	0.49	0.49	0.49	0.68	0.52	0.52	0.52	0.52	0.53	0.53	0.53	0.54	0.59	0.55	0.55	0.55	0.54	0.54		0.00	n/c	0.04	0.03	0.03	0.03	0.03	0.03	0.03	0.03	0.03	0.03	0.04	0.03	0.03
29-Q16181-2 (47-317)	0.51	0.50	0.49	0.49	0.49	0.49	0.49	0.49	0.49	0.49	0.49	0.49	0.68	0.52	0.52	0.52	0.52	0.53	0.53	0.53	0.54	0.59	0.55	0.55	0.55	0.54	0.54	0.00		n/c	0.04	0.03	0.03	0.03	0.03	0.03	0.03	0.03	0.03	0.03	0.04	0.03	0.03
30-O43236-8 (-)	n/c	n/c	n/c	n/c	n/c	n/c	n/c	n/c	n/c	n/c	n/c	n/c	n/c	n/c	n/c	n/c	n/c	n/c	n/c	n/c	n/c	n/c	n/c	n/c	n/c	n/c	n/c	n/c	n/c		n/c	n/c	n/c	n/c	n/c	n/c	n/c	n/c	n/c	n/c	n/c	n/c	n/c
31-O43236-6 (123-274)	0.53	0.54	0.49	0.49	0.49	0.49	0.49	0.49	0.49	0.49	0.50	0.50	0.68	0.63	0.62	0.62	0.62	0.61	0.61	0.61	0.64	0.61	0.61	0.61	0.61	0.59	0.59	0.42	0.42	n/c		0.03	0.03	0.03	0.03	0.03	0.03	0.04	0.04	0.04	0.04	0.04	0.03	0.03
32-O43236-7 (660-940)	0.53	0.54	0.49	0.49	0.49	0.49	0.49	0.49	0.49	0.49	0.48	0.48	0.68	0.56	0.56	0.56	0.56	0.55	0.55	0.55	0.56	0.58	0.55	0.55	0.55	0.55	0.55	0.40	0.40	n/c	0.12		0.00	0.00	0.00	0.00	0.00	0.03	0.03	0.03	0.03	0.04	0.02	0.03
33-O43236-4 (157-437)	0.53	0.54	0.49	0.49	0.49	0.49	0.49	0.49	0.49	0.49	0.48	0.48	0.68	0.56	0.56	0.56	0.56	0.55	0.55	0.55	0.56	0.58	0.55	0.55	0.55	0.55	0.55	0.40	0.40	n/c	0.12	0.00		0.00	0.00	0.00	0.00	0.03	0.03	0.03	0.03	0.04	0.02	0.03
34-O43236-3 (134-414)	0.53	0.54	0.49	0.49	0.49	0.49	0.49	0.49	0.49	0.49	0.48	0.48	0.68	0.56	0.56	0.56	0.56	0.55	0.55	0.55	0.56	0.58	0.55	0.55	0.55	0.55	0.55	0.40	0.40	n/c	0.12	0.00	0.00		0.00	0.00	0.00	0.03	0.03	0.03	0.03	0.04	0.02	0.03
35-O43236-2 (123-403)	0.53	0.54	0.49	0.49	0.49	0.49	0.49	0.49	0.49	0.49	0.48	0.48	0.68	0.56	0.56	0.56	0.56	0.55	0.55	0.55	0.56	0.58	0.55	0.55	0.55	0.55	0.55	0.40	0.40	n/c	0.12	0.00	0.00	0.00		0.00	0.00	0.03	0.03	0.03	0.03	0.04	0.02	0.03
36-O43236 (142-422)	0.53	0.54	0.49	0.49	0.49	0.49	0.49	0.49	0.49	0.49	0.48	0.48	0.68	0.56	0.56	0.56	0.56	0.55	0.55	0.55	0.56	0.58	0.55	0.55	0.55	0.55	0.55	0.40	0.40	n/c	0.12	0.00	0.00	0.00	0.00		0.00	0.03	0.03	0.03	0.03	0.04	0.02	0.03
37-O43236-5 (1-275)	0.53	0.54	0.49	0.49	0.49	0.49	0.49	0.49	0.49	0.49	0.48	0.48	0.79	0.56	0.57	0.57	0.57	0.55	0.55	0.55	0.56	0.58	0.55	0.55	0.55	0.55	0.55	0.40	0.40	n/c	0.12	0.00	0.00	0.00	0.00	0.00		0.03	0.03	0.03	0.03	0.04	0.02	0.03
38-Q15019-3 (35-316)	0.52	0.53	0.52	0.52	0.52	0.52	0.52	0.52	0.52	0.52	0.50	0.50	0.68	0.55	0.56	0.56	0.56	0.55	0.55	0.55	0.57	0.59	0.56	0.56	0.56	0.55	0.55	0.39	0.39	n/c	0.39	0.34	0.34	0.34	0.34	0.34	0.35		0.00	0.00	0.03	0.04	0.03	0.03
39-Q15019 (35-306)	0.52	0.53	0.52	0.52	0.52	0.52	0.52	0.52	0.52	0.52	0.50	0.50	0.68	0.55	0.56	0.56	0.56	0.55	0.55	0.55	0.57	0.59	0.56	0.56	0.56	0.55	0.55	0.39	0.39	n/c	0.39	0.34	0.34	0.34	0.34	0.34	0.35	0.00		0.00	0.03	0.04	0.03	0.03
40-Q15019-2 (70-341)	0.52	0.53	0.52	0.52	0.52	0.52	0.52	0.52	0.52	0.52	0.50	0.50	0.68	0.55	0.56	0.56	0.56	0.55	0.55	0.55	0.57	0.59	0.56	0.56	0.56	0.55	0.55	0.39	0.39	n/c	0.39	0.34	0.34	0.34	0.34	0.34	0.35	0.00	0.00		0.03	0.04	0.03	0.03
41-Q8WYJ6 (28-310)	0.56	0.56	0.54	0.54	0.54	0.54	0.54	0.54	0.54	0.54	0.51	0.51	0.68	0.56	0.57	0.57	0.57	0.58	0.58	0.58	0.59	0.60	0.58	0.58	0.58	0.57	0.57	0.45	0.45	n/c	0.37	0.34	0.34	0.34	0.34	0.34	0.34	0.39	0.39	0.39		0.02	0.03	0.03
42-Q8WYJ6-2 (28-172)	0.56	0.58	0.53	0.53	0.53	0.53	0.53	0.53	0.53	0.53	0.52	0.52	0.68	0.59	0.61	0.61	0.61	0.64	0.64	0.64	0.67	0.62	0.62	0.62	0.62	0.60	0.60	0.44	0.44	n/c	0.32	0.37	0.37	0.37	0.37	0.37	0.38	0.40	0.40	0.40	0.10		0.04	0.04
43-Q99719 (42-314)	0.53	0.54	0.51	0.51	0.51	0.51	0.51	0.51	0.51	0.51	0.49	0.49	0.68	0.56	0.56	0.56	0.56	0.54	0.54	0.54	0.55	0.58	0.55	0.55	0.55	0.56	0.56	0.41	0.41	n/c	0.20	0.18	0.18	0.18	0.18	0.18	0.18	0.36	0.36	0.36	0.34	0.37		0.02
44-Q99719-2 (51-312)	0.59	0.61	0.55	0.55	0.55	0.55	0.55	0.55	0.55	0.55	0.54	0.54	0.68	0.62	0.62	0.62	0.62	0.60	0.60	0.60	0.61	0.58	0.61	0.61	0.61	0.62	0.62	0.48	0.48	n/c	0.20	0.26	0.26	0.26	0.26	0.26	0.26	0.41	0.41	0.41	0.39	0.37	0.11	

Appendix 6 - **Identity matrix of the G-domain sequences from all human septin isoforms.** The number of amino acid differences per site from between sequences are shown (obtained by dividing the number of amino acid differences by the total number of sites compared between the two sequences). Standard error estimates are shown above the diagonal. This analysis involved 44 amino acid sequences. All ambiguous positions were removed for each sequence pair (pairwise deletion option). There was a total of 287 positions in the final dataset. Evolutionary analyses were conducted in MEGA11. The presence of n/c in the results denotes cases in which it was not possible to estimate evolutionary distances.

Source: By the author.

Identity matrix of the C-terminal domain sequences from all human septin isoforms

	1	2	3	4	5	6	7	8	9	10	11	12	13	14	15	16	17	18	19	20	21	22	23	24	25	26	27	28	29	30	31	32	33	34	35	36	37	38	39	40	41	42	43	44
1-Q8IYM1 (318-358)		0.00	0.08	0.08	0.08	0.08	0.08	0.08	0.08	0.08	0.08	0.09	n/c	0.04	0.03	0.03	0.03	0.04	0.04	0.04	0	n/c	0.04	0.04	0.04	0.04	0.04	0.00	0.00	n/c	n/c	0.07	0.07	0.07	0.07	0.07	0.1	0.04	0.04	0.04	0.06	n/c	0.05	0.05
2-Q8IYM1-2 (272-312)	0.00		0.08	0.08	0.08	0.08	0.08	0.08	0.08	0.08	0.08	0.09	n/c	0.04	0.03	0.03	0.03	0.04	0.04	0.04	0	n/c	0.04	0.04	0.04	0.04	0.04	0.00	0.00	n/c	n/c	0.07	0.07	0.07	0.07	0.07	0.1	0.04	0.04	0.04	0.06	n/c	0.05	0.05
3-Q9UHD8-9 (344-362)	0.84	0.84		0.00	0.00	0.00	0.00	0.00	0.00	0.00	0.08	0.11	n/c	0.07	0.07	0.07	0.07	0.07	0.07	0.07	0.1	n/c	0.07	0.07	0.07	0.09	0.09	0.10	0.10	n/c	n/c	0.08	0.08	0.08	0.08	0.08	0.1	0.09	0.09	0.09	0.09	n/c	0.09	0.07
4-Q9UHD8-8 (456-474)	0.84	0.84	0.00		0.00	0.00	0.00	0.00	0.00	0.00	0.08	0.11	n/c	0.07	0.07	0.07	0.07	0.07	0.07	0.07	0.1	n/c	0.07	0.07	0.07	0.09	0.09	0.10	0.10	n/c	n/c	0.08	0.08	0.08	0.08	0.08	0.1	0.09	0.09	0.09	0.09	n/c	0.09	0.07
5-Q9UHD8-7 (549-567)	0.84	0.84	0.00	0.00		0.00	0.00	0.00	0.00	0.00	0.08	0.11	n/c	0.07	0.07	0.07	0.07	0.07	0.07	0.07	0.1	n/c	0.07	0.07	0.07	0.09	0.09	0.10	0.10	n/c	n/c	0.08	0.08	0.08	0.08	0.08	0.1	0.09	0.09	0.09	0.09	n/c	0.09	0.07
6-Q9UHD8-5 (561-579)	0.84	0.84	0.00	0.00	0.00		0.00	0.00	0.00	0.00	0.08	0.11	n/c	0.07	0.07	0.07	0.07	0.07	0.07	0.07	0.1	n/c	0.07	0.07	0.07	0.09	0.09	0.10	0.10	n/c	n/c	0.08	0.08	0.08	0.08	0.08	0.1	0.09	0.09	0.09	0.09	n/c	0.09	0.07
7-Q9UHD8-2 (550-568)	0.84	0.84	0.00	0.00	0.00	0.00		0.00	0.00	0.00	0.08	0.11	n/c	0.07	0.07	0.07	0.07	0.07	0.07	0.07	0.1	n/c	0.07	0.07	0.07	0.09	0.09	0.10	0.10	n/c	n/c	0.08	0.08	0.08	0.08	0.08	0.1	0.09	0.09	0.09	0.09	n/c	0.09	0.07
8-Q9UHD8 (568-586)	0.84	0.84	0.00	0.00	0.00	0.00	0.00		0.00	0.00	0.08	0.11	n/c	0.07	0.07	0.07	0.07	0.07	0.07	0.07	0.1	n/c	0.07	0.07	0.07	0.09	0.09	0.10	0.10	n/c	n/c	0.08	0.08	0.08	0.08	0.08	0.1	0.09	0.09	0.09	0.09	n/c	0.09	0.07
9-Q9UHD8-3 (404-422)	0.84	0.84	0.00	0.00	0.00	0.00	0.00	0.00		0.00	0.08	0.11	n/c	0.07	0.07	0.07	0.07	0.07	0.07	0.07	0.1	n/c	0.07	0.07	0.07	0.09	0.09	0.10	0.10	n/c	n/c	0.08	0.08	0.08	0.08	0.08	0.1	0.09	0.09	0.09	0.09	n/c	0.09	0.07
10-Q9UHD8-4 (317-335)	0.84	0.84	0.00	0.00	0.00	0.00	0.00	0.00	0.00		0.08	0.11	n/c	0.07	0.07	0.07	0.07	0.07	0.07	0.07	0.1	n/c	0.07	0.07	0.07	0.09	0.09	0.10	0.10	n/c	n/c	0.08	0.08	0.08	0.08	0.08	0.1	0.09	0.09	0.09	0.09	n/c	0.09	0.07
11-Q9UH03 (332-358)	0.81	0.81	0.84	0.84	0.84	0.84	0.84	0.84	0.84	0.84		0.12	n/c	0.05	0.04	0.04	0.04	0.04	0.04	0.04	0	n/c	0.04	0.04	0.04	0.04	0.04	0.04	0.04	n/c	n/c	0.09	0.09	0.09	0.09	0.09	0.1	0.07	0.07	0.07	0.08	n/c	0.08	0.08
12-Q9UH03-2 (332-350)	0.83	0.83	0.76	0.76	0.76	0.76	0.76	0.76	0.76	0.76	0.63		n/c	0.07	0.07	0.07	0.07	0.07	0.07	0.07	0.1	n/c	0.07	0.07	0.07	0.07	0.07	0.05	0.05	n/c	n/c	0.08	0.08	0.08	0.08	0.08	0.1	0.00	0.00	0.00	0.08	n/c	0.07	0.07
13-Q9UH03-3 (-)	n/c	n/c	n/c	n/c	n/c	n/c	n/c	n/c	n/c	n/c	n/c	n/c	n/c	n/c	n/c	n/c	n/c	n/c	n/c	n/c	n/c	n/c	n/c	n/c	n/c	n/c	n/c	n/c	n/c	n/c	n/c	n/c	n/c	n/c	n/c	n/c	n/c	n/c	n/c	n/c	n/c	n/c	n/c
14-Q6ZU15 (316-432)	0.93	0.93	0.89	0.89	0.89	0.89	0.89	0.89	0.89	0.89	0.93	0.89	n/c		0.05	0.05	0.05	0.05	0.05	0.05	0	n/c	0.05	0.05	0.05	0.05	0.05	0.04	0.04	n/c	n/c	0.05	0.05	0.05	0.05	0.05	0	0.05	0.05	0.05	0.04	n/c	0.05	0.04
15-Q9P0V9-2 (330-503)	0.95	0.95	0.89	0.89	0.89	0.89	0.89	0.89	0.89	0.89	0.96	0.89	n/c	0.37		0.01	0.01	0.04	0.04	0.04	0	n/c	0.04	0.04	0.05	0.04	0.04	0.04	0.04	n/c	n/c	0.04	0.04	0.04	0.04	0.04	0	0.06	0.06	0.06	0.04	n/c	0.06	0.04
16-Q9P0V9 (330-454)	0.95	0.95	0.89	0.89	0.89	0.89	0.89	0.89	0.89	0.89	0.96	0.89	n/c	0.38	0.02		0.00	0.04	0.04	0.04	0	n/c	0.04	0.04	0.04	0.04	0.04	0.04	0.04	n/c	n/c	0.04	0.04	0.04	0.04	0.04	0	0.06	0.06	0.06	0.04	n/c	0.06	0.04
17-Q9P0V9-3 (307-431)	0.95	0.95	0.89	0.89	0.89	0.89	0.89	0.89	0.89	0.89	0.96	0.89	n/c	0.38	0.02	0.00		0.04	0.04	0.04	0	n/c	0.04	0.04	0.04	0.04	0.04	0.04	0.04	n/c	n/c	0.04	0.04	0.04	0.04	0.04	0	0.06	0.06	0.06	0.04	n/c	0.06	0.04
18-Q92599-4 (308-442)	0.93	0.93	0.89	0.89	0.89	0.89	0.89	0.89	0.89	0.89	0.96	0.89	n/c	0.47	0.43	0.38	0.38		0.03	0.01	0	n/c	0.04	0.04	0.04	0.04	0.04	0.04	0.04	n/c	n/c	0.05	0.05	0.05	0.05	0.05	0.1	0.05	0.05	0.05	0.05	n/c	0.06	0.04
19-Q92599 (308-483)	0.93	0.93	0.89	0.89	0.89	0.89	0.89	0.89	0.89	0.89	0.96	0.89	n/c	0.48	0.56	0.39	0.39	0.10		0.00	0	n/c	0.04	0.04	0.04	0.04	0.04	0.04	0.04	n/c	n/c	0.05	0.05	0.05	0.05	0.05	0.1	0.05	0.05	0.05	0.05	n/c	0.06	0.04
20-Q92599-2 (308-429)	0.93	0.93	0.89	0.89	0.89	0.89	0.89	0.89	0.89	0.89	0.96	0.89	n/c	0.48	0.38	0.37	0.37	0.01	0.00		0	n/c	0.04	0.04	0.04	0.04	0.04	0.04	0.04	n/c	n/c	0.05	0.05	0.05	0.05	0.05	0.1	0.05	0.05	0.05	0.05	n/c	0.06	0.04
21-Q92599-3 (248-369)	0.93	0.93	0.89	0.89	0.89	0.89	0.89	0.89	0.89	0.89	0.96	0.89	n/c	0.48	0.38	0.37	0.37	0.01	0	0		n/c	0.04	0.04	0.04	0.04	0.04	0.04	0.04	n/c	n/c	0.05	0.05	0.05	0.05	0.05	0.1	0.05	0.05	0.05	0.05	n/c	0.06	0.04
22-Q14141-3 (-)	n/c	n/c	n/c	n/c	n/c	n/c	n/c	n/c	n/c	n/c	n/c	n/c	n/c	n/c	n/c	n/c	n/c	n/c	n/c	n/c	n/c	n/c	n/c	n/c	n/c	n/c	n/c	n/c	n/c	n/c	n/c	n/c	n/c	n/c	n/c	n/c	n/c	n/c	n/c	n/c	n/c	n/c	n/c
23-Q14141-4 (306-429)	0.93	0.93	0.89	0.89	0.89	0.89	0.89	0.89	0.89	0.89	0.96	0.89	n/c	0.48	0.42	0.40	0.40	0.36	0.35	0.34	0.3	n/c		0.01	0.00	0.04	0.04	0.04	0.04	n/c	n/c	0.05	0.05	0.05	0.05	0.05	0	0.05	0.05	0.05	0.04	n/c	0.05	0.04
24-Q14141 (306-434)	0.93	0.93	0.89	0.89	0.89	0.89	0.89	0.89	0.89	0.89	0.96	0.89	n/c	0.48	0.43	0.40	0.40	0.39	0.38	0.34	0.3	n/c	0.02		0.00	0.04	0.04	0.04	0.04	n/c	n/c	0.05	0.05	0.05	0.05	0.05	0	0.05	0.05	0.05	0.04	n/c	0.05	0.04
25-Q14141-2 (306-427)	0.93	0.93	0.89	0.89	0.89	0.89	0.89	0.89	0.89	0.89	0.96	0.89	n/c	0.48	0.41	0.40	0.40	0.35	0.34	0.34	0.3	n/c	0.00	0.00		0.03	0.03	0.04	0.04	n/c	n/c	0.05	0.05	0.05	0.05	0.05	0	0.05	0.05	0.05	0.04	n/c	0.05	0.04
26-Q9NVA2 (304-429)	0.93	0.93	0.84	0.84	0.84	0.84	0.84	0.84	0.84	0.84	0.96	0.89	n/c	0.46	0.42	0.40	0.40	0.30	0.30	0.29	0.3	n/c	0.20	0.21	0.18		0.00	0.04	0.04	n/c	n/c	0.05	0.05	0.05	0.05	0.05	0	0.05	0.05	0.05	0.04	n/c	0.05	0.04
27-Q9NVA2-2 (314-439)	0.93	0.93	0.84	0.84	0.84	0.84	0.84	0.84	0.84	0.84	0.96	0.89	n/c	0.46	0.42	0.40	0.40	0.30	0.30	0.29	0.3	n/c	0.20	0.21	0.18	0.00		0.04	0.04	n/c	n/c	0.05	0.05	0.05	0.05	0.05	0	0.05	0.05	0.05	0.04	n/c	0.05	0.04
28-Q16181 (317-436)	1.00	1.00	0.74	0.74	0.74	0.74	0.74	0.74	0.74	0.74	0.96	0.95	n/c	0.70	0.69	0.69	0.69	0.68	0.69	0.69	0.7	n/c	0.70	0.70	0.70	0.70	0.70		0.00	n/c	n/c	0.05	0.05	0.05	0.05	0.05	0	0.05	0.05	0.05	0.04	n/c	0.05	0.05
29-Q16181-2 (318-437)	1.00	1.00	0.74	0.74	0.74	0.74	0.74	0.74	0.74	0.74	0.96	0.95	n/c	0.70	0.69	0.69	0.69	0.68	0.69	0.69	0.7	n/c	0.69	0.70	0.70	0.70	0.70	0.00		n/c	n/c	0.05	0.05	0.05	0.05	0.05	0	0.05	0.05	0.05	0.04	n/c	0.05	0.05
30-O43236-6 (-)	n/c	n/c	n/c	n/c	n/c	n/c	n/c	n/c	n/c	n/c	n/c	n/c	n/c	n/c	n/c	n/c	n/c	n/c	n/c	n/c	n/c	n/c	n/c	n/c	n/c	n/c	n/c	n/c	n/c	n/c	n/c	n/c	n/c	n/c	n/c	n/c	n/c	n/c	n/c	n/c	n/c	n/c	n/c
31-O43236-8 (-)	n/c	n/c	n/c	n/c	n/c	n/c	n/c	n/c	n/c	n/c	n/c	n/c	n/c	n/c	n/c	n/c	n/c	n/c	n/c	n/c	n/c	n/c	n/c	n/c	n/c	n/c	n/c	n/c	n/c	n/c	n/c	n/c	n/c	n/c	n/c	n/c	n/c	n/c	n/c	n/c	n/c	n/c	n/c
32-O43236-7 (941-996)	0.73	0.73	0.84	0.84	0.84	0.84	0.84	0.84	0.84	0.84	0.74	0.84	n/c	0.85	0.87	0.87	0.87	0.80	0.80	0.80	0.8	n/c	0.84	0.84	0.84	0.85	0.85	0.85	0.85	n/c	n/c		0.00	0.00	0.00	0.00	0	0.08	0.08	0.08	0.06	n/c	0.07	0.07
33-O43236-4 (438-493)	0.73	0.73	0.84	0.84	0.84	0.84	0.84	0.84	0.84	0.84	0.74	0.84	n/c	0.85	0.87	0.87	0.87	0.80	0.80	0.80	0.8	n/c	0.84	0.84	0.84	0.85	0.85	0.85	0.85	n/c	n/c	0.00		0.00	0.00	0.00	0	0.08	0.08	0.08	0.06	n/c	0.07	0.07
34-O43236-3 (415-470)	0.73	0.73	0.84	0.84	0.84	0.84	0.84	0.84	0.84	0.84	0.74	0.84	n/c	0.85	0.87	0.87	0.87	0.80	0.80	0.80	0.8	n/c	0.84	0.84	0.84	0.85	0.85	0.85	0.85	n/c	n/c	0.00	0.00		0.00	0.00	0	0.08	0.08	0.08	0.06	n/c	0.07	0.07
35-O43236-2 (404-459)	0.73	0.73	0.84	0.84	0.84	0.84	0.84	0.84	0.84	0.84	0.74	0.84	n/c	0.85	0.87	0.87	0.87	0.80	0.80	0.80	0.8	n/c	0.84	0.84	0.84	0.85	0.85	0.85	0.85	n/c	n/c	0.00	0.00	0.00		0.00	0	0.08	0.08	0.08	0.06	n/c	0.07	0.07
36-O43236 (423-478)	0.73	0.73	0.84	0.84	0.84	0.84	0.84	0.84	0.84	0.84	0.74	0.84	n/c	0.85	0.87	0.87	0.87	0.80	0.80	0.80	0.8	n/c	0.84	0.84	0.84	0.85	0.85	0.85	0.85	n/c	n/c	0.00	0.00	0.00	0.00		0	0.08	0.08	0.08	0.06	n/c	0.07	0.07
37-O43236-5 (276-331)	0.73	0.73	0.84	0.84	0.84	0.84	0.84	0.84	0.84	0.84	0.74	0.84	n/c	0.85	0.87	0.87	0.87	0.8	0.8	0.8	0.8	n/c	0.84	0.84	0.84	0.85	0.85	0.85	0.85	n/c	n/c	0	0	0	0	0		0.08	0.08	0.08	0.06	n/c	0.07	0.07
38-Q15019-3 (317-371)	0.96	0.96	0.91	0.91	0.91	0.91	0.91	0.91	0.91	0.91	0.92	1.00	n/c	0.85	0.78	0.78	0.78	0.82	0.82	0.82	0.8	n/c	0.85	0.85	0.85	0.84	0.84	0.80	0.80	n/c	n/c	0.66	0.66	0.66	0.66	0.66	0.7		0.00	0.00	0.07	n/c	0.08	0.00
39-Q15019 (307-361)	0.96	0.96	0.91	0.91	0.91	0.91	0.91	0.91	0.91	0.91	0.92	1.00	n/c	0.85	0.78	0.78	0.78	0.82	0.82	0.82	0.8	n/c	0.85	0.85	0.85	0.84	0.84	0.80	0.80	n/c	n/c	0.66	0.66	0.66	0.66	0.66	0.7	0.00		0.00	0.07	n/c	0.08	0.00
40-Q15019-2 (342-396)	0.96	0.96	0.91	0.91	0.91	0.91	0.91	0.91	0.91	0.91	0.92	1.00	n/c	0.85	0.78	0.78	0.78	0.82	0.82	0.82	0.8	n/c	0.85	0.85	0.85	0.84	0.84	0.80	0.80	n/c	n/c	0.66	0.66	0.66	0.66	0.66	0.7	0.00	0.00		0.07	n/c	0.08	0.00
41-Q8WYJ6 (311-372)	0.81	0.81	0.82	0.82	0.82	0.82	0.82	0.82	0.82	0.82	0.83	0.84	n/c	0.87	0.90	0.90	0.90	0.84	0.84	0.84	0.8	n/c	0.87	0.87	0.87	0.90	0.90	0.90	0.90	n/c	n/c	0.47	0.47	0.47	0.47	0.47	0.5	0.66	0.66	0.66		n/c	0.07	0.05
42-Q8WYJ6-2 (-)	n/c	n/c	n/c	n/c	n/c	n/c	n/c	n/c	n/c	n/c	n/c	n/c	n/c	n/c	n/c	n/c	n/c	n/c	n/c	n/c	n/c	n/c	n/c	n/c	n/c	n/c	n/c	n/c	n/c	n/c	n/c	n/c	n/c	n/c	n/c	n/c	n/c	n/c	n/c	n/c	n/c	n/c	n/c
43-Q99719 (315-369)	0.85	0.85	0.79	0.79	0.79	0.79	0.79	0.79	0.79	0.79	0.81	0.89	n/c	0.81	0.81	0.81	0.81	0.76	0.76	0.76	0.8	n/c	0.85	0.85	0.85	0.83	0.83	0.87	0.87	n/c	n/c	0.43	0.43	0.43	0.43	0.43	0.4	0.63	0.63	0.63	0.37	n/c		0.07
44-Q99719-2 (313-346)	0.91	0.91	0.89	0.89	0.89	0.89	0.89	0.89	0.89	0.89	0.81	0.89	n/c	0.94	0.94	0.94	0.94	0.94	0.94	0.94	0.9	n/c	0.94	0.94	0.94	0.94	0.94	0.91	0.91	n/c	n/c	0.80	0.80	0.80	0.80	0.80	0.8	1.00	1.00	1.00	0.91	n/c	0.82	

Appendix 7 - **Identity matrix of the C-terminal domain sequences from all human septin isoforms.** The number of amino acid differences per site from between sequences are shown (obtained by dividing the number of amino acid differences by the total number of sites compared between the two sequences). Standard error estimates are shown above the diagonal. This analysis involved 44 amino acid sequences. All ambiguous positions were removed for each sequence pair (pairwise deletion option). There was a total of 181 positions in the final dataset. Evolutionary analyses were conducted in MEGA11. The presence of n/c in the results denotes cases in which it was not possible to estimate evolutionary distances.

Source: By the author.

ANNEX – Publications during the project

ROSA, H. V. D. *et al.* Molecular recognition at septin interfaces: the switches hold the key. **Journal of Molecular Biology**, v. 432, n. 21, p. 5784–5801, Oct. 2020.

LEONARDO, D. A. *et al.* Orientational ambiguity in septin coiled coils and its structural basis. **Journal of Molecular Biology**, v. 433, n. 9, p. 166889, Apr. 2021.

NOSKE, G. D. *et al.* A Crystallographic snapshot of SARS-CoV-2 main protease maturation process. **Journal of Molecular Biology**, v. 433, n. 18, p. 167118, Sept. 2021.

CAVINI, I. A. *et al.* The structural biology of septins and their filaments: an update. **Frontiers in Cell and Developmental Biology**, v. 9, p. 3246, Nov. 2021.